Université d'Ottawa · University of Ottawa

Université d'Ottawa · University of Ottawa

FACULTÉ DES ÉTUDES SUPÉRIEURES ET POSTDOCTORALES

FACULTY OF GRADUATE AND POSTDOCTORAL STUDIES

Christine SCALES

AUTEUR DE LA THÈSE - AUTHOR OF THESIS

M. A. Sc. (Electrical Engineering)

GRADE - DEGREE

School of Information Technology and Engineering

FACULTÉ, ÉCOLE, DÉPARTEMENT - FACULTY, SCHOOL, DEPARTMENT

TITRE DE LA THÈSE - TITLE OF THE THESIS

Magneto-plasmons in Optical Slab Waveguides

P. Berini

DIRECTEUR DE LA THÈSE - THESIS SUPERVISOR

CO-DIRECTEUR DE LA THÈSE - THESIS CO-SUPERVISOR

EXAMINATEURS DE LA THÈSE - THESIS EXAMINERS

D. McNamara

L. Roy

J.-M. De Koninck, Ph.D.

LE DOYEN DE LA FACULTÉ DES ÉTUDES SUPÉRIEURES ET POSTDOCTORALES

DEAN OF THE FACULTY OF GRADUATE AND POSTDOCTORAL STUDIES

Magneto-Plasmons in Optical Slab Waveguides

By

Christine Scales

A thesis submitted to the
School of Graduate Studies and Research
in partial fulfillment of the requirements for the degree of

Master of Applied Science

Ottawa-Carleton Institute for Electrical Engineering
School of Information Technology and Engineering
University of Ottawa
Ottawa, Ontario

Your file Votre référence
ISBN: 0-494-01600-0
Our file Notre référence
ISBN: 0-494-01600-0

Abstract

The effect of an externally applied magnetic field on the propagation characteristics of a plasmon-polariton wave supported by an infinitely wide thin metal waveguide was investigated. In order to do so, the dispersion relation was derived, from Maxwell's equations, enabling accurate modelling of the situation of interest. The general dispersion relation, including the constraint equation, for magneto-plasmons was derived in general, and then, specifically for a magnetic field applied along three orthogonal cartesian axes. The losses in the metal were included in the dispersion equation so that a better understanding of the influence of an externally applied magnetic field may be provided.

The dispersion relation is used as the basis of a software model of magneto-plasmons in thin metal films. This model is validated against specific cases in the literature with and without an externally applied magnetic field. The specific formulations in the literature were deemed to be incorrect, and have been corrected and the results have been interpreted. The model is then used to simulate thin gold films bounded by silicon dioxide at an infrared wavelength. The modelling results include the effect of the externally applied magnetic field on the propagation constant and the corresponding field components for all three cartesian orientations of externally applied magnetic field. The results from these simulations are presented and interpreted.

An indium tin slab in air with an externally applied magnetic field in three orthogonal cartesian orientations is modelled. Numerous branches are found in each orientation. The modes in these branches exhibit complex behaviour; both plasmon-polariton modes and total internal reflection modes are present. A thin gold film bounded by semi-infinite silicon dioxide with an externally applied magnetic field in three orthogonal cartesian orientations is also modelled. The effect of a range of externally applied magnetic field

levels on both the symmetric bound mode and the asymmetric bound mode is examined for light at the free space wavelength of 1550nm.

Acknowledgements

I would like to thank my supervisor, Dr. Pierre Berini, for giving me the opportunity to work on this interesting project and for his valuable guidance, suggestions, comments and encouragement throughout the course of it. Every time I spoke with him about my work, I came away encouraged and enlightened. Thank you to Robert Charbonneau and Ian Breukelaar for their assistance with the modelling and theoretical work. I would like to thank Dr. Philip Wort of Spectalis Corp. for his assistance which led to the discovery of an error in the literature. I would also like to thank the other employees of Spectalis Corp. who have provided their assistance and support throughout this project.

Thank you to my friends and family who have supported me and encouraged me over the years. I would especially like to thank my husband, Nathan, for his constant support and love.

Thank you to Dr. Derek MacNamara, Dr. Langis Roy, Dr. Pierre Berini and Nathan Scales for reviewing my thesis and providing valuable comments and suggestions.

Finally I would like to thank the Natural Sciences and Engineering Research Council of Canada (NSERC) and the University of Ottawa for their financial support, and Spectalis Corp. for providing access to their resources for use throughout this project.

Contents

List of Figures

1. Introduction

1.1 Field of Research

In the telecommunications industry, faster, smaller and cheaper components are always in demand. For this reason, integrated optical communications components are of great interest. The basic building block of any optical communications component is an optical waveguide. Recently, it has been shown theoretically [1-3] and experimentally [4, 5] that optical waveguides can be built from printed metal lines that guide light as a plasmon-polariton mode. Such waveguides could prove to be the basis for passive printed integrated optical circuits, comprising waveguides, bends, Y-junctions and couplers, as well as active printed integrated optical circuits, such as variable optical attenuators, modulators, switches, amplifiers and sources.

1.1.1 Definition of Plasmon-Polaritons

An electromagnetic wave travelling through a polarizable medium is modified by the polarization it induces and becomes coupled to the medium [31, p1]. These coupled modes are called polaritons. Bulk polaritons are polaritons propagating in a boundless medium, whereas surface polaritons are polaritons propagating at the interface between two media by the coupling of electromagnetic radiation to surface dipole excitations [31, p143].

If a volume of metal is hit with an electron, a charge density will propagate through it. This is called a volume plasmon. If the propagation occurs at the surface of the metal, it is called a surface plasmon.

If a plasmon is coupled with a polariton the propagation involves both a photon and an electron. Such a coupling can occur at the interface of an electron supporting medium and a dielectric. From Maxwell's equations, it has been shown that the interface between two media with the real parts of their permittivities having opposite signs, for example, a metal and a dielectric, will support a surface plasmon-polariton mode [31, p17].

At infrared frequencies, metals and highly doped semiconductors have low absorption due to electron collisions. Therefore, they can be modelled as an almost free-electron gas or cold plasma, allowing their relative permittivity to be defined by the Drude free-electron theory as follows [31], [32] and [33]:

$$\varepsilon_r = 1 - \frac{\omega_0^2}{\omega(\omega - j\nu)} \tag{1.1}$$

This can be divided into real and imaginary components as follows:

$$\varepsilon_r = \varepsilon_r' - j\varepsilon_r'' \tag{1.2}$$

Therefore the real part is

$$\varepsilon_r' = 1 - \frac{\omega_0^2}{\omega^2 + \nu^2} \tag{1.3}$$

and the imaginary part is

$$\varepsilon_r'' = \frac{\omega_0^2 \nu}{\omega(\omega^2 + \nu^2)} \tag{1.4}$$

In equations (1.1), (1.3) and (1.4), ω is the angular frequency of the radiation, ν is the effective electron collision frequency and ω_0 is the plasma frequency which is defined as follows:

$$\omega_0^2 = \frac{Nq^2}{\varepsilon_0 m} \tag{1.5}$$

In equation (1.5), N is the density of conduction electrons in m^{-3}, q is the electronic charge in Coulombs, m is the effective optical mass of the electron in kg and ε_0 is the permittivity of free space in F/m. The real part of the relative permittivity will be negative if

$\omega^2 + \nu^2 < \omega_0^2$. The imaginary part of the relative permittivity represents the absorption of the material due to electron collisions, which results in optical losses. Hence, the term almost free-electron gas; a free-electron gas does not have any electron collisions, $\nu = 0$.

It has been shown that at infrared frequencies, metals and some highly doped semiconductors have a negative real part of their relative permittivities and can, therefore, support surface plasmon-polariton modes when in contact with another medium such as a dielectric with positive real part of its permittivity [31, p17].

It has also been shown that interfaces between metals or highly doped semiconductors and normal dielectrics can only support transverse magnetic modes [31, p17]. Therefore, surface plasmon-polaritons are transverse magnetic surface electromagnetic waves propagating at the interface between two media with oppositely signed real parts of their permittivities. These waves are characterized by an exponentially decaying amplitude with increasing distance from the interface such that the field's amplitude tends towards zero as the distance from the interface tends towards infinity [34]. The electric and magnetic fields associated with a surface plasmon-polariton wave are shown in Figure 1.1, in which the direction of the propagation of the light is in the negative z direction, that is, into the page.

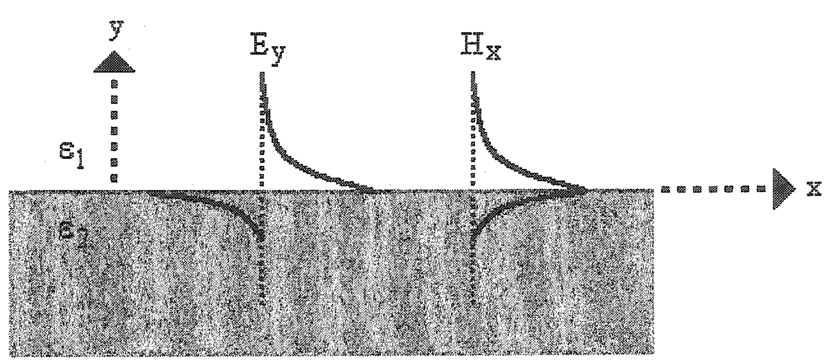

Figure 1.1 Fields associated with a plasmon polariton surface wave

1.1.2 Plasmon Polariton Waveguides

In the same manner that a plasmon-polariton wave can be supported by a semi-infinite metal-dielectric or semiconductor-dielectric interface, a plasmon-polariton wave can be supported and guided by a finite thickness, infinitely wide metal or semiconductor film bounded by a dielectric or even by a finite thickness, finite width metal or semiconductor film embedded in a dielectric. These two situations produce slightly different field solutions.

In the case of a finite thickness, infinitely wide metal or semiconductor film bounded by a dielectric, two plasmon-polariton modes are supported at both metal-dielectric or semiconductor-dielectric interfaces. If the film is thin enough, the plasmon-polariton modes guided by the two interfaces become coupled due to field tunnelling through the metal or semiconductor, producing a supermode [2]. The supermode may be either a symmetric mode or an asymmetric mode, as shown in Figure 1.2. These two modes are accompanied by evanescent fields which penetrate into the media bounding the metal film. The asymmetric mode has a propagation distance along the metal film which decreases as the metal film thickness decreases, while the propagation distance of the symmetric mode increases as the metal film thickness decreases. These modes are called the short-range surface plasmon wave and the long-range surface plasmon wave [25]. The difference in the propagation distances of these two modes is a direct result of the different fractions of the power carried by their evanescent fields. In a symmetric waveguide where the two media bounding the metal film have the same dielectric constant, the propagation distance of the symmetric mode will be longer than the propagation distance of the asymmetric mode in a thin film.

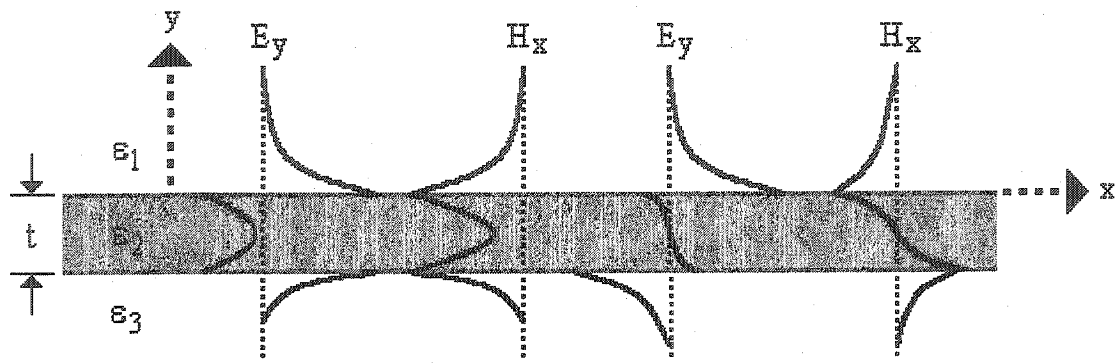

Figure 1.2 Fields associated with the symmetric (left) and asymmetric (right) plasmon polariton modes guided by an infinitely wide structure

Thin metal films finite in width, as shown in Figure 1.3, also support plasmon-polariton modes similar to those supported by an infinitely wide thin metal film. These waveguides provide lateral confinement as well as vertical confinement. Four fundamental modes were discovered, one for each combination of symmetric or asymmetric main electric field components in the vertical and horizontal confinement directions. The mode of most interest is the one that is symmetric in both vertical and horizontal confinement directions since its attenuation decreases significantly with decreasing metal thickness, in the same manner as the symmetric mode in the infinitely wide structure.

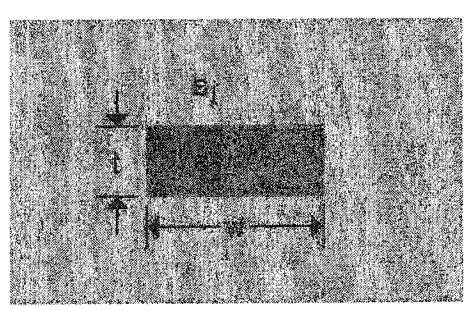

Figure 1.3 A thin metal film finite in width

1.2 Motivation

Active optical devices are an integral part of the optical integrated circuits of the future. Active devices provide modulation, emission, detection, attenuation, switching and sources, as well as, active wavelength selection. The recent discovery that light can be guided along thin finite width metal strips [1-5], has motivated the investigation of the properties of this new technology.

One possible way of influencing the propagation characteristics of surface plasmon waves is to apply an external magnetic field to the metal strip. Since metal waveguide technology is new, there is no literature on the effect of applying an external magnetic field to waveguides built with material combinations suitable for operation at infrared wavelengths. For this reason, a general theory was developed to describe this case. The theory that has been developed describes infinite width plasmon-polariton waveguide structures, and can be applied as a first approximation to finite width plasmon-polariton structures.

1.3 Thesis Objectives

The main purpose of this thesis is to investigate one of the possible ways of affecting finite width thin metal waveguides so as to make them active: application of magnetic field. Recently, it has been theoretically [1-3] and experimentally [4, 5] shown that a thin metal film finite in width is capable of supporting a bound plasmon-polariton propagating mode. Following this discovery, further exploration of the capabilities of this new optical waveguide technology is important.

The first objective of this thesis is to theoretically investigate the effect of an externally applied magnetic field on the propagation characteristics of a plasmon-polariton wave supported by an infinitely wide thin metal waveguide. In order to do so, it is necessary to derive relations using Maxwell's equations that enable accurate modelling of the situation of interest.

The second objective of this thesis is to use the newly developed theory to model plasmon-polariton waveguides made from a material combination that facilitates operation at near infra-red optical communications wavelengths.

1.4 Thesis Organization

Chapter 1 of this thesis provides an introduction to the field of research including a definition of plasmon-polaritons and plasmon-polariton waveguides. Next, a literary review of magneto-plasmons is presented in Chapter 2, in conjunction with a definition of magneto-plasmons and a derivation of the dielectric permittivity tensor of an almost free-electron gas in the presence of an externally applied magnetic field in the three cartesian orientations.

The general dispersion relation, including the constraint equation, is derived for magneto-plasmons in Chapter 3. The dispersion relation is derived in general, and then specifically for a magnetic field applied in all three possible cartesian orientations. The losses in the metal are included in the dispersion equation so that a better understanding of the influence of an externally applied magnetic field may be provided.

The dispersion relation is used as the basis of a software model of magneto-plasmons in thin metal films. In Chapter 4, this model is validated against specific cases in the literature with and without an externally applied magnetic field. It is then used to model thin gold films in silicon dioxide at an infrared wavelength. The modelling results presented in Chapter 5 include the effect of the externally applied magnetic field on the propagation constant and the corresponding field components for all three cartesian orientations of externally applied magnetic field.

The last chapter, Chapter 6, presents the conclusion and potential directions for future work. Finally, a list of bibliographic references is presented at the end of the thesis.

1.5 Thesis Contributions

In the last 30 years, surface magneto-plasmons have been investigated theoretically in several studies. However, most of the literature on the subject is not geared towards optical communications. In this thesis, an effort has been made to analyse the magneto-plasmons in structures that are practical at communications wavelengths.

The general dispersion relation for a structure with a permittivity tensor including losses, which may be induced by an externally applied magnetic field, has been formulated for what is believed to be the first time. This dispersion relation is used as the basis for a model which is used to reproduce simulations in previous work. The specific formulations in the previous work have been corrected and the results have been interpreted. Finally, this model is used to simulate magneto-plasmons in a thin gold film bounded by semi-infinite silicon dioxide at a free space wavelength of 1550nm for what is believed to be the first time. The results from these simulations are presented and interpreted.

2. Analytical Derivation and Literary Review

2.1 Definition of magneto-plasmons

Surface magneto-plasmons are surface plasmon-polaritons under the influence of an externally applied magnetic field. When a magnetic field is applied to a polarizable medium, such as a metal or highly doped semiconductor, it becomes anisotropic, meaning that propagation is variable as a function of direction [32].

2.1.1 Derivation of the dielectric permittivity tensor in the presence of a magnetic field

Metals and semiconductors, used in conjunction with dielectrics to form an interface capable of supporting surface plasmon-polaritons, can be modelled as a tenuous cold plasma. A cold plasma consists of equal positive and negative charges which have low thermal energies. In such a medium, only the interaction of the negative charges (electrons) with the wave will be considered since the positive ions are too massive to interact appreciably [32]. In the following analysis the permittivity of such a medium is derived.

The coordinate system that will be used in the following analysis is shown in Figure 2.1. The direction of wave propagation is taken to be in the *x-z* plane at an angle of ϕ with respect to the *z* axis. The electric field $\vec{E}$ associated with the wave may have any orientation perpendicular to the direction of propagation; it may be polarized in any manner. The applied dc magnetic field $\vec{B}_{DC}$ is chosen to be in the *z* direction. This simplifies the analysis without any loss of generality.

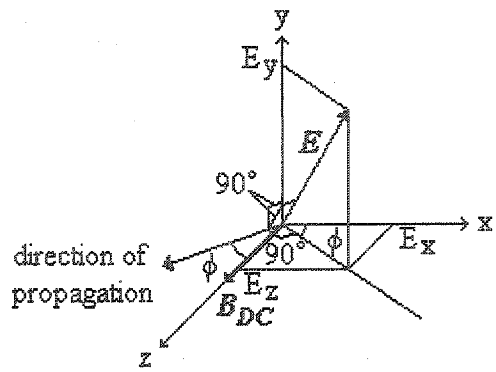

Figure 2.1 Coordinate system with magnetic field and direction of wave propagation

The forces that affect an electron of charge q and effective mass m in the presence of a wave and a magnetic flux density $\vec{B}_{DC}$ are the following:

the electric force is defined by

$$\vec{F}_e = q\vec{E} \tag{2.1}$$

and the magnetic force is defined by

$$\vec{F}_m = q(\vec{v} \times \vec{B}_{DC}) \tag{2.2}$$

where $\vec{v}$ is the velocity of the electron due to the wave in m/s.

The motion of the electron is damped by collisions with other electrons:

$$\vec{F}_d = -m\nu\vec{v} \tag{2.3}$$

where ν is the effective electron collision frequency.

The total force on the electron is given by Newton's second law of motion:

$$\vec{F} = m\vec{a} = m\frac{d\vec{v}}{dt} \tag{2.4}$$

where $\vec{a}$ is the acceleration of the particle in m/s^2 and t is time in seconds.

Combining these force relations, the total force being equal to the sum of the magnetic, electric and damping forces, yields the equation of motion of a particle subjected to external electric and magnetic fields [20]:

$$\vec{F} = q\vec{E} + q(\vec{v} \times \vec{B}_{DC}) = m\frac{d\vec{v}}{dt} + m\vec{v}\nu \tag{2.5}$$

To obtain the force per unit charge, equation (2.5) is divided by q:

$$\frac{\vec{F}}{q} = \vec{E} + \vec{v} \times \vec{B}_{DC} = \frac{m}{q}\frac{d\vec{v}}{dt} + \frac{m}{q}\vec{v}\nu \tag{2.6}$$

This vector equation can be expressed in terms of its three rectangular scalar components in cartesian coordinates as follows:

$$\frac{F_x}{q} = E_x + v_y B_{DCz} = \frac{m}{q}\frac{dv_x}{dt} + \frac{m}{q}v_x\nu \tag{2.7}$$

$$\frac{F_y}{q} = E_y - v_x B_{DCz} = \frac{m}{q}\frac{dv_y}{dt} + \frac{m}{q}v_y\nu \tag{2.8}$$

$$\frac{F_z}{q} = E_z = \frac{m}{q}\frac{dv_z}{dt} + \frac{m}{q}v_z\nu \tag{2.9}$$

Assuming time harmonic motion of the electron of the form

$$\vec{v} = \vec{v}_0 e^{j\omega t} \tag{2.10}$$

and a time harmonic wave of the form

$$\vec{E} = \vec{E}_0 e^{j\omega t}, \tag{2.11}$$

the derivatives go to $\frac{d}{dt} = j\omega$, where ω is the angular frequency of the radiation in radians. Therefore equations (2.7), (2.8) and (2.9) become

$$\frac{F_x}{q} = E_x + v_y B_{DCz} = \frac{m}{q}j\omega v_x + \frac{m}{q}v_x\nu \tag{2.12}$$

$$\frac{F_y}{q} = E_y - v_x B_{DCz} = \frac{m}{q}j\omega v_y + \frac{m}{q}v_y\nu \tag{2.13}$$

$$\frac{F_z}{q} = E_z = \frac{m}{q}j\omega v_z + \frac{m}{q}v_z\nu \tag{2.14}$$

Solving for the component velocities yields

$$v_x = \frac{(j\omega+\nu)(m/q)E_x + B_{DCz}E_y}{B_{DCz}^2 + (j\omega+\nu)^2(m^2/q^2)} \tag{2.15}$$

$$v_y = \frac{(j\omega+\nu)(m/q)E_y - B_{DCz}E_x}{B_{DCz}^2 + (j\omega+\nu)^2(m^2/q^2)} \tag{2.16}$$

$$v_z = \frac{E_z}{(j\omega+\nu)(m/q)} \tag{2.17}$$

From these relations it can be inferred that the wave will cause the charged particle to move in a helical path with axis coincident with the magnetic field (z direction) [32]. If the effect of collisions between particles in neglected ($\nu = 0$), v_x and v_y will become infinite for the frequency at which

$$B_{DCz}^2 = \frac{m^2\omega^2}{q^2} \tag{2.18}$$

indicating a strong interaction of the wave with the particles at this frequency. This frequency is called the gyro (or cyclotron) frequency:

$$\omega_g = \frac{q}{m}B_{DCz} \tag{2.19}$$

Substituting the gyro frequency from equation (2.19) into the component velocity equations (2.16) and (2.17) yields

$$v_x = \frac{q}{m}\frac{(j\omega+\nu)E_x + \omega_g E_y}{\omega_g^2 + (j\omega+\nu)^2} \tag{2.20}$$

$$v_y = \frac{q}{m}\frac{(j\omega+\nu) - \omega_g E_x}{\omega_g^2 + (j\omega+\nu)^2} \tag{2.21}$$

From Maxwell's equations, we have

$$\nabla\times\vec{H} = \vec{J}+j\omega\vec{D} = Nq\vec{v}+j\omega\varepsilon_0\vec{E} \qquad (2.22)$$

where $\vec{J}$ is the current density in A/m^2, $\vec{D}$ is the electric flux density in C/m^2 and N is the number of charged particles per unit volume. It is assumed that a movement of charged particles constitutes a conduction current [32]. (That is there is not diffusion current.) Expressing (2.22) in terms of its three rectangular components yields

$$(\nabla\times\vec{H})_x = j\omega\varepsilon_0 E_x + Nqv_x \qquad (2.23)$$

$$(\nabla\times\vec{H})_y = j\omega\varepsilon_0 E_y + Nqv_y \qquad (2.24)$$

$$(\nabla\times\vec{H})_z = j\omega\varepsilon_0 E_z + Nqv_z \qquad (2.25)$$

Introducing the component velocities from equations (2.20), (2.21) and (2.17) yields

$$(\nabla\times\vec{H})_x = \left[j\omega\varepsilon_0 + \frac{Nq^2(j\omega+\nu)}{m(\omega_g^2+(j\omega+\nu)^2)}\right]E_x + \left[\frac{Nq^2\omega_g}{m(\omega_g^2+(j\omega+\nu)^2)}\right]E_y \qquad (2.26)$$

$$(\nabla\times\vec{H})_y = -\left[\frac{Nq^2\omega_g}{m(\omega_g^2+(j\omega+\nu)^2)}\right]E_x + \left[j\omega\varepsilon_0 + \frac{Nq^2(j\omega+\nu)}{m(\omega_g^2+(j\omega+\nu)^2)}\right]E_y \qquad (2.27)$$

$$(\nabla\times\vec{H})_z = \left[j\omega\varepsilon_0 + \frac{Nq^2}{m(j\omega+\nu)}\right]E_z \qquad (2.28)$$

If the effect of collisions between particles is neglected ($\nu = 0$), the permittivity and the index of refraction of the medium become zero when the following condition is met:

$$\frac{Nq^2}{\varepsilon_0 m\omega^2} = 1 \qquad (2.29)$$

The frequency at which this condition is met called the critical or plasma frequency:

$$\omega_0^2 = \frac{Nq^2}{\varepsilon_0 m} \qquad (2.30)$$

Below the critical frequency, the real part of the permittivity is negative.

Substituting the critical frequency into equations (2.26), (2.27) and (2.28) yields

$$(\nabla\times\vec{H})_x = \left[j\omega\varepsilon_0 + \varepsilon_0\omega_0^2\frac{(j\omega+\nu)}{\omega_g^2+(j\omega+\nu)^2}\right]E_x + \left[\frac{\varepsilon_0\omega_0^2\omega_g}{\omega_g^2+(j\omega+\nu)^2}\right]E_y \qquad (2.31)$$

$$(\nabla\times\vec{H})_y = -\left[\frac{\varepsilon_0\omega_0^2\omega_g}{\omega_g^2+(j\omega+\nu)^2}\right]E_x + \left[j\omega\varepsilon_0 + \varepsilon_0\omega_0^2\frac{(j\omega+\nu)}{\omega_g^2+(j\omega+\nu)^2}\right]E_y \qquad (2.32)$$

$$(\nabla\times\vec{H})_z = \left[j\omega\varepsilon_0 + \frac{\varepsilon_0\omega_0^2}{j\omega+\nu}\right]E_z \qquad (2.33)$$

In general from Maxwell's equations, we have

$$\nabla\times\vec{H} = j\omega\tilde{\varepsilon}\cdot\vec{E} \qquad (2.34)$$

where $\tilde{\varepsilon}$ is the permittivity tensor. Based on the above, the permittivity tensor can be deduced from equations (2.31), (2.32) and (2.33):

$$\tilde{\varepsilon} = \varepsilon_0\begin{bmatrix} 1+\dfrac{\omega_0^2(\omega-j\nu)}{\omega(\omega_g^2-(\omega-j\nu)^2)} & \dfrac{-j\omega_0^2\omega_g}{\omega(\omega_g^2-(\omega-j\nu)^2)} & 0 \\ \dfrac{j\omega_0^2\omega_g}{\omega(\omega_g^2-(\omega-j\nu)^2)} & 1+\dfrac{\omega_0^2(\omega-j\nu)}{\omega(\omega_g^2-(\omega-j\nu)^2)} & 0 \\ 0 & 0 & 1-\dfrac{\omega_0^2}{\omega(\omega-j\nu)} \end{bmatrix} \qquad (2.35)$$

In the absence of an externally applied magnetic field, $\vec{B}=0 \Rightarrow \omega_g = 0$, the permittivity becomes isotropic:

$$\tilde{\varepsilon} = \varepsilon_0 \begin{bmatrix} 1 - \dfrac{\omega_0^2}{\omega(\omega - j\nu)} & 0 & 0 \\ 0 & 1 - \dfrac{\omega_0^2}{\omega(\omega - j\nu)} & 0 \\ 0 & 0 & 1 - \dfrac{\omega_0^2}{\omega(\omega - j\nu)} \end{bmatrix} \quad (2.36)$$

From equation (2.36), it can be seen that the relative permittivity is the following:

$$\varepsilon_r = 1 - \frac{\omega_0^2}{\omega(\omega - j\nu)} \quad (2.37)$$

We also know that the relative permittivity can be defined in terms of its real and imaginary components:

$$\varepsilon_r = \varepsilon_r' - j\varepsilon_r'' \quad (2.38)$$

From equation (2.37), it can be seen that the real part of the relative permittivity is

$$\varepsilon_r' = 1 - \frac{\omega_0^2}{\omega^2 + \nu^2} \quad (2.39)$$

and the imaginary part of the relative permittivity is

$$\varepsilon_r'' = \frac{\omega_0^2 \nu}{\omega(\omega^2 + \nu^2)} \quad (2.40)$$

Notice that the relative permittivity in the absence of an externally applied magnetic field is exactly the relative permittivity as obtained from the Drude free-electron theory and given previously in equations (1.2), (1.3) and (1.4).

2.1.2 Three orientations in the interface case

The above derivation of the dielectric tensor is for the generic case of a z-directed externally applied magnetic field in a homogeneous medium. A much more interesting case is the case of an interface that can support plasmon-polariton waves and, hence, magneto-plasmons, when a magnetic field is introduced. Such an interface consists of a dielectric with a dielectric constant that is isotropic and has a positive real part, and a plasma such as a metal or highly doped semiconductor with a dielectric index that is a tensor and has a negative real part. Figure 2.2 shows an interface along the x axis with the direction of wave propagation defined in the z-direction. The interface is defined as follows: for y>0, the permittivity is $\tilde{\varepsilon}_1$ (metal) and for y<0, the permittivity is ε_2 (dielectric).

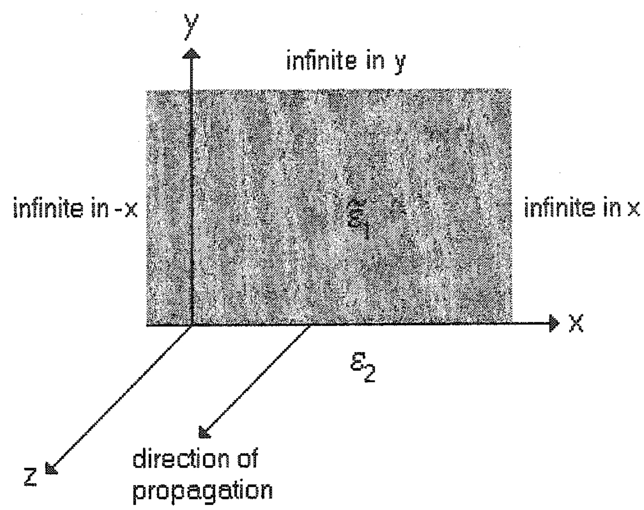

Figure 2.2 Direction of propagation of plasmon polariton wave at a semi-infinite interface (interface between semi-infinite half spaces)

Depending on the orientation of the externally applied magnetic field with respect to the interface and the direction of propagation of the wave, the values of the elements of the dielectric tensor in the plasma, $\tilde{\varepsilon}_1$, take on different positions. In the Faraday orientation, the magnetic field is in the direction of wave propagation (z-direction) and the dielectric tensor is the same as the one in equation (2.35) derived above. In the Voigt orientation, the magnetic field is perpendicular to the direction of wave propagation but parallel to the interface (x-direction) and the dielectric tensor is the following:

$$\tilde{\varepsilon} = \varepsilon_0 \begin{bmatrix} 1 - \dfrac{\omega_0^2}{\omega(\omega - j\nu)} & 0 & 0 \\ 0 & 1 + \dfrac{\omega_0^2(\omega - j\nu)}{\omega(\omega_g^2 - (\omega - j\nu)^2)} & \dfrac{-j\omega_0^2\omega_g}{\omega(\omega_g^2 - (\omega - j\nu)^2)} \\ 0 & \dfrac{j\omega_0^2\omega_g}{\omega(\omega_g^2 - (\omega - j\nu)^2)} & 1 + \dfrac{\omega_0^2(\omega - j\nu)}{\omega(\omega_g^2 - (\omega - j\nu)^2)} \end{bmatrix} \tag{2.41}$$

In the perpendicular orientation, the magnetic field is perpendicular to the direction of wave propagation and perpendicular to the interface (in the y-direction) and the dielectric tensor is the following:

$$\tilde{\varepsilon} = \varepsilon_0 \begin{bmatrix} 1 + \dfrac{\omega_0^2(\omega - j\nu)}{\omega(\omega_g^2 - (\omega - j\nu)^2)} & 0 & \dfrac{j\omega_0^2\omega_g}{\omega(\omega_g^2 - (\omega - j\nu)^2)} \\ 0 & 1 - \dfrac{\omega_0^2}{\omega(\omega - j\nu)} & 0 \\ \dfrac{-j\omega_0^2\omega_g}{\omega(\omega_g^2 - (\omega - j\nu)^2)} & 0 & 1 + \dfrac{\omega_0^2(\omega - j\nu)}{\omega(\omega_g^2 - (\omega - j\nu)^2)} \end{bmatrix} \tag{2.42}$$

As shown above, when a magnetic field is applied to a polarizable medium, the dielectric permittivity of that medium becomes a tensor. In addition to the three field components of a transverse magnetic wave, the interface supports supplemental field components which arise from the off-diagonal components in the dielectric permittivity tensor introduced by the externally applied magnetic field.

2.2 Historical Review

In the seventies and eighties, there was significant interest in the investigation of surface magneto-plasmons. Surface magneto-plasmons are surface plasmon-polaritons under the influence of an externally applied magnetic field. Surface plasmon-polaritons have been studied ever since the discovery, in 1968, of a method for exciting surface plasmon-polaritons using an attenuated total reflectance (ATR) setup [6-8]. Soon after, in 1972, the effect of the application of an external magnetic field on surface plasmon-polaritons was explored theoretically by Chiu and Quinn [9]. Magneto-plasmons have continued to be explored theoretically [10-20] as well as experimentally in the single interface case (interface between semi-infinite half spaces) [21-24], and theoretically in the double interface case (thin film bounded by semi-infinite half spaces) [25-29].

The effect of an externally applied dc magnetic field of arbitrary magnitude and orientation on surface plasmons supported by a metal or degenerate semiconductor has been studied in the "nonretarded" limit, in which the velocity of light is equal to unity, by K. W. Chiu and J. J. Quinn [9-10] in the lossless case. They found that when the magnetic field is applied normal to the surface (perpendicular orientation), the surface plasmon dispersion relation is strongly affected by the presence of the dc magnetic field. They found similar results when the magnetic field is applied parallel to the interface and to the direction of wave propagation (Faraday orientation). However, they found that when the magnetic field is applied perpendicular to the wave propagation but parallel to the interface (Voigt orientation) they found two branches of the dispersion curve corresponding to propagation in the positive and negative directions. The presence of the magnetic field breaks the symmetry between these directions and the two branches exchange places upon changing the sign of the magnetic field [10]. This orientation generates non-reciprocal wave propagation.

Similar results to those found in the study of magneto-plasmons in the single interface case have been found in the double interface case. In particular, M. S. Kushwaha and P. Halevi derived the dispersion relation for the thin film case in all three orientations separately. They found that, in both the Faraday orientation and the perpendicular orientation, the spectrum splits and a gap in the spectrum is created. They observe one spectrum split in the Faraday case and two spectrum splits involving both s-polarized (transverse electric) and p-polarized (transverse magnetic) waves in the perpendicular case. In the Voigt case, they found that the dispersion curve has two branches corresponding to propagation in the positive and negative directions, as in the single interface case. Each of these positive and negative branches then splits into two more branches and creates one gap in the spectrum each.

The general dispersion equation derived in the next chapter has been developed in a similar manner to the way that Kushwaha and Halevi developed the specific dispersion equations for all three orientations. Upon doing so, it was discovered that Kushwaha and Halevi made an error in the simplification of the dispersion equation which affects both the perpendicular case and the Voigt case but has no effect on the Faraday case. However, an additional branch of the dispersion equation was found through the simulation of the general dispersion equation in the Faraday case. Simulation of the general dispersion equation in the perpendicular case produced results similar to Kushwaha and Halevi's perpendicular results. However, the spectrum splits in three places rather than two places. The first two splits have a similar form to those simulated by Kushwaha and Halevi but do not occur in the same place. Simulation of the general dispersion equation in the Voigt case produced quite different results from Kushwaha and Halevi's Voigt results. The spectrum splits twice instead of once. The discrepancy between the results obtained in this thesis and those reported by Kushwaha and Halevi in references [28, 29] are believed to result from errors in their formulation.

The theoretical development by Kushwaha and Halevi is quite clear and easily understood, and can therefore be applied to other slab structures not yet examined in the literature. For this reason, it was chosen as the basis for the development of the general dispersion equation and for the same reason it is paramount that the errors be noted so that they are not perpetuated in further research.

3. Derivation of the Dispersion Relation

The first step in the investigation of magneto-plasmons is to derive the dispersion relation. In the case of finite width thin metal films, a powerful numerical modal analysis tool is required, since an analytic formulation for the dispersion relation cannot be obtained. This is not the case for infinite width thin metal films, where the dispersion equation can be obtained analytically. Finite width thin metal films have similar modes and will respond to an external magnetic field in a similar manner to infinite width thin metal films. Therefore, by modelling infinite width thin metal films it is possible to get an understanding of the effect of an externally applied magnetic field on finite width thin metal films without the complex modelling usually required. The following model is for magneto-plasmons in infinite width thin metal films.

The dispersion relation for magneto-plasmons in a thin, semiconducting film bounded by dissimilar or conducting media was derived by Kushwaha and Halevi. They looked at certain limiting cases, in three possible orientations of externally applied magnetic fields: Faraday (z-direction) [27], Voigt (x-direction) [28], and perpendicular (y-direction) [29]. In this thesis, the general dispersion relation for an infinite width thin metal film or semiconductor film supported above and below by dielectrics in the presence of an externally applied dc magnetic field is developed independent of the orientation of the magnetic field in both the lossless and the lossy cases. The general dispersion relation is then given for three magnetic field orientations: Faraday (z-direction), Voigt (x-direction), and Perpendicular (y-direction), with reference to Figure 3.1.

The orientation of the infinite width thin metal film with respect to the cartesian coordinates used in the following derivation is shown in Figure 3.1. The metal film lies in the x-z plane. Its thickness in the y-direction is d and its width in the x-direction is infinite. The direction of wave propagation is in the positive z-direction.

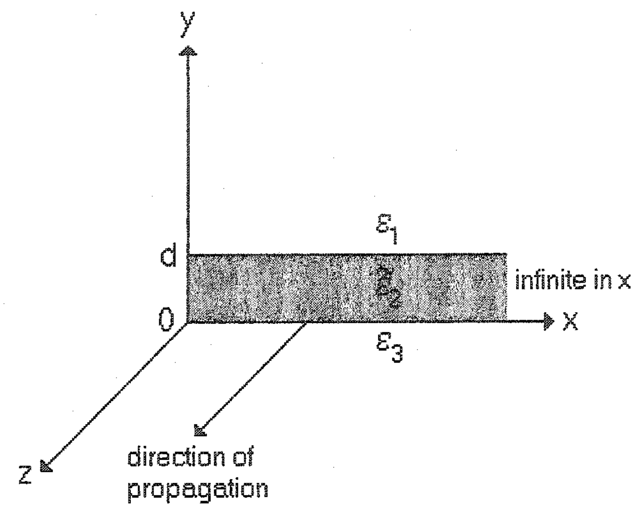

Figure 3.1 Orientation of the thin film and direction of wave propagation in cartesian coordinates

The metal film is cladded by semi-infinite dielectrics above and below. The top cladding medium has a dielectric permittivity of ε_1 and the bottom cladding material has a dielectric permittivity of ε_3. The dielectric permittivity of the metal film is a tensor with the following general form:

$$\tilde{\varepsilon} = \begin{bmatrix} \varepsilon_{xx} & \varepsilon_{xy} & \varepsilon_{xz} \\ \varepsilon_{yx} & \varepsilon_{yy} & \varepsilon_{yz} \\ \varepsilon_{zx} & \varepsilon_{zy} & \varepsilon_{zz} \end{bmatrix} \tag{3.1}$$

3.1 Derivation of vector wave equation for full dielectric tensor

Maxwell's equations give the general relationships between the electric and magnetic field. However, they are coupled with these two variables. The vector wave equations are decoupled versions of Maxwell's equations.

Maxwell's equation as derived from Ampere's law, equation (3.2), and Maxwell's equation as derived from Faraday's law, equation (3.3), are all that is needed to solve for the electric and magnetic field components:

$$\nabla \times \vec{E} = -\frac{\partial \vec{B}}{\partial t} \tag{3.2}$$

$$\nabla \times \vec{H} = \frac{\partial \vec{D}}{\partial t} + \vec{J} \tag{3.3}$$

where $\vec{E}$ is the electric field intensity in V/m
$\vec{B}$ is the magnetic flux density in T
$\vec{H}$ is the magnetic field in A/m
$\vec{D}$ is the electric flux density in C/m^2
$\vec{J}$ is the current density in A/m^2
ω is the angular frequency in rad/sec
t is the time in seconds

In the situation under consideration there are no external sources, therefore $\vec{J} = 0$ and equations (3.3) becomes

$$\nabla \times \vec{H} = \frac{\partial \vec{D}}{\partial t} \tag{3.4}$$

If it is assumed that the fields have a temporal dependency of the form $e^{j\omega t}$, the time derivative in equations (3.4) and (3.4) becomes $j\omega$:

$$\nabla \times \vec{E} = -j\omega\vec{B} \tag{3.5}$$

$$\nabla \times \vec{H} = j\omega\vec{D} \tag{3.6}$$

By substituting the material constitutive relations, $\vec{B} = \mu\vec{H}$ (where μ is the permeability in H/m), and $\vec{D} = \tilde{\varepsilon}\vec{E}$ (where $\tilde{\varepsilon}$ is the permittivity tensor in F/m), into equations (3.5) and (3.6), the number of variables can be reduced to two:

$$\nabla \times \vec{E} = -j\omega\mu\vec{H} \tag{3.7}$$

$$\nabla \times \vec{H} = j\omega\tilde{\varepsilon}\vec{E} \tag{3.8}$$

The above two equations are two linearly independent vector equations with two unknowns: $\vec{E}$ and $\vec{H}$. They are coupled first order partial differential equations and as such are quite difficult to solve. For this reason they are usually rewritten in the equivalent form of vector wave equations. These equations are obtained by raising the order of the derivatives. This is done by taking the curl of equations (3.7) and (3.8):

$$\nabla\times\nabla\times\vec{E} = -j\omega\mu\nabla\times\vec{H} \tag{3.9}$$

$$\nabla\times\nabla\times\vec{H} = j\omega\tilde{\varepsilon}\nabla\times\vec{E} \tag{3.10}$$

Substituting equations (3.7) and (3.8) in equations (3.9) and (3.10) gives the vector wave equations for the electric field

$$\nabla\times\nabla\times\vec{E} = \omega^2\mu\tilde{\varepsilon}\vec{E} \tag{3.11}$$

and magnetic field

$$\nabla\times\nabla\times\vec{H} = -\omega^2\mu\tilde{\varepsilon}\vec{H} \tag{3.12}$$

3.2 Constraint Equation

The first step in deriving the dispersion relation is to derive the constraint equation, which gives the relationship between the complex directional propagation constants: γ_x, γ_y, γ_z. It depends on the coordinate system (cartesian is used here) and the form of the field components.

The fields are assumed to have the following spatial and temporal dependence:

$$\vec{E}(r,t) \propto e^{-\vec{\gamma}\cdot\vec{r}+j\omega t} \tag{3.13}$$

where r is the position vector, $r = (x, y, z)$
γ is the propagation vector (or wave vector), $\gamma = (\gamma_x, \gamma_y, \gamma_z)$

The components of the propagation vector (the propagation constants in x, y and z) can be decomposed into real and imaginary parts: $\gamma_i = \alpha_i + j\beta_i$, where α_i is the attenuation constant in the i direction in Np/m, β_i is the phase constant in the i direction in rad/m, and i is the direction of propagation constant (x, y or z).

Equation (3.13) can be expanded in cartesian coordinates as follows:

$$\begin{aligned} E_x &\propto e^{-\gamma_x x + j\omega t} \\ E_y &\propto e^{-\gamma_y y + j\omega t} \\ E_z &\propto e^{-\gamma_z z + j\omega t} \end{aligned} \tag{3.14}$$

Given that

$$\begin{aligned} \nabla\times\nabla\times\vec{A} = {} & \hat{x}\left(\frac{\partial^2 A_y}{\partial x\partial y} - \frac{\partial^2 A_x}{\partial y^2} - \frac{\partial A_x}{\partial z^2} + \frac{\partial^2 A_z}{\partial z\partial x}\right) \\ & + \hat{y}\left(\frac{\partial^2 A_z}{\partial y\partial z} - \frac{\partial^2 A_y}{\partial z^2} - \frac{\partial^2 A_y}{\partial x^2} + \frac{\partial^2 A_x}{\partial x\partial y}\right) \\ & + \hat{z}\left(\frac{\partial^2 A_x}{\partial x\partial z} - \frac{\partial^2 A_z}{\partial x^2} - \frac{\partial^2 A_z}{\partial y^2} + \frac{\partial^2 A_y}{\partial y\partial z}\right) \end{aligned} \tag{3.15}$$

and given the form of the field in equation (3.13) or equivalently in equation (3.14), equations (3.11) and (3.12) can be rewritten as follows:

$$\nabla\times\nabla\times\vec{E} = \hat{x}(-\gamma_y^2 E_x - \gamma_z^2 E_x) + \hat{y}(\gamma_y\gamma_z E_z - \gamma_z^2 E_y) + \hat{z}(-\gamma_y^2 E_z - \gamma_y\gamma_z E_y) \tag{3.16}$$

$$\nabla\times\nabla\times\vec{H} = \hat{x}(-\gamma_y^2 H_x - \gamma_z^2 H_x) + \hat{y}(\gamma_y\gamma_z H_z - \gamma_z^2 H_y) + \hat{z}(-\gamma_y^2 H_z - \gamma_y\gamma_z H_y) \tag{3.17}$$

The slab is infinite in the x direction, therefore the x-component of the propagation constant is zero, $\gamma_x = 0$.

Taking this into account and rewriting equations (3.16) and (3.17) in matrix form yields the following:

$$\nabla\times\nabla\times\vec{E} = \begin{bmatrix} -\gamma_y^2-\gamma_z^2 & 0 & 0 \\ 0 & -\gamma_z^2 & \gamma_y\gamma_z \\ 0 & \gamma_y\gamma_z & -\gamma_y^2 \end{bmatrix}\begin{bmatrix} E_x \\ E_y \\ E_z \end{bmatrix} \tag{3.18}$$

$$\nabla\times\nabla\times\vec{H} = \begin{bmatrix} -\gamma_y^2-\gamma_z^2 & 0 & 0 \\ 0 & -\gamma_z^2 & \gamma_y\gamma_z \\ 0 & \gamma_y\gamma_z & -\gamma_y^2 \end{bmatrix}\begin{bmatrix} H_x \\ H_y \\ H_z \end{bmatrix} \tag{3.19}$$

Substituting the permittivity tensor from equation (3.1) and equation (3.18) into the vector wave equation (3.11) and multiplying by -1 yields the following:

$$\begin{bmatrix} \gamma_y^2+\gamma_z^2+\omega^2\mu\varepsilon_{xx} & \omega^2\mu\varepsilon_{xy} & \omega^2\mu\varepsilon_{xz} \\ \omega^2\mu\varepsilon_{yx} & \gamma_z^2+\omega^2\mu\varepsilon_{yy} & -\gamma_y\gamma_z+\omega^2\mu\varepsilon_{yz} \\ \omega^2\mu\varepsilon_{zx} & -\gamma_y\gamma_z+\omega^2\mu\varepsilon_{zy} & \gamma_z^2+\omega^2\mu\varepsilon_{zz} \end{bmatrix}\begin{bmatrix} E_x \\ E_y \\ E_z \end{bmatrix} = 0 \tag{3.20}$$

Substituting the permittivity tensor from equation (3.1) and equation (3.19) into the vector wave equation (3.12) and multiplying by -1 yields the following:

$$\begin{bmatrix} \gamma_y^2+\gamma_z^2+\omega^2\mu\varepsilon_{xx} & \omega^2\mu\varepsilon_{xy} & \omega^2\mu\varepsilon_{xz} \\ \omega^2\mu\varepsilon_{yx} & \gamma_z^2+\omega^2\mu\varepsilon_{yy} & -\gamma_y\gamma_z+\omega^2\mu\varepsilon_{yz} \\ \omega^2\mu\varepsilon_{zx} & -\gamma_y\gamma_z+\omega^2\mu\varepsilon_{zy} & \gamma_z^2+\omega^2\mu\varepsilon_{zz} \end{bmatrix}\begin{bmatrix} H_x \\ H_y \\ H_z \end{bmatrix} = 0 \tag{3.21}$$

Equations (3.20) and (3.21) are two equivalent sets of linear equations for which a non-trivial solution is found by setting the determinant to zero.

3.2.1 General constraint equation

The constraint equation for the directional propagation constants is the solution of the vector wave equation in which the spatial and temporal form of the electric and magnetic fields has been substituted, equations (3.20) and (3.21). The solution is found by setting the determinant equal to zero.

By examining the symmetry of the dielectric tensor for all three orientations in equations (2.35), (2.41) and (2.42), it can been seen that the off-diagonal components of the general dielectric tensor given in equation (3.1) can be simplified in the following manner: $\varepsilon_{yx} = -\varepsilon_{xy}$; $\varepsilon_{zy} = -\varepsilon_{yz}$; $\varepsilon_{zx} = -\varepsilon_{xz}$. If the media are lossless, $\nu = 0$, the dielectric tensor becomes Hermitian, $\varepsilon_{ij} = \varepsilon_{ji}^*$, and thereby maintains the requirement that the electromagnetic field energy be conserved [30].

Setting the determinant of equation (3.20), or equivalently of equation (3.21), to zero and simplifying the general form of the dielectric tensor by symmetry gives the general constraint equation:

$$\begin{aligned}\gamma_y^2 = \frac{1}{2\varepsilon_{yy}}\Bigg[& -\gamma_z^2(\varepsilon_{yy}+\varepsilon_{zz}) + (-\omega^2\mu(\varepsilon_{yy}(\varepsilon_{xx}+\varepsilon_{zz}) + \varepsilon_{yz}^2 + \varepsilon_{xy}^2)) \\ & \pm\Big\{\gamma_z^4(\varepsilon_{yy}-\varepsilon_{zz})^2 \\ & + 2\gamma_z^2\omega^2\mu[(\varepsilon_{yy}-\varepsilon_{zz})(\varepsilon_{yy}(\varepsilon_{xx}-\varepsilon_{zz})-\varepsilon_{yz}^2) + \varepsilon_{yy}(\varepsilon_{xy}^2 - 2\varepsilon_{xz}^2) + \varepsilon_{zz}\varepsilon_{xy}^2] \\ & + \omega^4\mu^2[\varepsilon_{yy}^2((\varepsilon_{xx}-\varepsilon_{zz})^2 - 4\varepsilon_{xz}^2) + (\varepsilon_{yz}^2+\varepsilon_{xy}^2)^2 + 2\varepsilon_{yy}(\varepsilon_{xx}-\varepsilon_{zz})(\varepsilon_{xy}^2-\varepsilon_{yz}^2)]\Big\}^{\frac{1}{2}}\Bigg]\end{aligned} \tag{3.22}$$

When there is no magnetic field present, the dielectric tensor simplifies to a single dielectric constant value: $\varepsilon = \varepsilon_{xx} = \varepsilon_{yy} = \varepsilon_{zz}$ and $\varepsilon_{xy} = \varepsilon_{yx} = \varepsilon_{xz} = \varepsilon_{zx} = \varepsilon_{yz} = \varepsilon_{zy} = 0$. Therefore the constraint equation becomes the following:

$$\gamma_y^2 = -\gamma_z^2 - \omega^2\mu\varepsilon \tag{3.23}$$

This is the constraint equation in an isotropic medium, where there is no external magnetic field, with the directional propagation constant in the x-direction equal zero since the medium is infinite in this direction.

3.2.2 Constraint equation for the Faraday orientation

In the Faraday orientation, the magnetic field is in the direction of wave propagation (z-direction) and the dielectric tensor is given by equation (2.35). Substituting the form of the dielectric tensor in the Faraday orientation into the general constraint equation gives the Faraday constraint equation with losses:

$$\gamma_y^2 = \frac{1}{2\varepsilon_{xx}}\left[-(\varepsilon_{xx}+\varepsilon_{zz})(\gamma_z^2+\omega^2\mu\varepsilon_{xx})-\omega^2\mu\varepsilon_{xy}^2 \pm\left\{[(\varepsilon_{xx}-\varepsilon_{zz})(\gamma_z^2+\omega^2\mu\varepsilon_{xx})+\omega^2\mu\varepsilon_{xy}^2]^2+4\gamma_z^2\omega^2\mu\varepsilon_{xy}^2\varepsilon_{zz}\right\}^{\frac{1}{2}}\right] \tag{3.24}$$

In the lossless case, all of the tensor components are either purely real or purely imaginary and the constraint equation can be simplified as follows:

$$\gamma_y^2 = \frac{1}{2\varepsilon_{xx}}\left[-(\varepsilon_{xx}+\varepsilon_{zz})(\gamma_z^2+\omega^2\mu\varepsilon_{xx})+\omega^2\mu\varepsilon_{xy}^2 \pm\left\{[(\varepsilon_{xx}-\varepsilon_{zz})(\gamma_z^2+\omega^2\mu\varepsilon_{xx})-\omega^2\mu\varepsilon_{xy}^2]^2-4\gamma_z^2\omega^2\mu\varepsilon_{xy}^2\varepsilon_{zz}\right\}^{\frac{1}{2}}\right] \tag{3.25}$$

In the lossless case, the attenuation constants are null, $\alpha_y = \alpha_z = 0$, and the propagation constants only contain the phase constant portion: $\gamma_y = j\beta_y$ and $\gamma_z = j\beta_z$, therefore equation (3.25) becomes

$$-\beta_y^2 = \frac{1}{2\varepsilon_{xx}}\Bigg[-(\varepsilon_{xx}+\varepsilon_{zz})(-\beta_z^2+\omega^2\mu\varepsilon_{xx})+\omega^2\mu\varepsilon_{xy}^2 \qquad (3.26)$$

$$\pm\left\{[(\varepsilon_{xx}-\varepsilon_{zz})(-\beta_z^2+\omega^2\mu\varepsilon_{xx})-\omega^2\mu\varepsilon_{xy}^2]^2+4\beta_z^2\omega^2\mu\varepsilon_{xy}^2\varepsilon_{zz}\right\}^{\frac{1}{2}}\Bigg]$$

3.2.3 Constraint equation for the Voigt orientation

In the Voigt orientation, the magnetic field is perpendicular to the direction of wave propagation but parallel to the interface (x-direction) and the dielectric tensor is given by equation (2.41). Substituting the form of the dielectric tensor in the Voigt orientation into the general constraint equation gives the Voigt constraint equation with losses:

$$\gamma_y^2 = \frac{1}{2\varepsilon_{zz}}[-2\varepsilon_{zz}\gamma_z^2-\omega^2\mu(\varepsilon_{zz}(\varepsilon_{xx}+\varepsilon_{zz})+\varepsilon_{yz}^2)\pm\omega^2\mu(\varepsilon_{zz}(\varepsilon_{xx}-\varepsilon_{zz})-\varepsilon_{yz}^2)] \qquad (3.27)$$

Taking the positive part of the equation, yields the following root:

$$\gamma_y^2 = -\gamma_z^2-\omega^2\mu\left(\varepsilon_{zz}+\frac{\varepsilon_{yz}^2}{\varepsilon_{zz}}\right) \qquad (3.28)$$

Taking the negative part of the equation, yields the following root:

$$\gamma_y^2 = -\gamma_z^2-\omega^2\mu\varepsilon_{xx} \qquad (3.29)$$

This root, however, leads to TE (s-polarized) waves, which do not experience a magnetic force in the Voigt geometry, therefore, this root will not be included [28].

In the lossless case, all of the tensor components are either purely real or purely imaginary and the attenuation constants are null, therefore the constraint equation can be simplified as follows:

$$\beta_y^2 = -\beta_z^2+\omega^2\mu\left(\varepsilon_{zz}-\frac{\varepsilon_{yz}^2}{\varepsilon_{zz}}\right) \qquad (3.30)$$

3.2.4 Constraint equation for the perpendicular orientation

In the perpendicular orientation, the magnetic field is perpendicular to the direction of wave propagation and perpendicular to the interface (in the y-direction) and the dielectric tensor is given by equation (2.42). Substituting the form of the dielectric tensor in the perpendicular orientation into the general constraint equation gives the perpendicular constraint equation with losses:

$$\gamma_y^2 = \frac{1}{2\varepsilon_{yy}}\left[-\gamma_z^2(\varepsilon_{xx}+\varepsilon_{yy}) - 2\omega^2\mu\varepsilon_{xx}\varepsilon_{yy} \pm \{\gamma_z^4(\varepsilon_{xx}-\varepsilon_{yy})^2 - 4\omega^2\mu\varepsilon_{yy}\varepsilon_{xz}^2(\gamma_z^2+\omega^2\mu\varepsilon_{yy})\}^{\frac{1}{2}}\right] \tag{3.31}$$

In the lossless case, all of the tensor components are either purely real or purely imaginary and the attenuation constants are null, therefore the constraint equation can be simplified as follows:

$$-\beta_y^2 = \frac{1}{2\varepsilon_{yy}}\left[\beta_z^2(\varepsilon_{xx}+\varepsilon_{yy}) - 2\omega^2\mu\varepsilon_{xx}\varepsilon_{yy} \pm \{\beta_z^4(\varepsilon_{xx}-\varepsilon_{yy})^2 - 4\omega^2\mu\varepsilon_{yy}\varepsilon_{xz}^2(-\beta_z^2+\omega^2\mu\varepsilon_{yy})\}^{\frac{1}{2}}\right] \tag{3.32}$$

3.3 Dispersion Relation for Various Geometries

Next, the dispersion equation itself can be derived. The purpose of the dispersion equation is to give the electric and magnetic fields associated with the mode propagating in the film. To do this all that is needed is Faraday's law in differential form (equation (3.4)) and the vector wave equation in $\vec{E}$ (equation (3.11)):

$$\nabla\times\vec{E} = -\frac{\partial\vec{B}}{\partial t} \tag{3.33}$$

$$\nabla\times\nabla\times\vec{E}-\omega^2\mu\tilde{\varepsilon}\vec{E} = 0 \tag{3.34}$$

The full dielectric tensor is maintained in order to handle all applied magnetic field geometries. The form of the solution is given in equation (3.13) and rewritten here for the electric and magnetic field components:

$$\vec{E} = \vec{A}_E e^{j\omega t} e^{-\gamma_y y} e^{-\gamma_z z}, \gamma_x = 0 \tag{3.35}$$

where $\vec{A}_E$ is the coefficient vector, $\vec{A}_E = (E_x, E_y, E_z)$,

$$\vec{H} = \vec{A}_H e^{j\omega t} e^{-\gamma_y y} e^{-\gamma_z z}, \gamma_x = 0 \tag{3.36}$$

where $\vec{A}_H$ is the coefficient vector, $\vec{A}_H = (H_x, H_y, H_z)$.

Substituting the form of the solution into Faraday's law gives the following three equations:

$$\frac{\partial E_z}{\partial y} - \frac{\partial E_y}{\partial z} = -j\omega\mu H_x \tag{3.37}$$

$$\frac{\partial E_x}{\partial z} = -j\omega\mu H_y \tag{3.38}$$

$$\frac{\partial E_x}{\partial y} = j\omega\mu H_z \tag{3.39}$$

Substituting the form of the solution into the wave equation gives the following three equations:

$$-\frac{\partial^2 E_x}{\partial y^2} - \frac{\partial^2 E_x}{\partial z^2} = \omega^2\mu(\varepsilon_{xx}E_x + \varepsilon_{xy}E_y + \varepsilon_{xz}E_z) \tag{3.40}$$

$$\frac{\partial^2 E_z}{\partial y \partial z} - \frac{\partial^2 E_y}{\partial z^2} = \omega^2\mu(\varepsilon_{yx}E_x + \varepsilon_{yy}E_y + \varepsilon_{yz}E_z) \tag{3.41}$$

$$-\frac{\partial^2 E_z}{\partial y^2} - \frac{\partial^2 E_y}{\partial y \partial z} = \omega^2\mu(\varepsilon_{zx}E_x + \varepsilon_{zy}E_y + \varepsilon_{zz}E_z) \tag{3.42}$$

Because the solution has the spatial form $e^{-\gamma_z z}$, the derivatives in z become $\frac{\partial}{\partial z} = -\gamma_z$. Applying this form of the equation to all six equations, (3.37) to (3.42) yields the following:

$$\frac{\partial E_z}{\partial y} + \gamma_z E_y = -j\omega\mu H_x \tag{3.43}$$

$$-\gamma_z E_x = -j\omega\mu H_y \tag{3.44}$$

$$-\frac{\partial E_x}{\partial y} = -j\omega\mu H_z \tag{3.45}$$

$$-\frac{\partial^2 E_x}{\partial y^2} - \gamma_z^2 E_x = \omega^2\mu(\varepsilon_{xx}E_x + \varepsilon_{xy}E_y + \varepsilon_{xz}E_z) \tag{3.46}$$

$$-\gamma_z\frac{\partial E_z}{\partial y} - \gamma_z^2 E_y = \omega^2\mu(\varepsilon_{yx}E_x + \varepsilon_{yy}E_y + \varepsilon_{yz}E_z) \tag{3.47}$$

$$-\frac{\partial^2 E_z}{\partial y^2} - \gamma_z\frac{\partial E_y}{\delta y} = \omega^2\mu(\varepsilon_{zx}E_x + \varepsilon_{zy}E_y + \varepsilon_{zz}E_z) \tag{3.48}$$

3.3.1 Region I

In region I, the dielectric tensor becomes the dielectric constant of the upper cladding: $\tilde{\varepsilon} = \varepsilon_1$. If a guided mode is to be obtained then the wave must decay exponentially along y in the cladding, as shown in Figure 3.2. [42 Section 9.1] Therefore the solution is in the following form: $E^I(y) = E^I e^{-\gamma_{y1}y}$, where γ_{y1} is the propagation constant of region I which is the positive root of γ_{y1}^2, and E^I is a coefficient. An analogous solution can be written for the magnetic field.

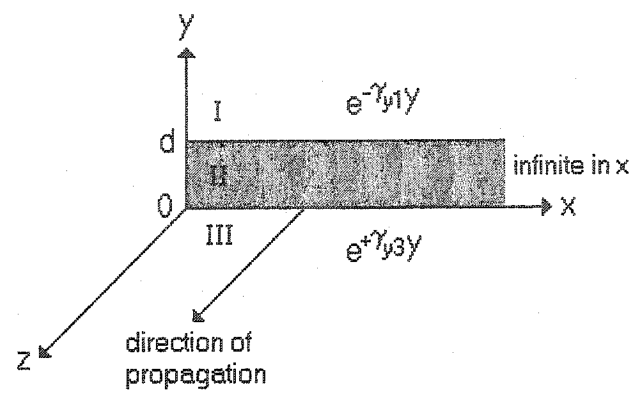

Figure 3.2 The form of the exponentially decaying fields in the cladding

Substituting this form of the solution into equations (3.43) to (3.48) gives the following:

$$-\gamma_{y1}E_z^I + \gamma_z E_y^I = -j\omega\mu H_x^I \tag{3.49}$$

$$-\gamma_z E_x^I = -j\omega\mu H_y^I \tag{3.50}$$

$$\gamma_{y1}E_x^I = -j\omega\mu H_z^I \tag{3.51}$$

$$-\gamma_{y1}^2 E_x^I - \gamma_z^2 E_x^I = \omega^2\mu\varepsilon_1 E_x^I \tag{3.52}$$

$$\gamma_z\gamma_{y1}E_z^I - \gamma_z^2 E_y^I = \omega^2\mu\varepsilon_1 E_y^I \tag{3.53}$$

$$-\gamma_{y1}^2 E_z^I + \gamma_z\gamma_{y1}E_y^I = \omega^2\mu\varepsilon_1 E_z^I \tag{3.54}$$

To reduce the number of unknowns, E_y^I, H_x^I and H_z^I will be written in terms of E_x^I and E_z^I.

From equation (3.54):

$$E_y^I = \frac{\gamma_{y1}^2 + \omega^2\mu\varepsilon_1}{\gamma_z\gamma_{y1}}E_z^I \tag{3.55}$$

Substitute equation (3.55) into equation (3.49):

$$H_x^I = \frac{j\omega\varepsilon_1}{\gamma_{y1}}E_z^I \tag{3.56}$$

From equation (3.51):

$$H_z^I = \frac{j\gamma_{y1}}{\omega\mu}E_x^I \tag{3.57}$$

3.3.2 Region III

In region III, the dielectric tensor becomes the dielectric constant of the lower cladding: $\tilde{\varepsilon} = \varepsilon_3$. The solution is in the form of an exponentially decaying wave, as in region I: $E^{III}(y) = E^{III}e^{\gamma_{y3}y}$, where γ_{y3} is the propagation constant of region III which is the positive root of γ_{y3}^2, and E^{III} is a coefficient. An analogous solution can be written for the magnetic field. Substituting this form of the equation into equations (3.43) to (3.48) gives the following:

$$\gamma_{y3}E_z^{III} + \gamma_z E_y^{III} = -j\omega\mu H_x^{III} \tag{3.58}$$

$$-\gamma_z E_x^{III} = -j\omega\mu H_y^{III} \tag{3.59}$$

$$-\gamma_{y3}E_x^{III} = -j\omega\mu H_z^{III} \tag{3.60}$$

$$-\gamma_{y3}^2 E_x^{III} - \gamma_z^2 E_x^{III} = \omega^2\mu\varepsilon_3 E_x^{III} \tag{3.61}$$

$$-\gamma_z\gamma_{y3}E_z^{III} - \gamma_z^2 E_y^{III} = \omega^2\mu\varepsilon_3 E_y^{III} \tag{3.62}$$

$$-\gamma_{y3}^2 E_z^{III} - \gamma_z\gamma_{y3}E_y^{III} = \omega^2\mu\varepsilon_3 E_z^{III} \tag{3.63}$$

To reduce the number of unknowns, E_y^{III}, H_x^{III} and H_z^{III} will be written in terms of E_x^{III} and E_z^{III}.

From equation (3.63):

$$E_y^{III} = \frac{-(\gamma_{y3}^2 + \omega^2\mu\varepsilon_3)}{\gamma_z\gamma_{y3}} E_z^{III} \tag{3.64}$$

Substitute equation (3.64) into equation (3.58):

$$H_x^{III} = \frac{-j\omega\varepsilon_3}{\gamma_{y3}} E_z^{III} \tag{3.65}$$

From equation (3.60):

$$H_z^{III} = \frac{-j\gamma_{y3}}{\omega\mu} E_x^{III} \tag{3.66}$$

3.3.3 Region II

In region II, the dielectric tensor remains in tensor form. A guided mode will have the form of a standing wave in the transverse direction in the core of the waveguide. Therefore, the solution is in the following standing wave form: $E(y) = e^{-\gamma_{y2p}y}E_1 + e^{\gamma_{y2p}y}E_2 + e^{-\gamma_{y2m}y}E_3 + e^{\gamma_{y2m}y}E_4$, where $\gamma_{y2p} = \sqrt{\gamma_{y2p}^2}$, where γ_{y2p}^2 is the solution to the constraint equation that has the form $A + \sqrt{B}$; $\gamma_{y2m} = \sqrt{\gamma_{y2m}^2}$, where γ_{y2m}^2 is the solution to the constraint equation that has the form $A - \sqrt{B}$; and E_1, E_2, E_3 and E_4 are the coefficients. An analogous solution can be written for the magnetic field.

Rewriting equations (3.43) to (3.48) for the $e^{-\gamma_{y2p}y}$ term of the solution gives the following:

$$-\gamma_{y2p}E_{1z} + \gamma_z E_{1y} = -j\omega\mu H_{1x} \tag{3.67}$$

$$-\gamma_z E_{1x} = -j\omega\mu H_{1y} \tag{3.68}$$

$$\gamma_{y2p}E_{1x} = -j\omega\mu H_{1z} \tag{3.69}$$

$$-\gamma_{y2p}^2 E_{1x} - \gamma_z^2 E_{1x} = \omega^2\mu(\varepsilon_{xx}E_{1x} + \varepsilon_{xy}E_{1y} + \varepsilon_{xz}E_{1z}) \tag{3.70}$$

$$\gamma_z\gamma_{y2p}E_{1z} - \gamma_z^2 E_{1y} = \omega^2\mu(\varepsilon_{yx}E_{1x} + \varepsilon_{yy}E_{1y} + \varepsilon_{yz}E_{1z}) \tag{3.71}$$

$$-\gamma_{y2p}^2 E_{1z} + \gamma_z \gamma_{y2p} E_{1y} = \omega^2 \mu(\varepsilon_{zx} E_{1x} + \varepsilon_{zy} E_{1y} + \varepsilon_{zz} E_{1z}) \quad (3.72)$$

Group the like terms in the last three equations:

$$(\gamma_{y2p}^2 + \gamma_z^2 + \omega^2 \mu \varepsilon_{xx}) E_{1x} + \omega^2 \mu \varepsilon_{xy} E_{1y} + \omega^2 \mu \varepsilon_{xz} E_{1z} = 0 \quad (3.73)$$

$$\omega^2 \mu \varepsilon_{yx} E_{1x} + (\omega^2 \mu \varepsilon_{yy} + \gamma_z^2) E_{1y} + (\omega^2 \mu \varepsilon_{yz} - \gamma_z \gamma_{y2p}) E_{1z} = 0 \quad (3.74)$$

$$\omega^2 \mu \varepsilon_{zx} E_{1x} + (\omega^2 \mu \varepsilon_{zy} - \gamma_z \gamma_{y2p}) E_{1y} + (\omega^2 \mu \varepsilon_{zz} + \gamma_{y2p}^2) E_{1z} = 0 \quad (3.75)$$

Write E_{1x} in terms of E_{1z}:

$$E_{1x} = \frac{-\omega^2 \mu[\varepsilon_{xy}(\omega^2 \mu \varepsilon_{zz} + \gamma_{y2p}^2) + \varepsilon_{xz}(\omega^2 \mu \varepsilon_{yz} + \gamma_z \gamma_{y2p})]}{(\omega^2 \mu \varepsilon_{yz} + \gamma_z \gamma_{y2p})(\gamma_{y2p}^2 + \gamma_z^2 + \omega^2 \mu \varepsilon_{xx}) - \omega^4 \mu^2 \varepsilon_{xy} \varepsilon_{xz}} E_{1z} \quad (3.76)$$

Write H_{1x} in terms of E_{1z}:

$$H_{1x} = \frac{j\omega[(\varepsilon_{zz}\gamma_z - \varepsilon_{yz}\gamma_{y2p})(\gamma_z^2 + \gamma_{y2p}^2 + \omega^2 \mu \varepsilon_{xx}) + \omega^2 \mu \varepsilon_{xz}(\varepsilon_{xy}\gamma_{y2p} + \varepsilon_{xz}\gamma_z)]}{(\omega^2 \mu \varepsilon_{yz} + \gamma_z \gamma_{y2p})(\gamma_z^2 + \gamma_{y2p}^2 + \omega^2 \mu \varepsilon_{xx}) - \omega^4 \mu^2 \varepsilon_{xy} \varepsilon_{xz}} E_{1z} \quad (3.77)$$

Write H_{1z} in terms of E_{1z}:

$$H_{1z} = \frac{-j\omega\gamma_{y2p}[\varepsilon_{xy}(\omega^2 \mu \varepsilon_{zz} + \gamma_{y2p}^2) + \varepsilon_{xz}(\omega^2 \mu \varepsilon_{yz} + \gamma_z \gamma_{y2p})]}{(\omega^2 \mu \varepsilon_{yz} + \gamma_z \gamma_{y2p})(\gamma_{y2p}^2 + \gamma_z^2 + \omega^2 \mu \varepsilon_{xx}) - \omega^4 \mu^2 \varepsilon_{xy} \varepsilon_{xz}} E_{1z} \quad (3.78)$$

In a similar manner, the other tangential components can also be written in terms of E_z for region II:

Coefficients of the $e^{\gamma_{y2p} y}$ terms:

$$E_{2x} = \frac{-\omega^2 \mu[\varepsilon_{xy}(\omega^2 \mu \varepsilon_{zz} + \gamma_{y2p}^2) + \varepsilon_{xz}(\omega^2 \mu \varepsilon_{yz} - \gamma_z \gamma_{y2p})]}{(\omega^2 \mu \varepsilon_{yz} - \gamma_z \gamma_{y2p})(\gamma_{y2p}^2 + \gamma_z^2 + \omega^2 \mu \varepsilon_{xx}) - \omega^4 \mu^2 \varepsilon_{xy} \varepsilon_{xz}} E_{2z} \quad (3.79)$$

$$H_{2x} = \frac{j\omega[(\varepsilon_{zz}\gamma_z + \varepsilon_{yz}\gamma_{y2p})(\gamma_z^2 + \gamma_{y2p}^2 + \omega^2 \mu \varepsilon_{xx}) + \omega^2 \mu \varepsilon_{xz}(\varepsilon_{xy}\gamma_z - \varepsilon_{xy}\gamma_{y2p})]}{(\omega^2 \mu \varepsilon_{yz} - \gamma_z \gamma_{y2p})(\gamma_z^2 + \gamma_{y2p}^2 + \omega^2 \mu \varepsilon_{xx}) - \omega^4 \mu^2 \varepsilon_{xy} \varepsilon_{xz}} E_{2z} \quad (3.80)$$

$$H_{2z} = \frac{j\omega\gamma_{y2p}[\varepsilon_{xy}(\omega^2\mu\varepsilon_{zz}+\gamma_{y2p}^2)+\varepsilon_{xz}(\omega^2\mu\varepsilon_{yz}-\gamma_z\gamma_{y2p})]}{(\omega^2\mu\varepsilon_{yz}-\gamma_z\gamma_{y2p})(\gamma_{y2p}^2+\gamma_z^2+\omega^2\mu\varepsilon_{xx})-\omega^4\mu^2\varepsilon_{xy}\varepsilon_{xz}}E_{2z} \tag{3.81}$$

Coefficients of the $e^{-\gamma_{y2m}y}$ terms:

$$E_{3x} = \frac{-\omega^2\mu[\varepsilon_{xy}(\omega^2\mu\varepsilon_{zz}+\gamma_{y2m}^2)+\varepsilon_{xz}(\omega^2\mu\varepsilon_{yz}+\gamma_z\gamma_{y2m})]}{(\omega^2\mu\varepsilon_{yz}+\gamma_z\gamma_{y2m})(\gamma_{y2m}^2+\gamma_z^2+\omega^2\mu\varepsilon_{xx})-\omega^4\mu^2\varepsilon_{xy}\varepsilon_{xz}}E_{3z} \tag{3.82}$$

$$H_{3x} = \frac{j\omega[(\varepsilon_{zz}\gamma_z-\varepsilon_{yz}\gamma_{y2m})(\gamma_z^2+\gamma_{y2m}^2+\omega^2\mu\varepsilon_{xx})+\omega^2\mu\varepsilon_{xz}(\varepsilon_{xy}\gamma_{y2m}+\varepsilon_{xz}\gamma_z)]}{(\omega^2\mu\varepsilon_{yz}+\gamma_z\gamma_{y2m})(\gamma_z^2+\gamma_{y2m}^2+\omega^2\mu\varepsilon_{xx})-\omega^4\mu^2\varepsilon_{xy}\varepsilon_{xz}}E_{1z} \tag{3.83}$$

$$H_{3z} = \frac{-j\omega\gamma_{ymp}[\varepsilon_{xy}(\omega^2\mu\varepsilon_{zz}+\gamma_{y2m}^2)+\varepsilon_{xz}(\omega^2\mu\varepsilon_{yz}+\gamma_z\gamma_{y2m})]}{(\omega^2\mu\varepsilon_{yz}+\gamma_z\gamma_{y2m})(\gamma_{y2m}^2+\gamma_z^2+\omega^2\mu\varepsilon_{xx})-\omega^4\mu^2\varepsilon_{xy}\varepsilon_{xz}}E_{3z} \tag{3.84}$$

Coefficients of the $e^{\gamma_{y2m}y}$ terms:

$$E_{4x} = \frac{-\omega^2\mu[\varepsilon_{xy}(\omega^2\mu\varepsilon_{zz}+\gamma_{y2m}^2)+\varepsilon_{xz}(\omega^2\mu\varepsilon_{yz}-\gamma_z\gamma_{y2m})]}{(\omega^2\mu\varepsilon_{yz}-\gamma_z\gamma_{y2m})(\gamma_{y2m}^2+\gamma_z^2+\omega^2\mu\varepsilon_{xx})-\omega^4\mu^2\varepsilon_{xy}\varepsilon_{xz}}E_{4z} \tag{3.85}$$

$$H_{4x} = \frac{j\omega[(\varepsilon_{zz}\gamma_z+\varepsilon_{yz}\gamma_{y2m})(\gamma_z^2+\gamma_{y2m}^2+\omega^2\mu\varepsilon_{xx})+\omega^2\mu\varepsilon_{xz}(\varepsilon_{xy}\gamma_z-\varepsilon_{xy}\gamma_{y2m})]}{(\omega^2\mu\varepsilon_{yz}-\gamma_z\gamma_{y2m})(\gamma_z^2+\gamma_{y2m}^2+\omega^2\mu\varepsilon_{xx})-\omega^4\mu^2\varepsilon_{xy}\varepsilon_{xz}}E_{4z} \tag{3.86}$$

$$H_{4z} = \frac{j\omega\gamma_{y2m}[\varepsilon_{xy}(\omega^2\mu\varepsilon_{zz}+\gamma_{y2m}^2)+\varepsilon_{xz}(\omega^2\mu\varepsilon_{yz}-\gamma_z\gamma_{y2m})]}{(\omega^2\mu\varepsilon_{yz}-\gamma_z\gamma_{y2m})(\gamma_{y2m}^2+\gamma_z^2+\omega^2\mu\varepsilon_{xx})-\omega^4\mu^2\varepsilon_{xy}\varepsilon_{xz}}E_{4z} \tag{3.87}$$

The three equations for region I, (3.55) to (3.57), have 5 unknown field coefficients. The three equations for region III, (3.64) to (3.66), also have 5 unknown field coefficients. The twelve equations for region II, (3.76) to (3.87), have 16 unknown field coefficients. In order to solve these equations for the dispersion relation, the boundary conditions at the interfaces must be enforced.

3.3.4 Matching the Tangential Field Components

A sufficient set of boundary conditions can be obtained by matching the tangential fields on either side of both interfaces ($y = 0$ and $y = d$). The boundary conditions for the tangential field components at a dielectric interface (no sources or surface currents) have been determined from Maxwell's equations and are required to be continuous across the boundary [42 Section 1.10].

The form of the solution for the electric field is shown in Figure 3.3 in terms of the unknown field coefficients and the directional propagation constants. The form of the solution for the magnetic field is equivalent to the form of the solution for the electric field shown in Figure 3.3. Each of the field coefficients shown in Figure 3.3 have x, y and z components. The tangential field components can be matched by substituting the value of y at the interface, either 0 or d, into the equations that represent the tangential field components (x and z coefficients) on either side and equating the two equations.

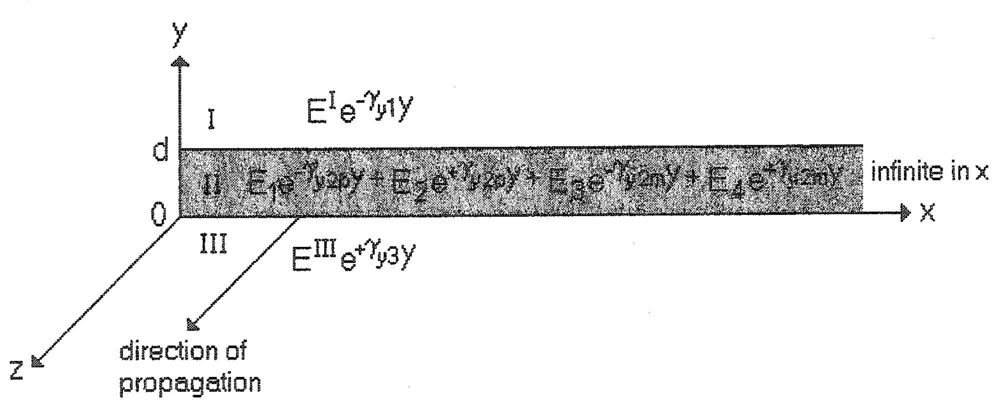

Figure 3.3 Equations that correspond to all three regions of the slab waveguide

Matching the tangential field components at the $y = 0$ boundary yields the following:

$$E_x^{III} = E_{1x} + E_{2x} + E_{3x} + E_{4x} \tag{3.88}$$

$$E_z^{III} = E_{1z} + E_{2z} + E_{3z} + E_{4z} \tag{3.89}$$

$$H_x^{III} = H_{1x} + H_{2x} + H_{3x} + H_{4x} \tag{3.90}$$

$$H_z^{III} = H_{1z} + H_{2z} + H_{3z} + H_{4z} \tag{3.91}$$

Substituting equations (3.76), (3.79), (3.82) and (3.85) into equation (3.88) gives the following:

$$\begin{aligned} E_x^{III} = -\omega^2\mu\Big[&\frac{A_p + \varepsilon_{xz}B_{p1}}{B_{p1}T_p - R}E_{1z} + \frac{A_p + \varepsilon_{xz}B_{p2}}{B_{p2}T_p - R}E_{2z} \\ &+ \frac{A_m + \varepsilon_{xz}B_{m1}}{B_{m1}T_m - R}E_{3z} + \frac{A_m + \varepsilon_{xz}B_{m2}}{B_{m2}T_m - R}E_{4z}\Big] \end{aligned} \tag{3.92}$$

where
$$\begin{aligned} A_p &= \varepsilon_{xy}(\omega^2\mu\varepsilon_{zz} + \gamma_{y2p}^2) \\ A_m &= \varepsilon_{xy}(\omega^2\mu\varepsilon_{zz} + \gamma_{y2m}^2) \\ B_{p1} &= \omega^2\mu\varepsilon_{yz} + \gamma_z\gamma_{y2p} \\ B_{p2} &= \omega^2\mu\varepsilon_{yz} - \gamma_z\gamma_{y2p} \\ B_{m1} &= \omega^2\mu\varepsilon_{yz} + \gamma_z\gamma_{y2m} \\ B_{m1} &= \omega^2\mu\varepsilon_{yz} - \gamma_z\gamma_{y2m} \\ T_p &= \gamma_{y2p}^2 + \gamma_z^2 + \omega^2\mu\varepsilon_{xx} \\ T_m &= \gamma_{y2m}^2 + \gamma_z^2 + \omega^2\mu\varepsilon_{xx} \\ R &= \omega^4\mu^2\varepsilon_{xy}\varepsilon_{xz} \end{aligned}$$

Substituting equations (3.65), (3.77), (3.80), (3.83) and (3.86) into equation (3.90) and dividing by $j\omega$ gives the following

$$\begin{aligned} \frac{-\varepsilon_3}{\gamma_{y3}}E_z^{III} = &\frac{[Q_{p1}T_p + S_{p1}]}{B_{p1}T_p - R}E_{1z} + \frac{[Q_{p2}T_p + S_{p2}]}{B_{p2}T_p - R}E_{2z} \\ &+ \frac{[Q_{m1}T_m + S_{m1}]}{B_{m1}T_m - R}E_{3z} + \frac{[Q_{m2}T_m + S_{m2}]}{B_{m2}T_m - R}E_{4z} \end{aligned} \tag{3.93}$$

where $Q_{p1} = \varepsilon_{zz}\gamma_z - \varepsilon_{yz}\gamma_{y2p}$

$$Q_{p2} = \varepsilon_{zz}\gamma_z + \varepsilon_{yz}\gamma_{y2p}$$
$$Q_{m1} = \varepsilon_{zz}\gamma_z - \varepsilon_{yz}\gamma_{y2m}$$
$$Q_{m2} = \varepsilon_{zz}\gamma_z + \varepsilon_{yz}\gamma_{y2m}$$
$$S_{p1} = \omega^2\mu\varepsilon_{xz}(\varepsilon_{xz}\gamma_z + \varepsilon_{xy}\gamma_{y2p})$$
$$S_{p2} = \omega^2\mu\varepsilon_{xz}(\varepsilon_{xz}\gamma_z - \varepsilon_{xy}\gamma_{y2p})$$
$$S_{m1} = \omega^2\mu\varepsilon_{xz}(\varepsilon_{xz}\gamma_z + \varepsilon_{xy}\gamma_{y2m})$$
$$S_{m2} = \omega^2\mu\varepsilon_{xz}(\varepsilon_{xz}\gamma_z - \varepsilon_{xy}\gamma_{y2m})$$

Substituting equations (3.66), (3.78), (3.81), (3.84) and (3.87) into equation (3.91) and dividing by $j\omega$ gives the following

$$\frac{-\gamma_{y3}}{\omega^2\mu}E_x^{III} = -\frac{\gamma_{y2p}[A_p + \varepsilon_{xz}B_{p1}]}{B_{p1}T_p - R}E_{1z} + \frac{\gamma_{y2p}[A_p + \varepsilon_{xz}B_{p2}]}{B_{p2}T_p - R}E_{2z} + \frac{\gamma_{y2m}[A_m + \varepsilon_{xz}B_{m1}]}{B_{m1}T_m - R}E_{3z} - \frac{\gamma_{y2m}[A_m + \varepsilon_{xz}B_{m2}]}{B_{m2}T_m - R}E_{4z} \tag{3.94}$$

Matching the tangential field components at the $y = d$ boundary yields the following:

$$e^{-\gamma_{y1}d}E_x^I = e^{-\gamma_{y2p}d}E_{1x} + e^{\gamma_{y2p}d}E_{2x} + e^{-\gamma_{y2m}d}E_{3x} + e^{\gamma_{y2m}d}E_{4x} \tag{3.95}$$

$$e^{-\gamma_{y1}d}E_z^I = e^{-\gamma_{y2p}d}E_{1z} + e^{\gamma_{y2p}d}E_{2z} + e^{-\gamma_{y2m}d}E_{3z} + e^{\gamma_{y2m}d}E_{4z} \tag{3.96}$$

$$e^{-\gamma_{y1}d}H_x^I = e^{-\gamma_{y2p}d}H_{1x} + e^{\gamma_{y2p}d}H_{2x} + e^{-\gamma_{y2m}d}H_{3x} + e^{\gamma_{y2m}d}H_{4x} \tag{3.97}$$

$$e^{-\gamma_{y1}d}H_z^I = e^{-\gamma_{y2p}d}H_{1z} + e^{\gamma_{y2p}d}H_{2z} + e^{-\gamma_{y2m}d}H_{3z} + e^{\gamma_{y2m}d}H_{4z} \tag{3.98}$$

Substituting equations (3.76), (3.79), (3.82) and (3.85) into equation (3.95) gives the following:

$$e^{-\gamma_{y1}d}E_x^I = -\omega^2\mu\left[\frac{A_p + \varepsilon_{xz}B_{p1}}{B_{p1}T_p - R}e^{-\gamma_{y2p}d}E_{1z} + \frac{A_p + \varepsilon_{xz}B_{p2}}{B_{p2}T_p - R}e^{\gamma_{y2p}d}E_{2z} + \frac{A_m + \varepsilon_{xz}B_{m1}}{B_{m1}T_m - R}e^{-\gamma_{y2m}d}E_{3z} + \frac{A_m + \varepsilon_{xz}B_{m2}}{B_{m2}T_m - R}e^{\gamma_{y2m}d}E_{4z}\right] \tag{3.99}$$

Substituting equations (3.65), (3.77), (3.80), (3.83) and (3.86) into equation (3.97) and dividing by $j\omega$ gives the following:

$$\begin{aligned}\frac{\varepsilon_1}{\gamma_{y1}}E_z^I = {} & \frac{[Q_{p1}T_p + S_{p1}]}{B_{p1}T_p - R}e^{-\gamma_{y2p}d}E_{1z} + \frac{[Q_{p2}T_p + S_{p2}]}{B_{p2}T_p - R}e^{\gamma_{y2p}d}E_{2z} \\ & + \frac{[Q_{m1}T_m + S_{m1}]}{B_{m1}T_m - R}e^{-\gamma_{y2m}d}E_{3z} + \frac{[Q_{m2}T_m + S_{m2}]}{B_{m2}T_m - R}e^{\gamma_{y2m}d}E_{4z}\end{aligned} \tag{3.100}$$

Substituting equations (3.66), (3.78), (3.81), (3.84) and (3.87) into equation (3.98) and dividing by $j\omega$ gives the following:

$$\begin{aligned}\frac{\gamma_{y1}}{\omega^2\mu}E_x^I = {} & -\frac{\gamma_{y2p}[A_p + \varepsilon_{xz}B_{p1}]}{B_{p1}T_p - R}e^{-\gamma_{y2p}d}E_{1z} + \frac{\gamma_{y2p}[A_p + \varepsilon_{xz}B_{p2}]}{B_{p2}T_p - R}e^{\gamma_{y2p}d}E_{2z} \\ & + \frac{\gamma_{y2m}[A_m + \varepsilon_{xz}B_{m1}]}{B_{m1}T_m - R}e^{-\gamma_{y2m}d}E_{3z} - \frac{\gamma_{y2m}[A_m + \varepsilon_{xz}B_{m2}]}{B_{m2}T_m - R}e^{\gamma_{y2m}d}E_{4z}\end{aligned} \tag{3.101}$$

Equations (3.89), (3.92), (3.93), (3.94), (3.96), (3.99), (3.100) and (3.101) form a set of eight equations with eight unknowns. This is system is the dispersion relation:

$$\begin{bmatrix} 0 & 0 & 0 & -1 & 1 & 1 & 1 & 1 \\ 0 & 1 & 0 & 0 & \omega^2\mu A1 & \omega^2\mu A2 & \omega^2\mu A3 & \omega^2\mu A4 \\ 0 & 0 & 0 & \frac{\varepsilon_3}{\gamma_{y3}} & Q1 & Q2 & Q3 & Q4 \\ 0 & \frac{\gamma_{y3}}{\omega^2\mu} & 0 & 0 & -\gamma_{y2p}A1 & \gamma_{y2p}A2 & \gamma_{y2m}A3 & -\gamma_{y2m}A4 \\ 0 & 0 & -e^{-\gamma_{y1}d} & 0 & e^{-\gamma_{y2p}d} & e^{\gamma_{y2p}d} & e^{-\gamma_{y2m}d} & e^{\gamma_{y2m}d} \\ e^{-\gamma_{y1}d} & 0 & 0 & 0 & \omega^2\mu A1e^{-\gamma_{y2p}d} & \omega^2\mu A2e^{\gamma_{y2p}d} & \omega^2\mu A3e^{-\gamma_{y2m}d} & \omega^2\mu A4e^{\gamma_{y2m}d} \\ 0 & 0 & -\frac{\varepsilon_1}{\gamma_{y1}} & 0 & Q1e^{-\gamma_{y2p}d} & Q2e^{\gamma_{y2p}d} & Q3e^{-\gamma_{y2m}d} & Q4e^{\gamma_{y2m}d} \\ -\frac{\gamma_{y1}}{\omega^2\mu} & 0 & 0 & 0 & -\gamma_{y2p}A1e^{-\gamma_{y2p}d} & \gamma_{y2p}A2e^{\gamma_{y2p}d} & \gamma_{y2m}A3e^{-\gamma_{y2m}d} & -\gamma_{y2m}A4e^{\gamma_{y2m}d} \end{bmatrix} \begin{bmatrix} E_x^I \\ E_x^{III} \\ E_z^I \\ E_z^{III} \\ E_{1z} \\ E_{2z} \\ E_{3z} \\ E_{4z} \end{bmatrix} = 0 \tag{3.102}$$

where

$$A1 = \frac{A_p + \varepsilon_{xz}B_{p1}}{B_{p1}T_p - R} \quad A2 = \frac{A_p + \varepsilon_{xz}B_{p2}}{B_{p2}T_p - R}, \quad A3 = \frac{A_m + \varepsilon_{xz}B_{m1}}{B_{m1}T_m - R}, \quad A4 = \frac{A_m + \varepsilon_{xz}B_{m2}}{B_{m2}T_m - R},$$

$$Q1 = \frac{Q_{p1}T_p + S_{p1}}{B_{p1}T_p - R}, \qquad Q2 = \frac{Q_{p2}T_p + S_{p2}}{B_{p2}T_p - R}, \qquad Q3 = \frac{Q_{m1}T_m + S_{m1}}{B_{m1}T_m - R} \qquad \text{and}$$

$$Q4 = \frac{Q_{m2}T_m + S_{m2}}{B_{m2}T_m - R}.$$

3.4 Conclusion

The general dispersion relation derived above can be used to analytically solve for the modes supported by infinitely wide thin metal or highly doped semiconductor films under the influence of an exterally applied magnetic field in the x-direction, y-direction or z-direction. In the literature, the specific dispersion relations for an externally applied magnetic field along these three directions (x, y, z) were derived by Halevi and Kushwaha [27, 28 and 29] for an infinitely wide thin film without any losses. It should be noted that in the literature, Halevi and Kushwaha [27, 28 and 29] simplify their dispersion relation equations in a similar manner to that shown above. However, they make an error while simplifying that shows up when the x-y off-diagonal elements of the permittivity tensor are null, $\varepsilon_{xy}=\varepsilon_{yx}=0$, which is the case for the perpendicular and Voigt configurations. Here their relation has been extended to the general case and losses are included and the simplification error has been corrected.

4. Model for Magneto-plasmons in Thin Metal Films

4.1 Numerical Model

The modes supported by an infinitely wide thin metal film bounded by dielectrics under the influence of an externally applied magnetic field can be found by solving the dispersion equation in conjunction with the constraint equation, as derived in the previous chapter. The constraint equation gives the relationship between the directional propagation constants: γ_x, γ_y, γ_z. In the case of a slab waveguide, which is infinite in the x-direction, according to the geometry used in the previous chapters, the propagation constant along x, γ_x, is zero. Therefore, the constraint equation defines the propagation constant for the mode, γ_z, in terms of the transverse decay constant or propagation constant in y, γ_y, or vice-versa. The dispersion equation is a set of eight equations with ten unknowns, which generates a homogeneous matrix problem of the following form:

$$[A]\vec{E} = 0 \tag{4.1}$$

where $\vec{E}$ represents the eight unknown field components and $[A]$ represents the homogeneous matrix of the coefficients of the eight unknowns which are combinations of the permittivity tensor and the directional propagation constants, as can be seen in equation (3.102). Given that the constraint equation defines the propagation constant for the mode (γ_z) in terms of the transverse decay constant (γ_y), the propagation constant for the mode (γ_z) is the only unknown and can be found by forcing the determinant of the matrix to zero.

A code was written to find the modes supported by a thin metal film bounded by dielectrics under the influence of an externally applied magnetic field. Given an initial guess for the propagation constant of the mode (γ_z), the corresponding transverse decay constant (γ_y) values are found from the roots of the constraint equation. Next, these directional propagation constants are substituted into the homogeneous matrix of the dispersion equation and its determinant is found. Muller's method [43] is used to interatively find the propagation constant values for the mode (γ_z) for which the determinant of the dispersion equation is zero.

Once the propagation constant for the mode of interest has been found, it can be back substituted into the dispersion relation, equations (3.89), (3.92), (3.94), (3.96), (3.99), (3.100) and (3.101), to get the x and z directed electric field components in regions I and III, and the z directed electric field components in region II. These field components along with the propagation constant can then be substituted into the equations indicated in Table 4.1 to get the corresponding field components.

Table 4.1 Equations and corresponding field components

Equation	Field Component
(3.50)	H_y^I
(3.55)	E_y^I
(3.56)	H_x^I
(3.57)	H_z^I
(3.59)	H_y^{III}
(3.64)	E_y^{III}
(3.65)	H_x^{III}
(3.66)	H_z^{III}
(3.67) to (3.72)	E_x, E_y and H in II

Before proceeding with the simulation results obtained from the code for the structures of interest it is important to compare the simulation results obtained from this code with results presented in the literature, thus validating the code for use in subsequent simulations.

4.2 Validation of Model with no Externally Applied Magnetic Field

The first comparison of simulated results with results in the literature is for the modes supported by an infinitely wide thin metal film bounded by dielectrics without an externally applied magnetic field. Charbonneau [44] studied this case for an infinitely wide thin gold film bounded by semi-infinite silicon dioxide. His results along with the results from simulations performed with the code described at the beginning of this chapter are shown in Figure 4.1 and Figure 4.2. These results are the simulated dispersion curves of a thin gold film, with a refractive index of N_{Au}=0.555-j10.66, bounded by semi-infinite silicon dioxide with a refractive index of N_{SiO_2}=1.44402, at a free space wavelength of 1550nm. The refractive index ($N = n - jk$) can be easily converted to the relative permittivity using the following equation:

$$\tilde{\varepsilon}_r = N^2 = n^2 - k^2 - j2nk \tag{4.2}$$

The simulation results in Figure 4.1 are for the normalized attenuation constant as a function of the thickness of the metal film, and the simulation results in Figure 4.2 are for the normalized phase constant as a function of the thickness of the metal film. The propagation constant, γ_z, can be written in terms of its real and imaginary parts, α_z and β_z, respectively:

$$\gamma_z = \alpha_z + j\beta_z \tag{4.3}$$

The real part of the propagation constant is the attenuation constant and the imaginary part of the propagation constant is the phase constant. The attenuation constant and the phase constant are normalized in Figure 4.1 and Figure 4.2 by dividing by the free space wave constant, β_0:

$$\beta_0 = \frac{2\pi}{\lambda_0} \tag{4.4}$$

where λ_0 is the free space wavelength. The ratio, α_z/β_0, gives the imaginary part of the index of refraction.

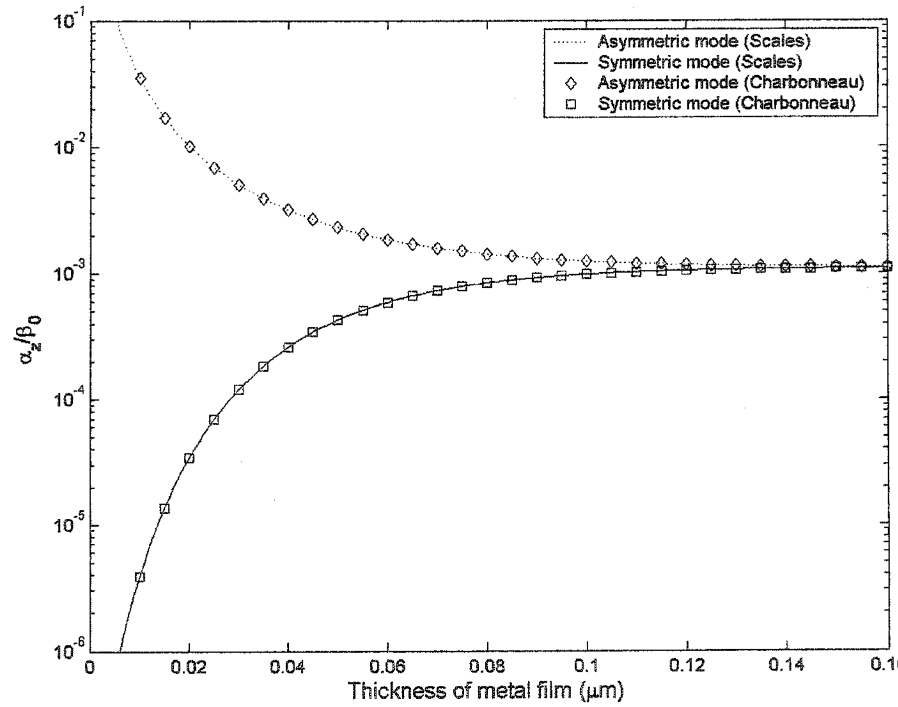

Figure 4.1 Comparison of simulated dispersion curves for the normalized attenuation constant of two bound modes supported by a thin Au film bounded by semi-infinite SiO_2, at free space wavelength of 1550nm, obtained from the code described in this chapter and from reference [44]. The indices of refraction are N_{Au}=0.555-j10.66 and N_{SiO_2}=1.44402 for gold and silicon dioxide, respectively.

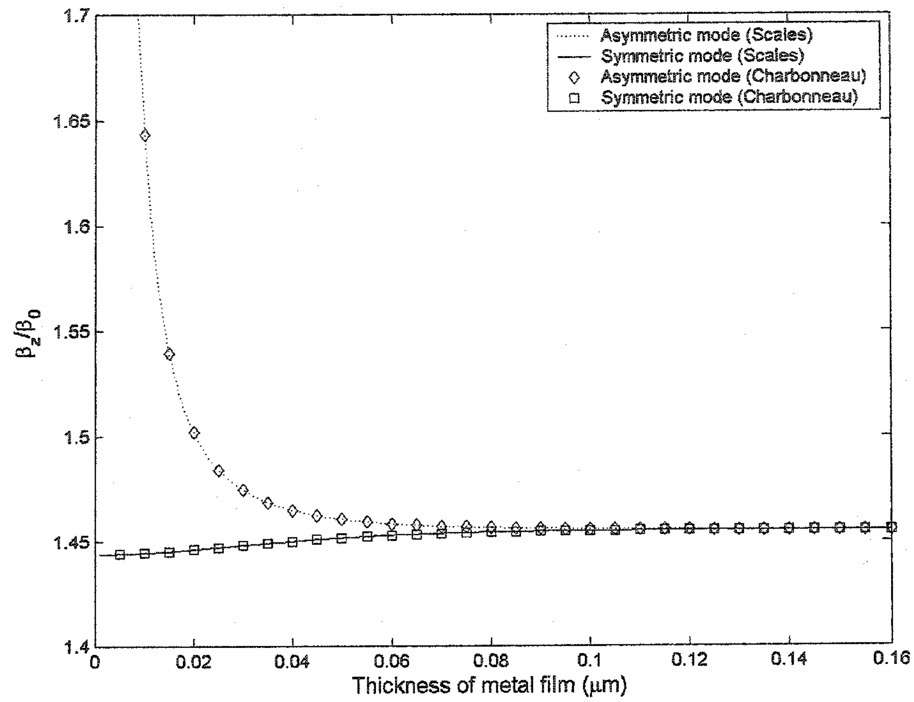

Figure 4.2 Comparison of simulated dispersion curves for the normalized phase constant of two bound modes supported by a thin Au film bounded by semi-infinite SiO_2, at free space wavelength of 1550nm, obtained from the code described in this chapter and from reference [44]. The indices of refraction are N_{Au}=0.555-j10.66 and N_{SiO_2}=1.44402 for gold and silicon dioxide, respectively.

It can be seen that, in both the symmetric and asymmetric cases, the attenuation constants and the propagation constants from simulations performed with the code described at the beginning of this chapter are in good agreement with the results presented in the literature [44]. Therefore, the model presented at the beginning of this chapter is valid in the case where no external magnetic field is applied.

The modes supported by an infinitely wide thin metal film bounded by dielectrics without an externally applied magnetic field will be explored in more detail in the Chapter 5.

4.3 Validation of Model with an Externally Applied Magnetic Field

Next, it is important to compare simulated results with results in the literature for the modes supported by a thin metal film bounded by semi-infinite dielectric when an external magnetic field is applied. M. S. Kushwaha and P. Halevi studied this case for a very thin unsupported film corresponding to highly doped InSb bounded by air with an external magnetic field applied in the Faraday [27], Voigt [28] and perpendicular [29] configurations. Their results along with the results from simulations performed with the code described at the beginning of this chapter are shown in Figure 4.3 for the Faraday orientation, in Figure 4.18 for the Voigt orientation, and in Figure 4.29 for the perpendicular orientation. These results are the simulated dispersion curves of a thin InSb film in air where the relative permittivity of air is unity and the relative permittivity of the thin InSb film has the following tensor form in the Faraday configuration:

$$\tilde{\varepsilon}_r = \begin{bmatrix} \varepsilon_L + \dfrac{\omega_0^2}{(\omega_g^2 - \omega^2)} & \dfrac{-j\omega_0^2\omega_g}{\omega(\omega_g^2 - \omega^2)} & 0 \\ \dfrac{j\omega_0^2\omega_g}{\omega(\omega_g^2 - \omega^2)} & \varepsilon_L + \dfrac{\omega_0^2}{(\omega_g^2 - \omega^2)} & 0 \\ 0 & 0 & \varepsilon_L - \dfrac{\omega_0^2}{\omega^2} \end{bmatrix} \tag{4.5}$$

where ω_0 is the plasma frequency as defined in equation (2.30), ω_g is the cyclotron frequency as defined in equation (2.19), ω is the angular frequency, and ε_L is the background dielectric constant of the film and is equal to 15.7. If the relative permittivity of the thin InSb film in equation (4.5) is compared with the permittivity tensor in equation (2.35) for a polarizable medium with an external magnetic field in the Faraday direction, it can be seen that it is similar but the losses have been neglected here, $\nu = 0$, and the background dielectric constant is no longer unity, which is the usual case, but is equal to

ε_L. The relative permittivity of the thin InSb film for the other two orientations of magnetic field, Voigt and perpendicular, is the same as the tensor for the Faraday case, except the elements are positioned differently, in the same manner as in equations (2.41) and (2.42), respectively. In order to be consistent with Kushwaha and Halevi, the thickness of the film is set to $2\,\mu\text{m}$ in all three configurations. However, it should not be expected that the results are invariant with thickness. The plasma frequency has the following value:

$$\omega_0 = \frac{0.02\pi c}{d} \tag{4.6}$$

where c is the speed of light in a vacuum and d is the thickness of the film. In the Faraday configuration, the cyclotron frequency is set to the plasma frequency: $\omega_g = \omega_0$. In the Voigt configuration, the cyclotron frequency is set to half the plasma frequency: $\omega_g = \frac{1}{2}\omega_0$. In the perpendicular configuration, the cyclotron frequency is set to half the plasma frequency divided by the square root of the background dielectric constant of the film medium: $\omega_g = \frac{1}{2}\frac{\omega_0}{\sqrt{\varepsilon_L}}$. The externally applied magnetic fields in each case can be calculated with equation (2.19) with the elementary charge being equal to $1.60\text{x}10^{-19}$C and the electron mass being equal to $9.11\text{x}10^{-31}$kg. The external magnetic field applied in the Faraday configuration is approximately 54 Tesla. The external magnetic field applied in the Voigt configuration is approximately 27 Tesla. The external magnetic field applied in the perpendicular configuration is approximately 7 Tesla.

The dispersion curves for all three orientations have been found with the code described at the beginning of this chapter over the frequencies used by Kushwaha and Halevi. They have been plotted in Figure 4.3, Figure 4.18 and Figure 4.29, using the same axes as were used in the literature [27, 28 and 29]. Every branch has been explored meticulously to the best of the limitations of the modelling code. Different and additional branches have been found above those found in the literature, as will be seen in the next three sections.

4.3.1 External Magnetic Field in Faraday Configuration

The simulated dispersion curves for the normalized frequency, ω/ω_0, versus normalized propagation constant, $\gamma_z c/\omega_0$, for a very thin unsupported semiconducting film with an external magnetic field in the Faraday configuration obtained from the code described in this chapter and from reference [27] are plotted in Figure 4.3. It can be seen from Figure 4.3 that the simulated results obtained from the code described in this chapter are in good agreement with those obtained in the literature with the exception of an extra branch in the results obtained from the code described in this chapter.

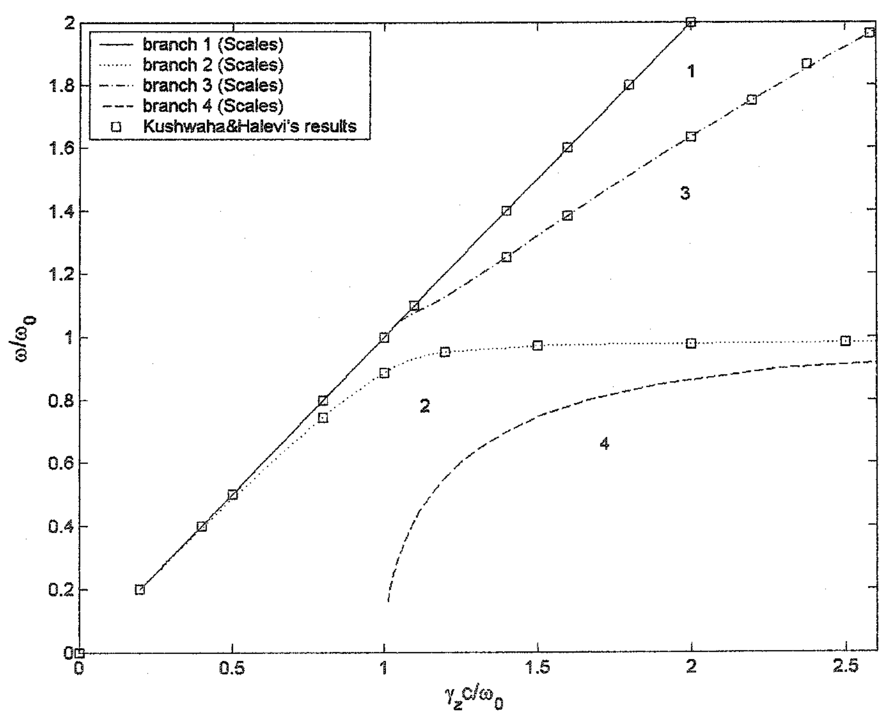

Figure 4.3 Comparison of simulated dispersion curves for the normalized frequency, ω/ω_0 versus normalized propagation constant $\gamma_z c/\omega_0$ for a very thin unsupported semiconducting film with an external magnetic field in the Faraday configuration, obtained from the code described in this chapter and from reference [27]

The relative permittivity tensor components for the InSb slab as a function of normalized frequency over the range that was examined in the literature for the Faraday orientation is shown in Figure 4.4. In this orientation the cyclotron frequency is set equal to the plasma frequency: $\omega_g = \omega_0$. When the angular frequency is also equal to the plasma frequency, $\omega/\omega_0 = 1$, the denominators of all of the non-zero tensor components, except for ε_{zz}, become zero and therefore the components themselves become infinite. It can be seen in Figure 4.4 that the tensor components with a resonance at $\omega/\omega_0 = 1$, tend asymptotically towards positive infinity as the resonance is approached from below and tend asymptotically towards negative infinity as the resonance is approached from above. The diagonal tensor components ε_{xx} and ε_{yy} are negative for $1 < \omega/\omega_0 < 1.0317$ and the diagonal tensor component ε_{zz} is negative for $\omega/\omega_0 < 0.2525$. The diagonal tensor components are positive for the other frequencies.

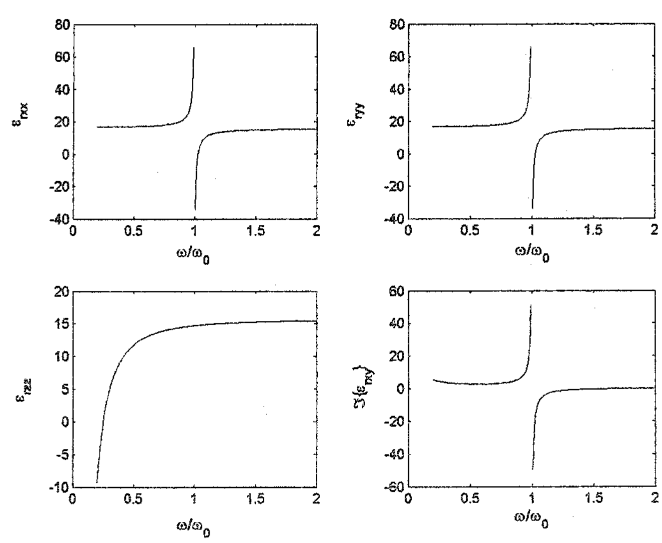

Figure 4.4 The relative permittivity tensor components for the InSb slab as a function of normalized frequency, ω/ω_0, over the range that was examined in the literature for the Faraday orientation of externally applied magnetic field

From Figure 4.3, it can be noted that two of the branches (2 and 4) of the dispersion curve tend asymptotically towards positive infinity as they approach the point $\omega/\omega_0 = 1$. When the angular frequency is greater than the plasma frequency, another branch (3) begins to appear in the dispersion curve.

In order to get a better understanding of the nature of the modes in these dispersion curve branches, the fields have been plotted at a specific point on each branch. The orientation of the film and the direction of wave propagation in cartesian coordinates are shown in Figure 4.5. Notice that the film thickness is from y=0 to y=d, where d is 2μm in this case. The field components and Poynting vectors are plotted along the y-axis in the following figures.

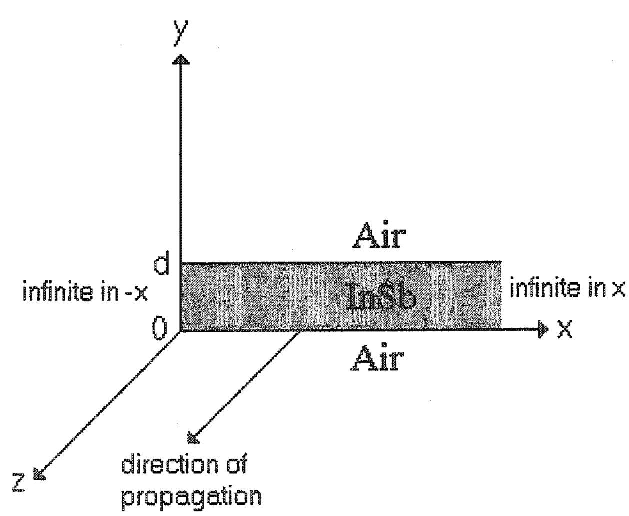

Figure 4.5 Orientation of the unsupported InSb film and direction of wave propagation in cartesian coordinates

Along with the field components, the Poynting vector is also plotted. The real part of the Poynting vector represents power flow while the imaginary part represents stored energy. The time averaged Poynting vector, which represents power flow, is calculated with the following equation:

$$\vec{S} = \frac{1}{2}\Re(\vec{E} \times \vec{H}^*) \tag{4.7}$$

Equation (4.7) can be written in terms of its three rectangular components as follows:

$$S_x = \frac{1}{2}\Re(E_y \times H_z^* - E_z \times H_y^*) \tag{4.8}$$

$$S_y = -\frac{1}{2}\Re(E_x \times H_z^* - E_z \times H_x^*) \tag{4.9}$$

$$S_z = \frac{1}{2}\Re(E_x \times H_y^* - E_y \times H_x^*) \tag{4.10}$$

The fields for the mode in branch 1 are plotted at $\omega/\omega_0 = 1.5$. They are shown in Figure 4.6 and Figure 4.7, and the Poynting vector is shown in Figure 4.8. The field component with the largest magnitude is the major field component. The primary fields, in Figure 4.6, are the fields, along with the major field component, that define a TE or TM mode. The InSb film is between y = 0 and y = 2 μm. It can be seen that mode in branch 1 is mainly transverse magnetic in nature since E_y is the major field component. All six field components exist, therefore, the mode is not purely TM. It can also be seen that the major field component is almost symmetric, therefore it can be said that the mode is a slightly perturbed symmetric mode. This is a symmetric plasmon-polariton mode that is perturbed by an externally applied magnetic field.

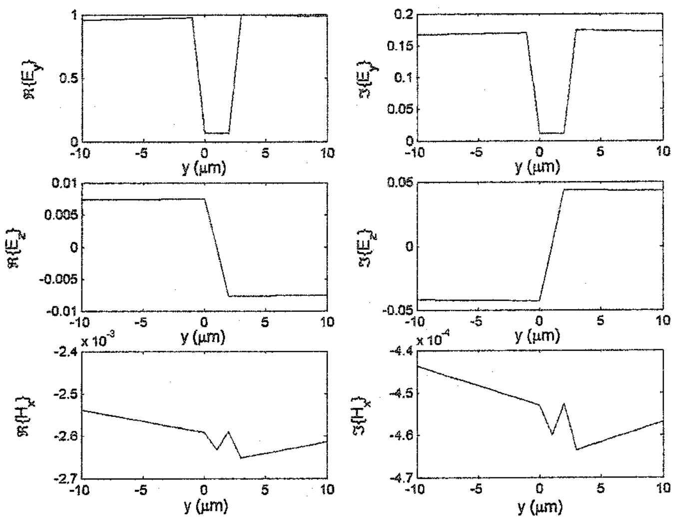

Figure 4.6 The primary field components (E_y, E_z, H_x) for branch 1 of the simulated dispersion curves for a very thin unsupported semiconducting film with an external magnetic field in the Faraday configuration, at $\omega/\omega_0=1.5$.

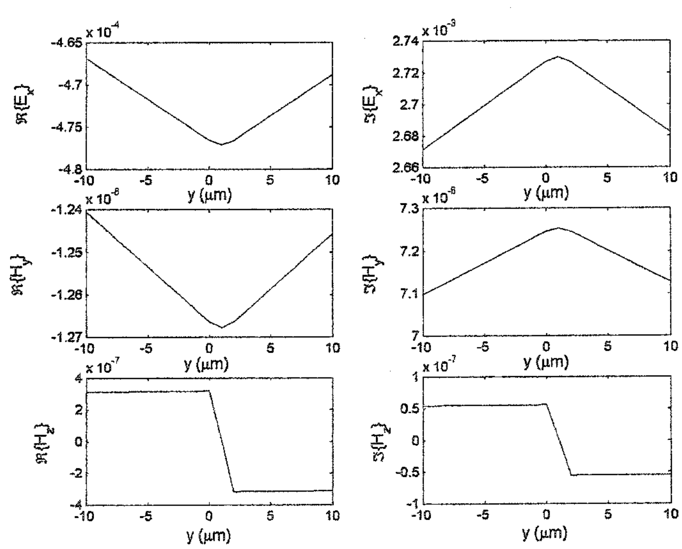

Figure 4.7 The secondary field components (E_x, H_y, H_z) for branch 1 of the simulated dispersion curves for a very thin unsupported semiconducting film with an external magnetic field in the Faraday configuration, at $\omega/\omega_0=1.5$.

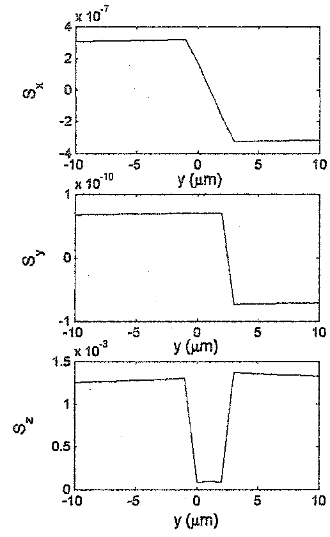

Figure 4.8 The Poynting vector components (S_x, S_y, S_z) for branch 1 of the simulated dispersion curves for a very thin unsupported semiconducting film with an external magnetic field in the Faraday configuration, at $\omega/\omega_0 = 1.5$.

The fields for the mode in branch 2 are plotted at $\omega/\omega_0 = 0.6$. They are shown in Figure 4.9 and Figure 4.10, and the Poynting vector is shown in Figure 4.11. It can be seen that the mode in branch 2 is mainly transverse magnetic in nature since E_y is the major field component. All six field components exist, therefore, the mode is not purely TM in nature. It can also be seen that the major field component is asymmetric, therefore, the mode is an asymmetric mode. This looks like an asymmetric plasmon-polariton mode, whose fields and Poynting vector are shown in Figure 5.4 and Figure 5.5, that is perturbed by an externally applied magnetic field. It should also be noted that the secondary field components are quite large compared to the primary field components and are characteristic of a transverse electric total internal reflection mode as shown in Figure 4.13 for the total internal reflection mode in branch 3. The mode shown in branch 2 is therefore a combination of a plasmon-polariton mode and a total internal reflection mode.

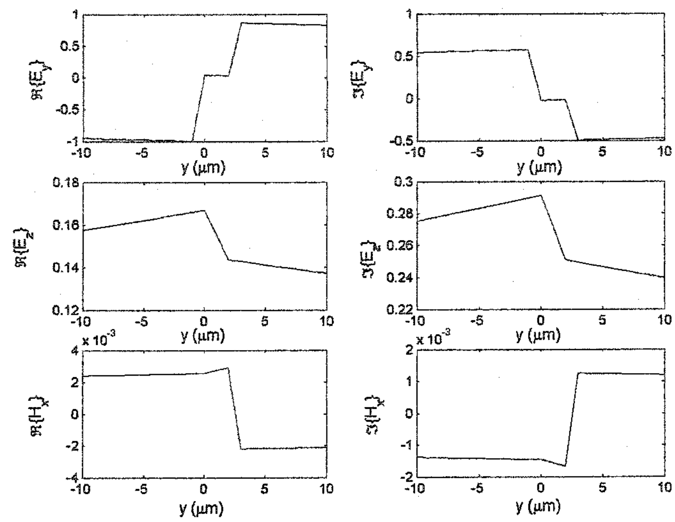

Figure 4.9 The primary field components (E_y, E_z, H_x) for branch 2 of the simulated dispersion curves for a very thin unsupported semiconducting film with an external magnetic field in the Faraday configuration, at ω/ω_0=0.6.

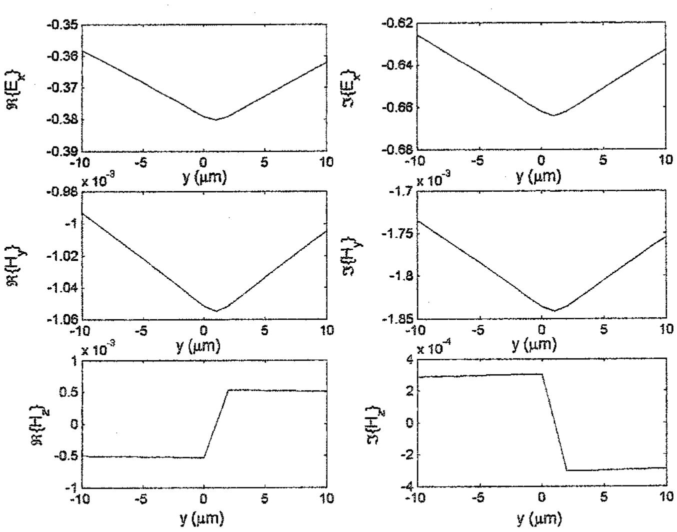

Figure 4.10 The secondary field components (E_x, H_y, H_z) for branch 2 of the simulated dispersion curves for a very thin unsupported semiconducting film with an external magnetic field in the Faraday configuration, at ω/ω_0=0.6

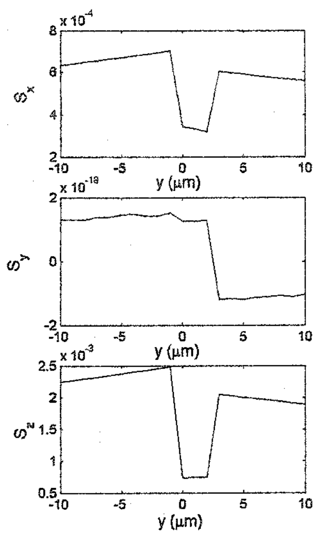

Figure 4.11 The Poynting vector components (S_x, S_y, S_z) for branch 2 of the simulated dispersion curves for a very thin unsupported semiconducting film with an external magnetic field in the Faraday configuration, at ω/ω_0 =0.6.

The fields for the mode in branch 3 are plotted at $\omega/\omega_0 = 1.5$. They are shown in Figure 4.12 and Figure 4.13, and the Poynting vector is shown in Figure 4.14. It can be seen that mode in branch 3 is mainly transverse electric in nature since E_x is the major field component. All six field components exist, therefore, the mode is not purely TE. It can also be seen that the major field component is symmetric, therefore, the mode is a symmetric mode. Plasmon-polariton modes are TM modes with maximum fields at the interfaces. The mode in branch 3 does not exhibit this behaviour therefore it is not a plasmon-polariton mode. It behaves more like a total internal reflection mode which can be either TE or TM.

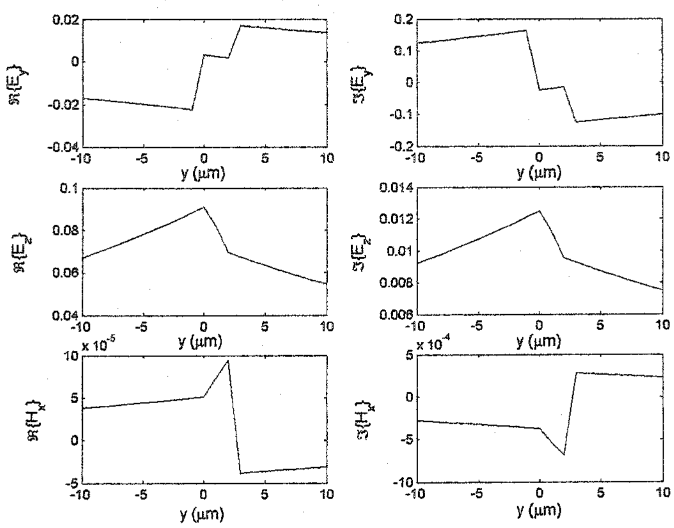

Figure 4.12 The secondary field components (E_y, E_z, H_x) for branch 3 of the simulated dispersion curves for a very thin unsupported semiconducting film with an external magnetic field in the Faraday configuration, at $\omega/\omega_0=1.5$.

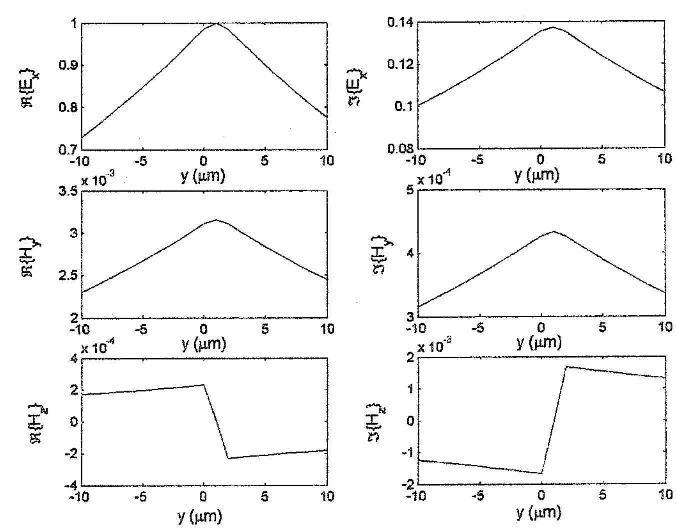

Figure 4.13 The primary field components (E_x, H_y, H_z) for branch 3 of the simulated dispersion curves for a very thin unsupported semiconducting film with an external magnetic field in the Faraday configuration, at $\omega/\omega_0=1.5$.

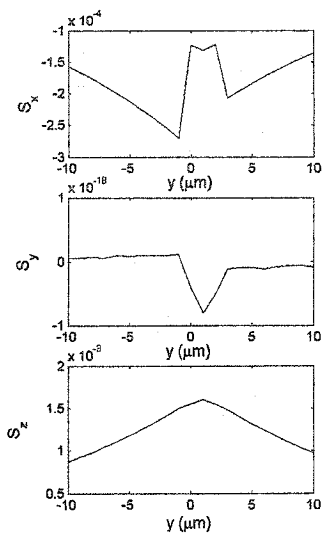

Figure 4.14 The Poynting vector components (S_x, S_y, S_z) for branch 3 of the simulated dispersion curves for a very thin unsupported semiconducting film with an external magnetic field in the Faraday configuration, at $\omega/\omega_0 = 1.5$.

The fields for the mode in branch 4 are plotted at $\omega/\omega_0 = 0.6$. They are shown in Figure 4.15 and Figure 4.16, and the Poynting vector is shown in Figure 4.17. It can be seen that the mode in branch 4 is mainly transverse magnetic in nature since E_y is the major field component. All six field components exist, therefore, the mode is not purely transverse magnetic. It can also be seen that the major field component is asymmetric, therefore, the mode is an asymmetric mode. This is an asymmetric plasmon-polariton mode that is perturbed by an externally applied magnetic field.

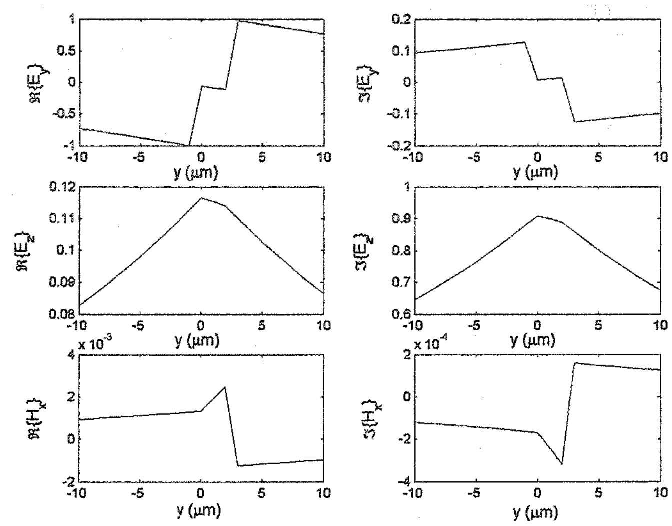

Figure 4.15 The primary field components (E_y, E_z, H_x) for branch 4 of the simulated dispersion curves for a very thin unsupported semiconducting film with an external magnetic field in the Faraday configuration, at $\omega/\omega_0 = 0.6$.

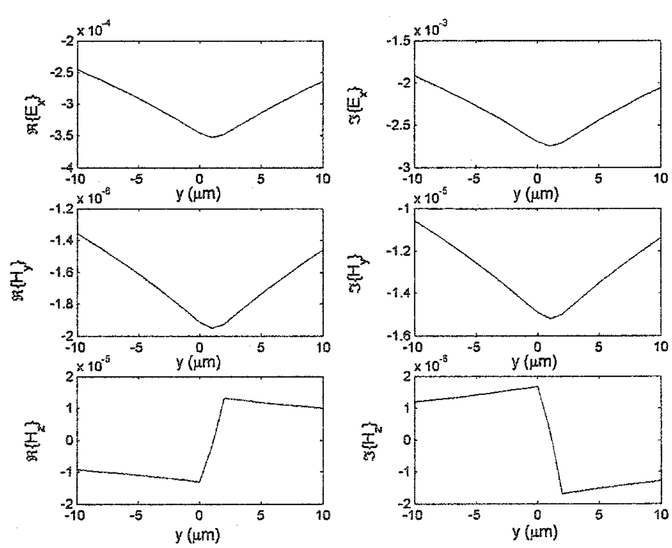

Figure 4.16 The secondary field components (E_x, H_y, H_z) for branch 4 of the simulated dispersion curves for a very thin unsupported semiconducting film with an external magnetic field in the Faraday configuration, at $\omega/\omega_0 = 0.6$.

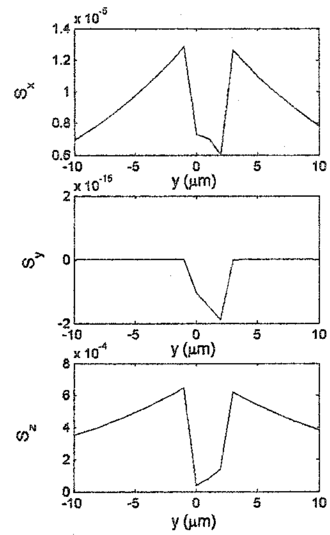

Figure 4.17 The Poynting vector components (S_x, S_y, S_z) for branch 4 of the simulated dispersion curves for a very thin unsupported semiconducting film with an external magnetic field in the Faraday configuration, at $\omega/\omega_0 = 0.6$.

There are four modes whose dispersion curves are shown in Figure 4.3 for an externally applied magnetic field in the Faraday orientation. By examining the fields, it has been found that the mode in branch 1 is a symmetric plasmon-polariton mode, the mode in branch 3 is a transverse electric total internal reflection mode, the mode in branch 4 is an asymmetric plasmon-polariton mode and the mode in branch 2 is a combination of an asymmetric plasmon-polariton mode and a transverse electric total internal reflection mode.

When no external magnetic field is present, the existence of plasmon-polariton modes requires that the real parts of the diagonal components of the permittivity tensor be of opposite sign for the media that make up the interface or interfaces. In this structure this requirement means that the real parts of the diagonal components of the permittivity tensor are negative since the permittivity of the surrounding medium, air, is positive. As noted previously, the diagonal components of the permittivity tensor are negative only for small intervals. Plasmon-polariton modes would not normally exist over most of the frequencies examined. However, the presence of an externally applied magnetic field induces plasmon-polariton modes in the structure through the emergence of the off-diagonal elements in the permittivity tensor.

Typically, both an asymmetric plasmon-polariton mode and a symmetric plasmon-polariton mode exist in the same structure, and both a transverse electric total internal reflection mode and a transverse magnetic total internal reflection mode exist in the same structure. This is not the case in the structure under the influence of an externally applied magnetic field in the Faraday orientation. The externally applied magnetic field may cause a mode to evolve into another mode or it may actually cause a mode to appear. For this reason, the modes seen here are likely not those that would be seen in the same structure with no externally applied magnetic field.

4.3.2 External Magnetic Field in Voigt Configuration

The simulated dispersion curves for the normalized frequency, ω/ω_0, versus normalized propagation constant, $\gamma_z c/\omega_0$, for a thin unsupported semiconducting film with an external magnetic field in the Voigt configuration obtained from the code described in this chapter and from reference [28] are plotted in Figure 4.18. It can be seen from Figure 4.18 that the simulated results obtained from the code described in this chapter are not in agreement with those presented in the literature. In the literature, Halevi and Kushwaha [28] simplify their dispersion relation equations in a similar manner to that shown in the previous chapter. However, they make an error while simplifying that shows up when the x-y off-diagonal elements of the permittivity tensor are null, $\varepsilon_{xy}=\varepsilon_{yx}=0$, which is the case for the perpendicular and Voigt configurations. When this simplification error is included in the simulations performed with the code described at the beginning of the chapter, the results agree closely with those from the literature, shown as diamonds and squares, respectively, in Figure 4.18. When the simplification error is removed from the simulations performed with the code described at the beginning of the chapter, the results differ significantly from those in the literature.

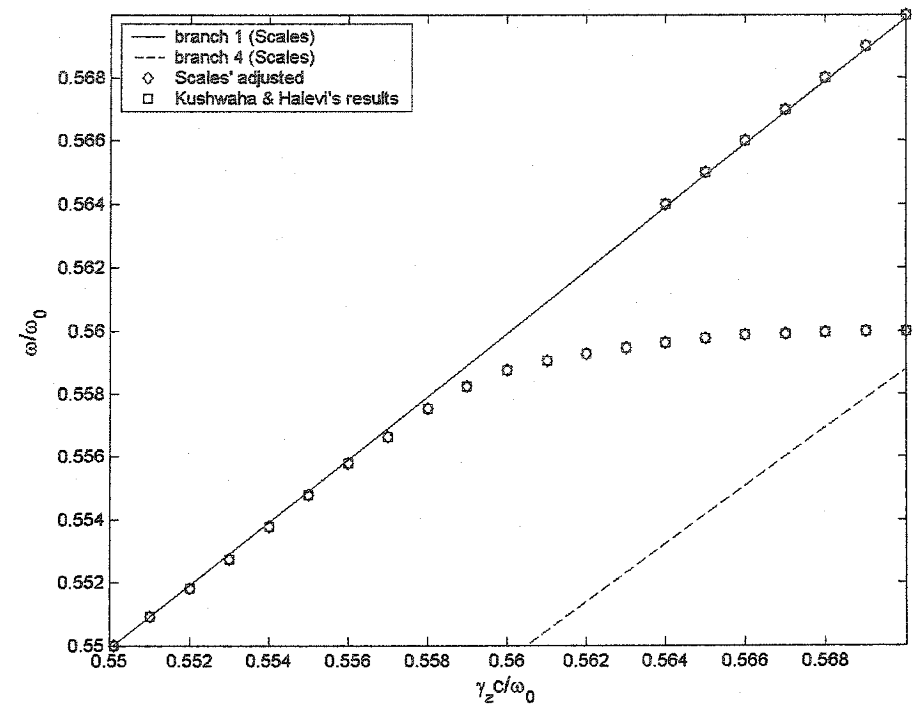

Figure 4.18 Comparison of simulated dispersion curves for the normalized frequency, ω/ω_0 versus normalized propagation constant $\gamma_z c/\omega_0$ for a very thin unsupported semiconducting film with an external magnetic field in the Voigt configuration, obtained from the code described in this chapter and from reference [28].

Figure 4.18 shows the portion of the dispersion curves that is given in the literature [28], for comparison. It is not only interesting to compare with the literature but also to see the behaviour of the dispersion curves over a wider range of values. The simulation results for the dispersion curves obtained from the code discussed at the beginning of the chapter for an external magnetic field applied in the Voigt configuration are shown in Figure 4.19.

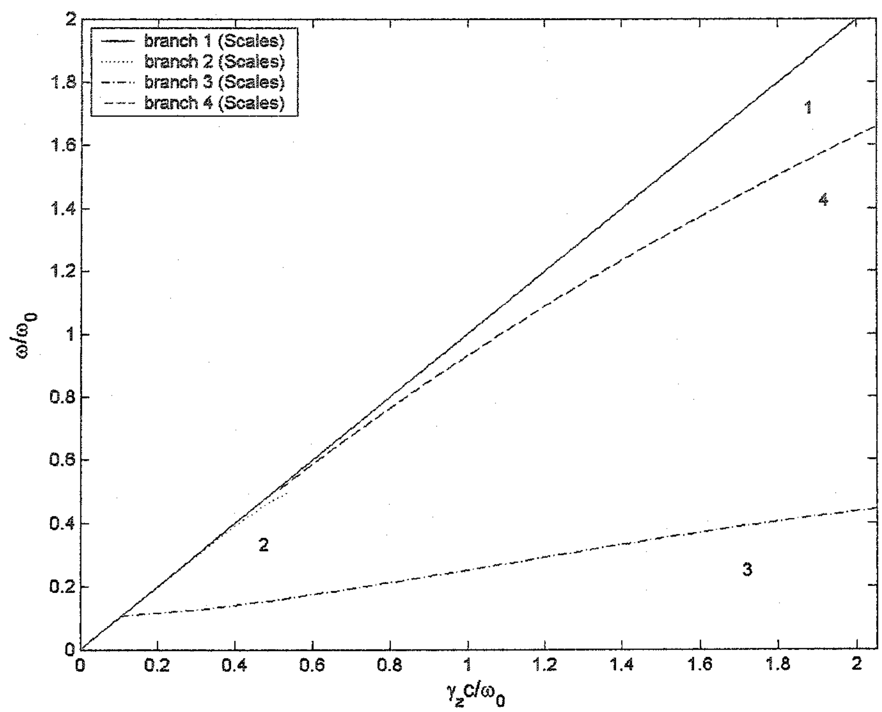

Figure 4.19 Simulated dispersion curves for the normalized frequency, ω/ω_0 versus normalized propagation constant $\gamma_z c/\omega_0$ for a very thin unsupported semiconducting film with an external magnetic field in the Voigt configuration, obtained from the code described in this chapter.

The relative permittivity tensor components for the InSb slab as a function of normalized frequency over the range shown in Figure 4.19 for the Voigt orientation is shown in Figure 4.20. In this orientation the cyclotron frequency is set equal to half the plasma frequency: $\omega_g = \frac{1}{2}\omega_0$. When the angular frequency is also equal to half the plasma frequency, $\omega/\omega_0 = 0.5$, the denominators of all of the non-zero tensor components, except for ε_{xx}, become zero and therefore the components themselves become infinite. It can be seen in Figure 4.20 that the tensor components with a resonance at $\omega/\omega_0 = 0.5$, tend asymptotically towards positive infinity as the resonance is approached from below and tend asymptotically towards negative infinity as the resonance is approached from above. The diagonal tensor component ε_{xx} is negative for $\omega/\omega_0 < 0.2524$ and the diagonal tensor components ε_{yy} and ε_{zz} are negative for $0.5 < \omega/\omega_0 < 0.5601$. The diagonal tensor components are positive for the other frequencies.

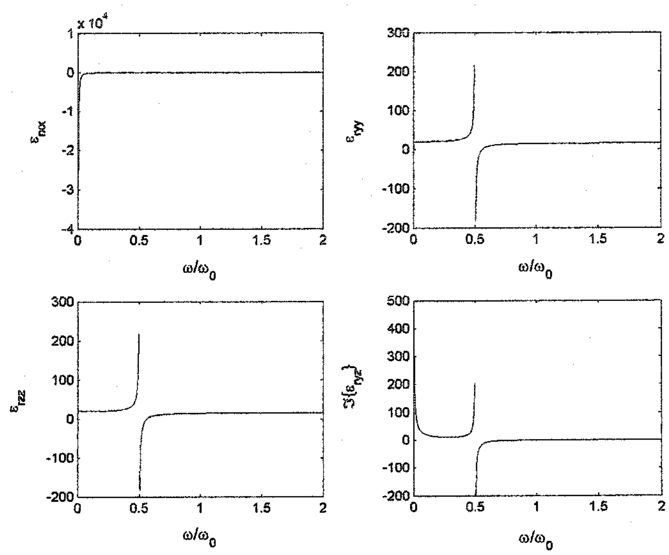

Figure 4.20 The relative permittivity tensor components for the InSb slab as a function of normalized frequency, ω/ω_0, over the range that was examined in the literature for the Voigt orientation of externally applied magnetic field

From Figure 4.19, it can be seen that one of the branches (2) of the dispersion curve tends towards positive infinity as the angular frequency approaches the point where $\omega/\omega_0 = 0.5$. When the angular frequency is greater than one half the plasma frequency, another branch (4) begins to appear in the dispersion curve.

It can be seen from Figure 4.19 that there are four branches to the dispersion curve in the Voigt case. In order to get a better understanding of these branches in the dispersion curve, the fields have been plotted at a specific point on each branch. Due to the transverse application of the external magnetic field in the Voigt orientation, no additional field components are created and the modes remain transverse magnetic in nature. Therefore only the transverse magnetic field components have been plotted since the other three are null.

The fields for the mode in branch 1 are plotted at $\omega/\omega_0 = 1.0$. They are shown in Figure 4.21 and the Poynting vector is shown in Figure 4.22. It can be seen that the major field component, E_y, is almost symmetric, therefore it can be said that the mode is a slightly perturbed symmetric mode. This is a symmetric plasmon-polariton mode that is perturbed by an externally applied magnetic field.

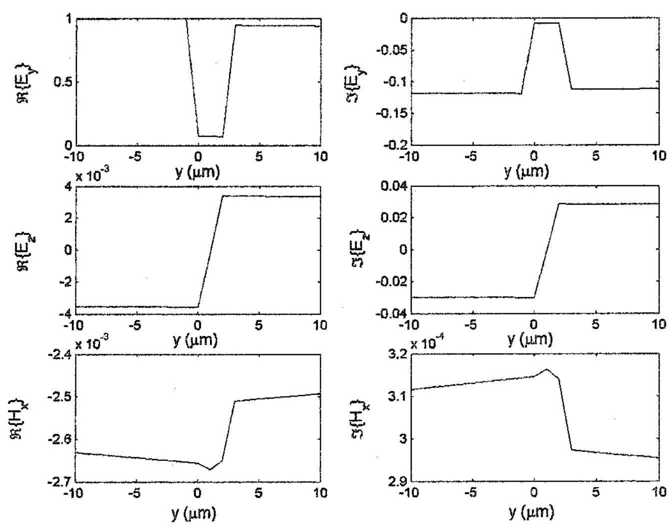

Figure 4.21 The field components (E_y, E_z, H_x) for branch 1 of the simulated dispersion curves for a very thin unsupported semiconducting film with an external magnetic field in the Voigt configuration, at $\omega/\omega_0 = 1.0$.

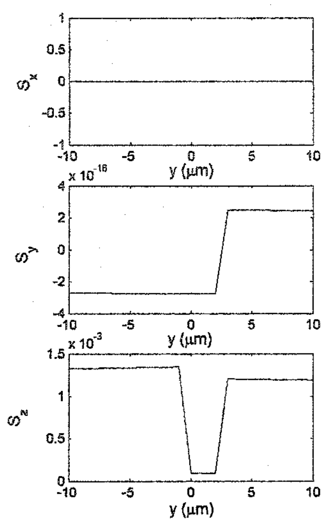

Figure 4.22 The Poynting vector components (S_x, S_y, S_z) for branch 1 of the simulated dispersion curves for a very thin unsupported semiconducting film with an external magnetic field in the Voigt configuration, at $\omega/\omega_0 = 1.0$.

The fields for the mode in branch 2 are plotted at $\omega/\omega_0 = 0.45$. They are shown in Figure 4.23 and the Poynting vector is shown in Figure 4.24. It can be seen that the major field component, E_y, is asymmetric, therefore the mode is an asymmetric mode. This is an asymmetric plasmon-polariton mode that is perturbed by an externally applied magnetic field. By comparing the Poynting vectors in Figure 4.22 and Figure 4.24, it can be seen that both branches 1 and 2 have similar power flow distributions.

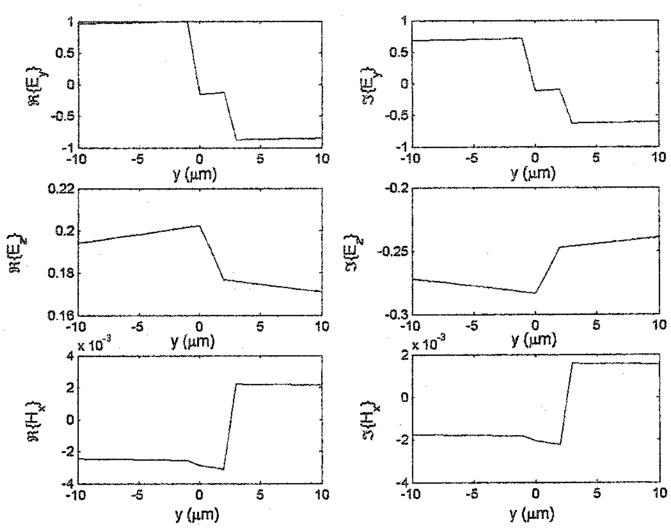

Figure 4.23 The field components (E_y, E_z, H_x) for branch 2 of the simulated dispersion curves for a very thin unsupported semiconducting film with an external magnetic field in the Voigt configuration, at $\omega/\omega_0 = 0.45$.

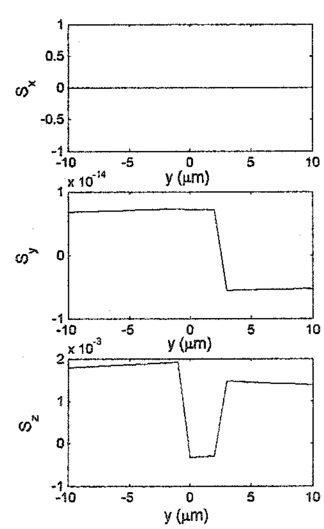

Figure 4.24 The Poynting vector components (S_x, S_y, S_z) for branch 2 of the simulated dispersion curves for a very thin unsupported semiconducting film with an external magnetic field in the Voigt configuration, at $\omega/\omega_0 = 0.45$.

The fields for the mode in branch 3 are plotted at $\omega/\omega_0 = 0.25$. They are shown in Figure 4.25 and the Poynting vector is shown in Figure 4.26. It can be seen that the major field component, E_y, is asymmetric, therefore, the mode is an asymmetric transverse magnetic mode. It can be seen from the Poynting vector in Figure 4.26 that most of the mode power is in the InSb slab rather than the surrounding air. This is indicative of a total internal reflection mode rather than a plasmon-polariton mode. Therefore, this is an asymmetric transverse magnetic total internal reflection mode that is perturbed by an externally applied magnetic field.

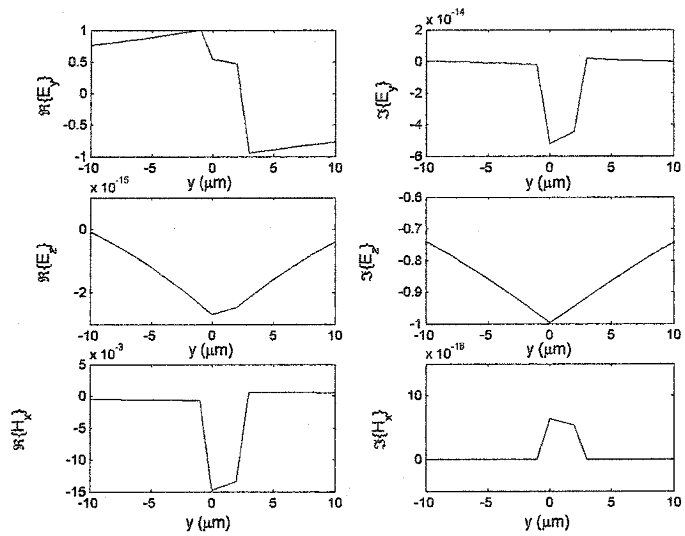

Figure 4.25 The field components (E_y, E_z, H_x) for branch 3 of the simulated dispersion curves for a very thin unsupported semiconducting film with an external magnetic field in the Voigt configuration, at $\omega/\omega_0 = 0.25$.

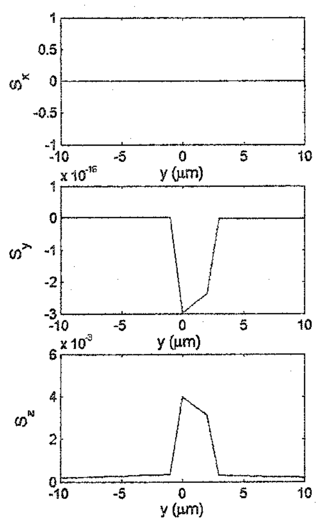

Figure 4.26 The Poynting vector components (S_x, S_y, S_z) for branch 3 of the simulated dispersion curves for a very thin unsupported semiconducting film with an external magnetic field in the Voigt configuration, at $\omega/\omega_0 = 0.25$.

The fields for the mode in branch 4 are plotted at $\omega/\omega_0 = 1.0$. They are shown in Figure 4.27 and the Poynting vector is shown in Figure 4.28. It can be seen that the major field component, E_y, is asymmetric, therefore the mode is an asymmetric mode. This is an asymmetric plasmon-polariton mode that is perturbed by an externally applied magnetic field.

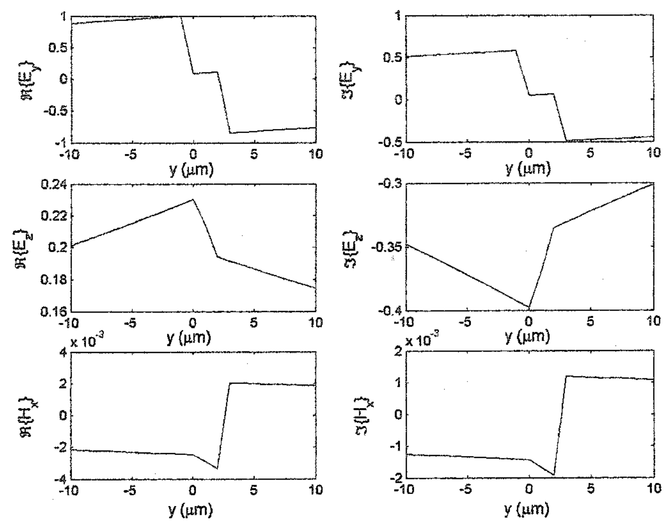

Figure 4.27 The field components (E_y, E_z, H_x) for branch 4 of the simulated dispersion curves for a very thin unsupported semiconducting film with an external magnetic field in the Voigt configuration, at $\omega/\omega_0 = 1.0$.

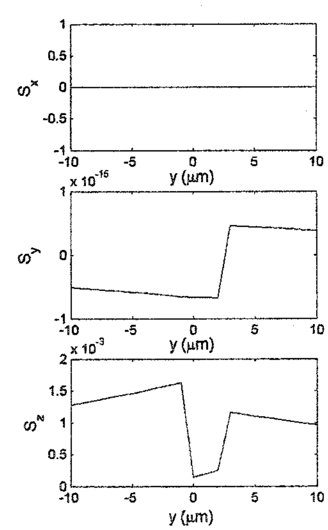

Figure 4.28 The Poynting vector components (S_x, S_y, S_z) for branch 4 of the simulated dispersion curves for a very thin unsupported semiconducting film with an external magnetic field in the Voigt configuration, at $\omega/\omega_0 = 1.0$.

By comparing Figure 4.22, Figure 4.24 and Figure 4.28 it can be seen that branches 1, 2 and 4 all have similar power flow distributions, with the majority of the power in the surrounding air rather than the InSb slab, which is indicative of plasmon-polariton modes. Notice also that the fields for branch 2, in Figure 4.23, and branch 4, in Figure 4.27 are very similar. The mode in branch 2 exists below the resonance at $\omega/\omega_0 = 0.5$, whereas the mode in branch 4 exists above the resonance. At a given frequency, only one symmetric plasmon-polariton mode and one asymmetric plasmon-polariton mode is present. The transverse magnetic total internal reflection mode splits from the symmetric plasmon-polariton mode at around $\omega/\omega_0 = 0.105$.

When no external magnetic field is present, the existence of plasmon-polariton modes requires that the real parts of the diagonal components of the permittivity tensor be of opposite sign for the media that make up the interface or interfaces. In this structure this requirement means that the diagonal components of the permittivity tensor are negative since the permittivity of the surrounding medium, air, is positive. As noted previously, the diagonal components of the permittivity tensor are negative only for small intervals. Plasmon-polariton modes would not normally exist over most of the frequencies examined. However, the presence of an externally applied magnetic field induces plasmon-polariton modes in the structure.

4.3.3 External Magnetic Field in Perpendicular Configuration

The simulated dispersion curves for the normalized frequency, $\sqrt{\varepsilon_L}\omega/\omega_0$, versus normalized propagation constant, $\sqrt{\varepsilon_L}\gamma_z c/\omega_0$, for a very thin unsupported semiconducting film with an external magnetic field in the perpendicular configuration obtained from the code described in this chapter and from reference [29] are plotted in Figure 4.29. The modes in the region above $\sqrt{\varepsilon_L}\omega/\omega_0 = 1$ have been re-plotted in Figure 4.30 for clarity.

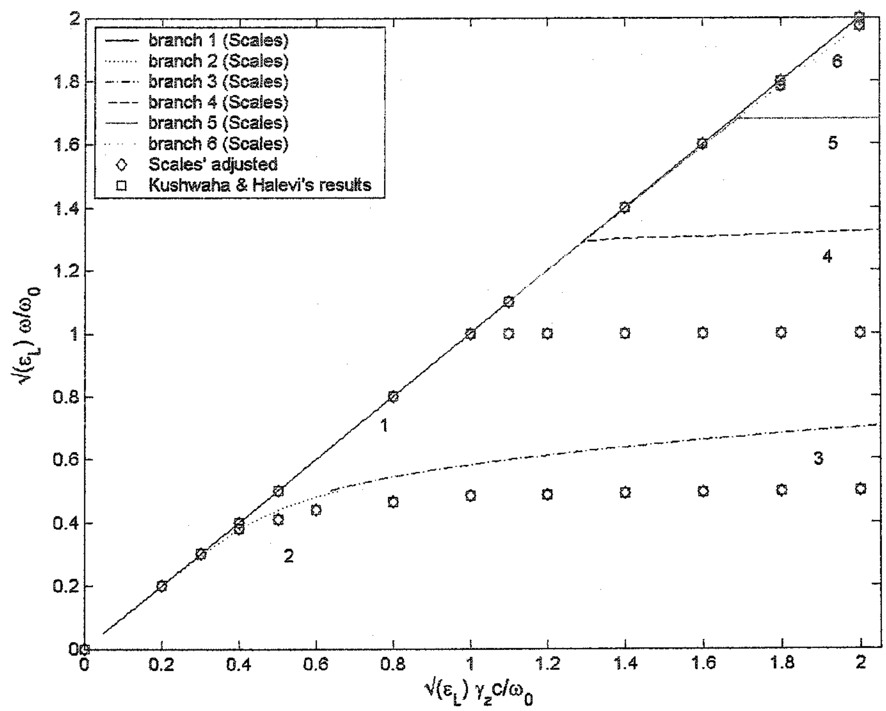

Figure 4.29 Comparison of simulated dispersion curves for the normalized frequency, $\sqrt{\varepsilon_L}\omega/\omega_0$ versus normalized propagation constant, $\sqrt{\varepsilon_L}\gamma_z c/\omega_0$ for a very thin unsupported semiconducting film with an external magnetic field in the perpendicular configuration, obtained from the code described in this chapter and from reference [29].

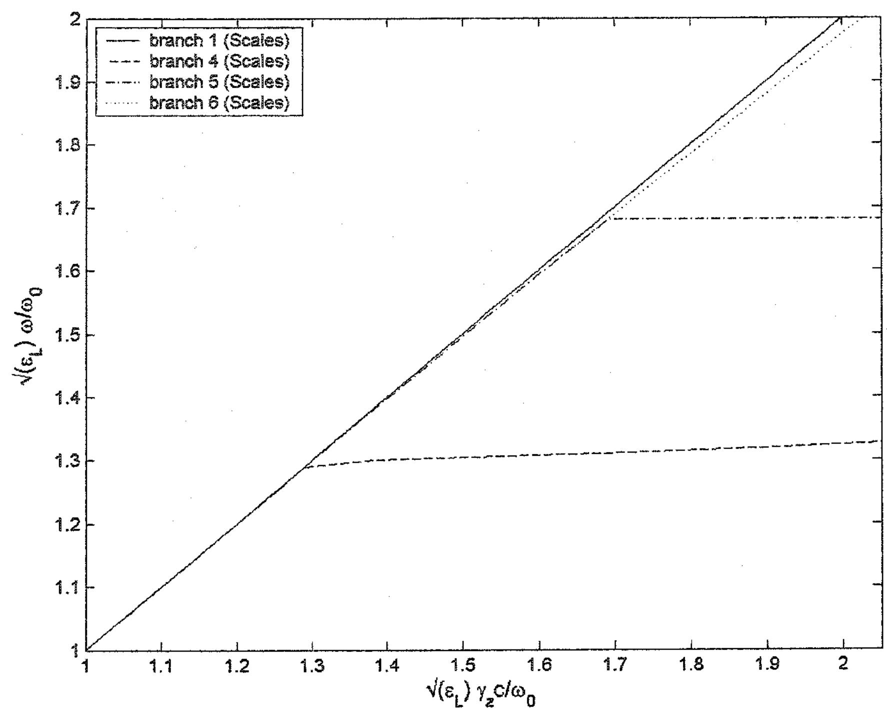

Figure 4.30 Close up of simulated dispersion curves for the normalized frequency, $\sqrt{\varepsilon_L}\omega/\omega_0$ versus normalized propagation constant, $\sqrt{\varepsilon_L}\gamma_z c/\omega_0$ for a very thin unsupported semiconducting film with an external magnetic field in the perpendicular configuration.

It can be seen from Figure 4.29 that the simulated results obtained from the code described in this chapter are not in agreement with those presented in the literature. In the literature, Halevi and Kushwaha [29] simplify their dispersion relation equations in a similar manner to that shown in the previous chapter. However, they make an error while simplifying that shows up when the x-y off-diagonal elements of the permittivity tensor are null, $\varepsilon_{xy}=\varepsilon_{yx}=0$, which is the case for the perpendicular and Voigt configurations. When this simplification error is included in the simulations performed with the code described at the beginning of the chapter, the results agree closely with those from the literature, shown as diamonds and squares, respectively, in Figure 4.29. When the simplification error is removed from the simulations performed with the code described at the beginning of the chapter, the results differ significantly from those in the literature.

The relative permittivity tensor components for the InSb slab as a function of normalized frequency over the range that was examined in the literature for the perpendicular orientation are shown in Figure 4.31. In this orientation, the cyclotron frequency is set to half the plasma frequency divided by the square root of the background dielectric constant of the film medium: $\omega_g = \frac{1}{2}\frac{\omega_0}{\sqrt{\varepsilon_L}}$. When the angular frequency is also equal to half the plasma frequency divided by the square root of the background dielectric constant of the film medium, $\sqrt{\varepsilon_L}\omega/\omega_0 = 0.5$, the denominators of all of the non-zero tensor components, except for ε_{yy}, become zero and therefore the components themselves become infinite. It can be seen in Figure 4.31 that the tensor components with a resonance at $\sqrt{\varepsilon_L}\omega/\omega_0 = 0.5$, tend asymptotically towards positive infinity as the resonance is approached from below and tend asymptotically towards negative infinity as the resonance is approached from above. These tensor components also cross zero at $\sqrt{\varepsilon_L}\omega/\omega_0 =$ 1.1175, whereas the tensor component ε_{yy} crosses zero at $\sqrt{\varepsilon_L}\omega/\omega_0 = 1$. The diagonal tensor components ε_{xx} and ε_{zz} are negative for $0.5 < \sqrt{\varepsilon_L}\omega/\omega_0 < 1.1175$ and the diagonal tensor component ε_{yy} is negative for $\sqrt{\varepsilon_L}\omega/\omega_0 < 1$. The diagonal tensor components are positive for the other frequencies.

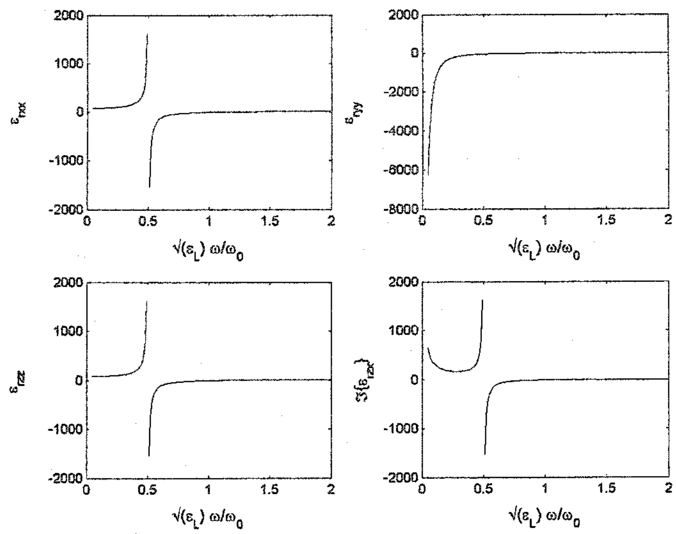

Figure 4.31 The relative permittivity tensor components for the InSb slab as a function of normalized frequency, $\sqrt{\varepsilon_L}\omega/\omega_0$, over the range that was examined in the literature for the perpendicular orientation of externally applied magnetic field

It can be seen from Figure 4.29 that there are six branches to the dispersion curve in the perpendicular case. In order to get a better understanding of these branches in the dispersion curve, the fields have been plotted at a specific point on each branch. The fields for the mode in branch 1 are plotted at $\sqrt{\varepsilon_L}\omega/\omega_0 = 0.8$. They are shown in Figure 4.32 and Figure 4.33, and the Poynting vector is shown in Figure 4.34. It can be seen that mode in branch 1 is mainly transverse magnetic in nature since E_y is the major field component. All six field components exist, therefore, the mode is not purely TM. It can also be seen that the major field component is asymmetric, therefore the mode is an asymmetric mode. From the Poynting vector in Figure 4.34 it can be seen that the majority of the power is in the surrounding air rather than the InSb slab. This is an asymmetric plasmon-polariton mode that is perturbed by an externally applied magnetic field.

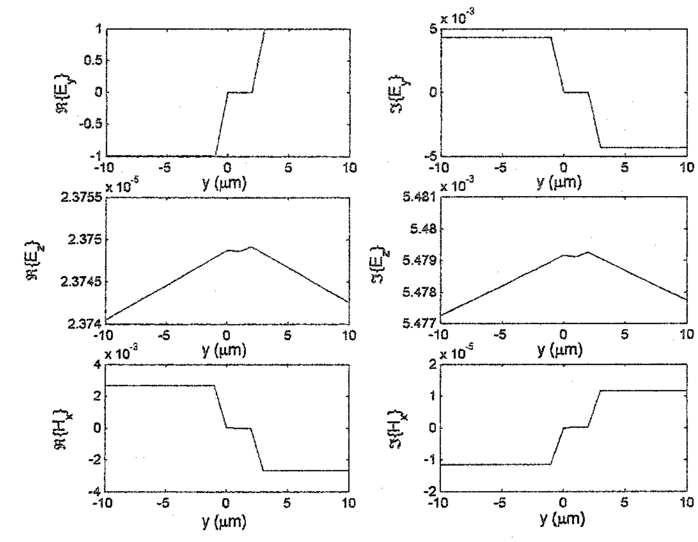

Figure 4.32 The primary field components (E_y, E_z, H_x) for branch 1 of the simulated dispersion curves for a very thin unsupported semiconducting film with an external magnetic field in the perpendicular configuration, at $\sqrt{\varepsilon_L}\omega/\omega_0$=0.8.

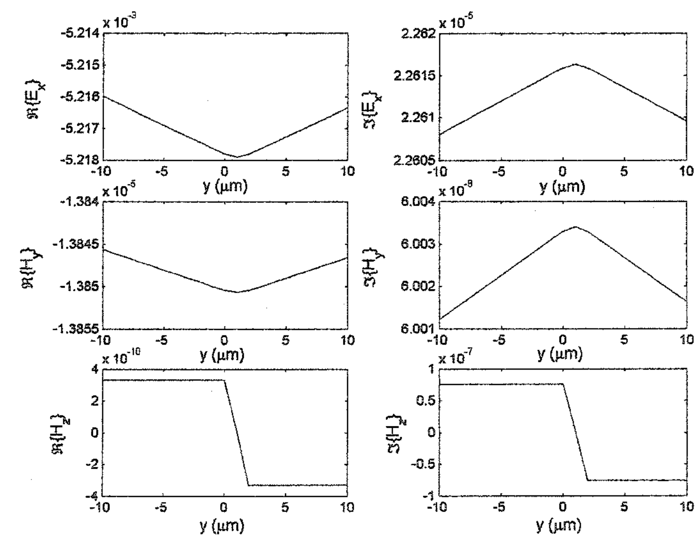

Figure 4.33 The secondary field components (E_x, H_y, H_z) for branch 1 of the simulated dispersion curves for a very thin unsupported semiconducting film with an external magnetic field in the perpendicular configuration, at $\sqrt{\varepsilon_L}\omega/\omega_0$=0.8.

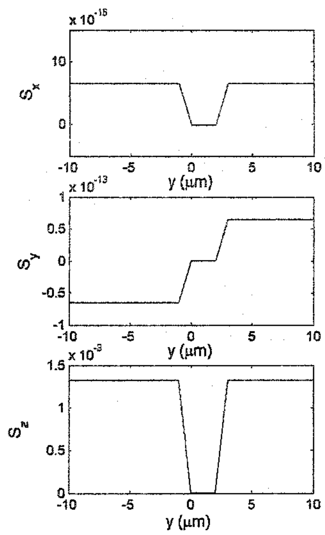

Figure 4.34 The Poynting vector components (S_x, S_y, S_z) for branch 1 of the simulated dispersion curves for a very thin unsupported semiconducting film with an external magnetic field in the perpendicular configuration, at $\sqrt{\varepsilon_L}\omega/\omega_0$ =0.8.

The fields for the mode in branch 2 are plotted at $\sqrt{\varepsilon_L}\omega/\omega_0 = 0.44$. They are shown in Figure 4.35 and Figure 4.36, and the Poynting vector is shown in Figure 4.37. It can be seen that both E_x and E_y are significant field components in the mode in branch 2. It can also be seen that the E_y component is asymmetric and the E_x component is symmetric, therefore the mode is asymmetric in y and symmetric in x. From the Poynting vector component in the z direction, it can be seen that the majority of the power is flowing in the positive z-direction above and below the InSb slab however a significant portion of the power is also flowing in the positive z direction inside the InSb slab. There is very little power in the x and y directions. This mode cannot be a plasmon-polariton mode since it is not TM or close to TM in nature. It is not a total internal reflection mode either since the majority of the power is flowing outside of the InSb slab. However, the majority of the power in the E_x and H_y field components is in the InSb slab. This mode may be a combination of the two types of modes.

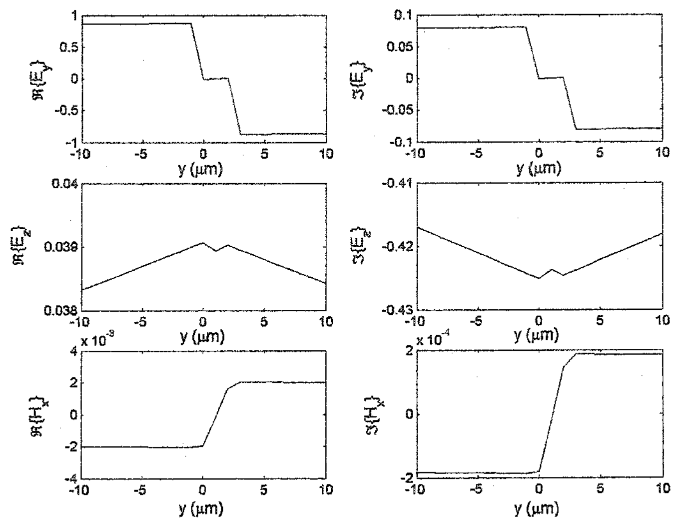

Figure 4.35 The field components (E_y, E_z, H_x) for branch 2 of the simulated dispersion curves for a very thin unsupported semiconducting film with an external magnetic field in the perpendicular configuration, at $\sqrt{\varepsilon_L}\omega/\omega_0$ =0.44.

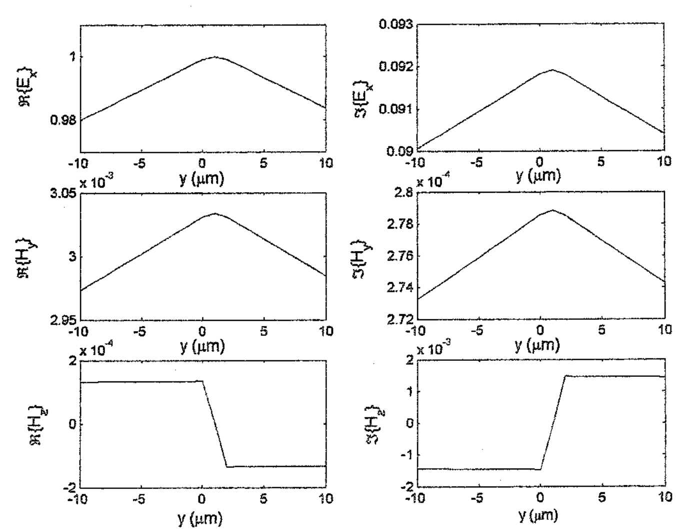

Figure 4.36 The field components (E_x, H_y, H_z) for branch 2 of the simulated dispersion curves for a very thin unsupported semiconducting film with an external magnetic field in the perpendicular configuration, at $\sqrt{\varepsilon_L}\omega/\omega_0$ =0.44.

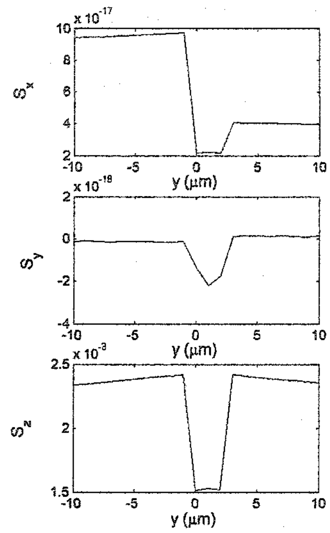

Figure 4.37 The Poynting vector components (S_x, S_y, S_z) for branch 2 of the simulated dispersion curves for a very thin unsupported semiconducting film with an external magnetic field in the perpendicular configuration, at $\sqrt{\varepsilon_L}\omega/\omega_0=0.44$.

The fields for the mode in branch 3 are plotted at $\sqrt{\varepsilon_L}\omega/\omega_0 = 0.6$. They are shown in Figure 4.38 and Figure 4.39, and the Poynting vector is shown in Figure 4.40. It can be seen that the mode in branch 3 is mainly transverse magnetic in nature since E_y is the major field component. All six field components exist, therefore, the mode is not purely TM. It can also be seen that the major field component is asymmetric, therefore the mode is an asymmetric mode. From the Poynting vector in Figure 4.40, it can be seen that the majority of the power is above and below the InSb slab. However, the majority of the power in secondary field components, E_x, H_y and H_z, is in the InSb slab as is the case for the mode in branch 2. It should also be noted that the mode in branch 2 exists only for frequencies below the resonance at $\sqrt{\varepsilon_L}\omega/\omega_0 = 0.5$ and the mode in branch 3 exists only for frequencies above the resonance. Therefore, the mode in branch 3 replaces the mode in branch 2 for frequencies above the resonance. The mode in branch 3 looks more like an asymmetric plasmon-polariton mode that is perturbed by an externally applied magnetic field than the mode in branch 2.

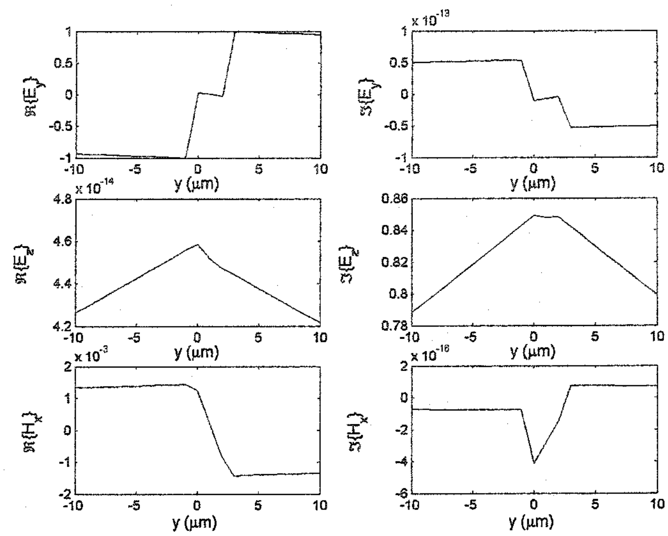

Figure 4.38 The primary field components (E_y, E_z, H_x) for branch 3 of the simulated dispersion curves for a very thin unsupported semiconducting film with an external magnetic field in the perpendicular configuration, at $\sqrt{\varepsilon_L}\,\omega/\omega_0=0.6$.

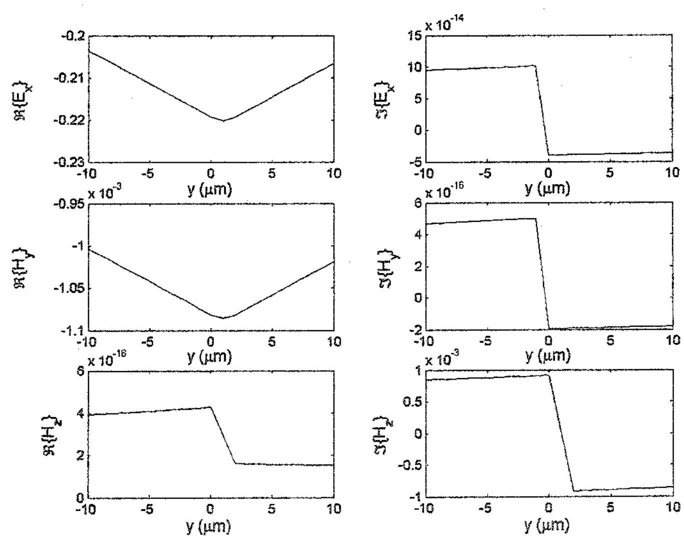

Figure 4.39 The secondary field components (E_x, H_y, H_z) for branch 3 of the simulated dispersion curves for a very thin unsupported semiconducting film with an external magnetic field in the perpendicular configuration, at $\sqrt{\varepsilon_L}\,\omega/\omega_0=0.6$.

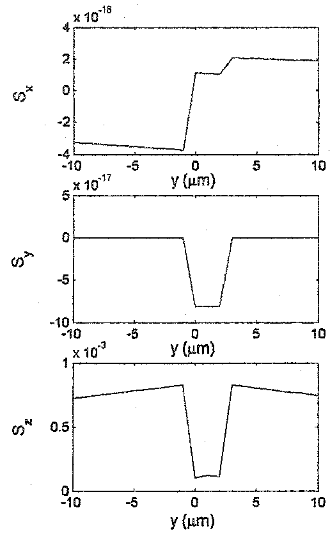

Figure 4.40 The Poynting vector components (S_x, S_y, S_z) for branch 3 of the simulated dispersion curves for a very thin unsupported semiconducting film with an external magnetic field in the perpendicular configuration, at $\sqrt{\varepsilon_L}\omega/\omega_0$=0.6.

The fields for the mode in branch 4 are plotted at $\sqrt{\varepsilon_L}\omega/\omega_0 = 1.3$. They are shown in Figure 4.41 and Figure 4.42, and the Poynting vector is shown in Figure 4.43. It can be seen that mode in branch 4 is mainly transverse magnetic in nature since E_y is the major field component. All six field components exist, therefore, the mode is not purely TM. It can also be seen that the major field component is asymmetric, therefore the mode is an asymmetric mode. From the Poynting vector in Figure 4.43, it can be seen that the majority of the power is above and below the InSb slab. This is an asymmetric plasmon-polariton mode that is perturbed by an externally applied magnetic field. By comparing the fields for the mode in branch 1 with the fields for the mode in branch 4 it can be seen that they are very similar. The mode in branch 4 splits off from the mode in branch 1 at around $\sqrt{\varepsilon_L}\omega/\omega_0 = 1$, which is the point at which the permittivity tensor component ε_{yy} changes sign. Below the split off point the modes in branches 1 and 4 are degenerate. That is why the fields are so similar. The existence of an externally applied magnetic field removes the degeneracy above the split off point.

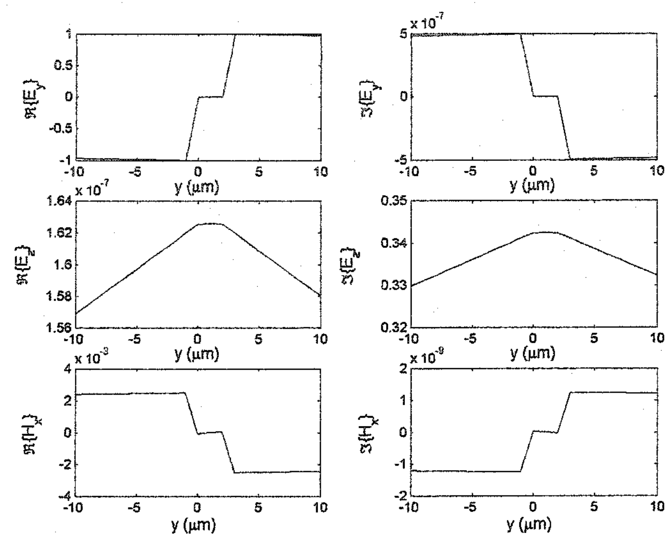

Figure 4.41 The primary field components (E_y, E_z, H_x) for branch 4 of the simulated dispersion curves for a very thin unsupported semiconducting film with an external magnetic field in the perpendicular configuration, at $\sqrt{\varepsilon_L}\omega/\omega_0 = 1.3$.

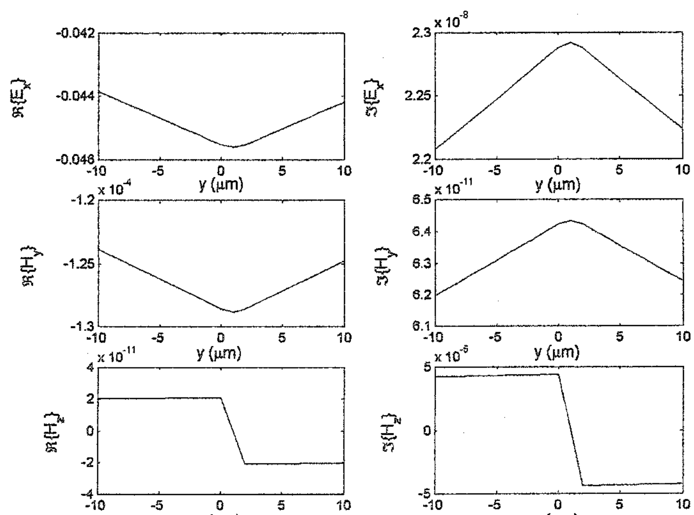

Figure 4.42 The secondary field components (E_x, H_y, H_z) for branch 4 of the simulated dispersion curves for a very thin unsupported semiconducting film with an external magnetic field in the perpendicular configuration, at $\sqrt{\varepsilon_L}\omega/\omega_0 = 1.3$.

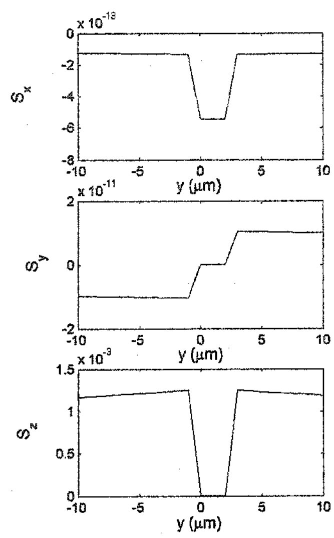

Figure 4.43 The Poynting vector components (S_x, S_y, S_z) for branch 4 of the simulated dispersion curves for a very thin unsupported semiconducting film with an external magnetic field in the perpendicular configuration, at $\sqrt{\varepsilon_L}\omega/\omega_0$ =1.3.

The fields for the mode in branch 5 are plotted at $\sqrt{\varepsilon_L}\omega/\omega_0$ = 1.68. They are shown in Figure 4.44 and Figure 4.45, and the Poynting vector is shown in Figure 4.46. It can be seen that the mode in branch 5 is mainly transverse electric in nature since E_x is the major field component. All six field components exist, therefore, the mode is not purely TE. It can also be seen that the major field component is symmetric, therefore the mode is a symmetric mode. From the Poynting vector in Figure 4.46, it can be seen that the majority of the power is in the InSb slab, which is indicative of a total internal reflection mode. This is a symmetric transverse electric total internal reflection mode that is perturbed by an externally applied magnetic field. The mode in branch 5 exists for frequencies above approximately $\sqrt{\varepsilon_L}\omega/\omega_0$ = 1, which is the point at which the permittivity tensor component ε_{yy} changes sign.

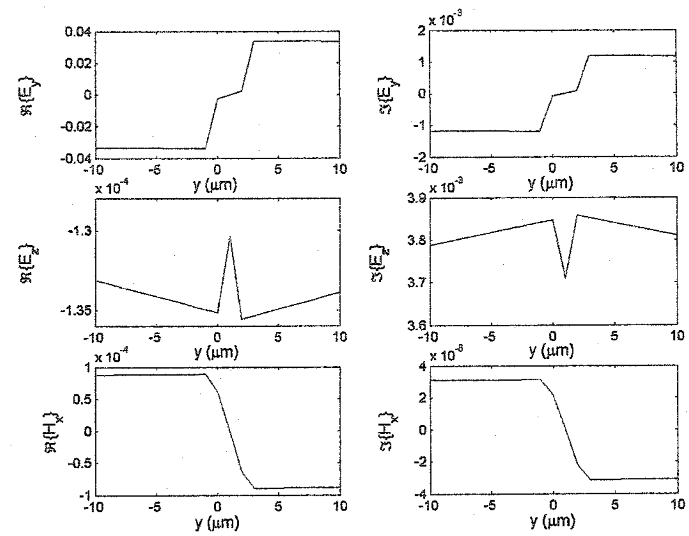

Figure 4.44 The secondary field components (E_y, E_z, H_x) for branch 5 of the simulated dispersion curves for a very thin unsupported semiconducting film with an external magnetic field in the perpendicular configuration, at $\sqrt{\varepsilon_L}\omega/\omega_0=1.68$.

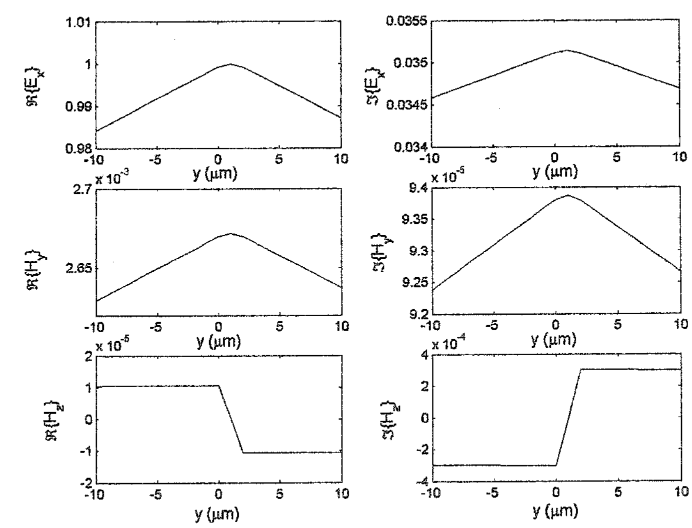

Figure 4.45 The primary field components (E_x, H_y, H_z) for branch 5 of the simulated dispersion curves for a very thin unsupported semiconducting film with an external magnetic field in the perpendicular configuration, at $\sqrt{\varepsilon_L}\omega/\omega_0=1.68$.

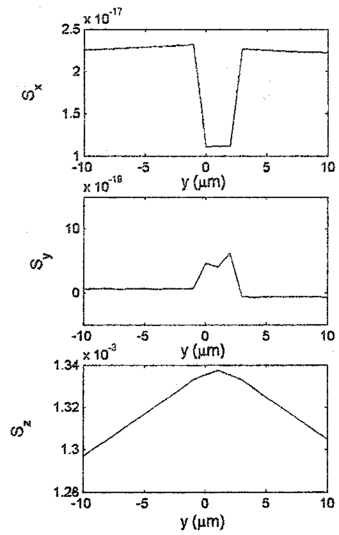

Figure 4.46 The Poynting vector components (S_x, S_y, S_z) for branch 5 of the simulated dispersion curves for a very thin unsupported semiconducting film with an external magnetic field in the perpendicular configuration, at $\sqrt{\varepsilon_L}\omega/\omega_0=1.68$.

The fields for the mode in branch 6 are plotted at $\sqrt{\varepsilon_L}\omega/\omega_0 = 1.9$. They are shown in Figure 4.47 and Figure 4.48, and the Poynting vector is shown in Figure 4.49. It can be seen that the mode in branch 6 is mainly transverse electric in nature since E_x is the major field component. All six field components exist, therefore, the mode is not purely TE. It can also be seen that the major field component is symmetric, therefore the mode is a symmetric mode. From the Poynting vector in Figure 4.49, it can be seen that the majority of the power is in the InSb slab, which is indicative of a total internal reflection mode. This is a symmetric transverse electric total internal reflection mode that is perturbed by an externally applied magnetic field. By comparing the fields for the mode in branch 5, in Figure 4.44 and Figure 4.45, with the field components for the mode in branch 6, Figure 4.47 and Figure 4.48, it can be seen that they are very similar. This is because the modes in branches 5 and 6 are degenerate modes until the mode in branch 6 becomes distinct from the mode in branch 5 around $\sqrt{\varepsilon_L}\omega/\omega_0 = 1.6$. The existence of an externally applied magnetic field removes the degeneracy above the split off point.

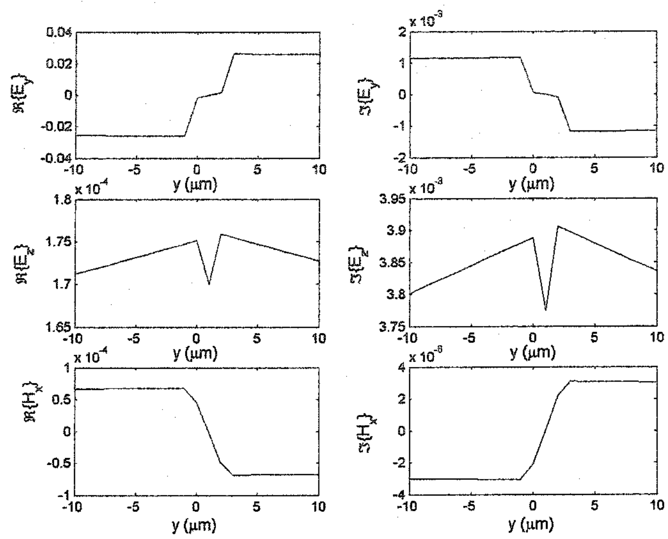

Figure 4.47 The secondary field components (E_y, E_z, H_x) for branch 6 of the simulated dispersion curves for a very thin unsupported semiconducting film with an external magnetic field in the perpendicular configuration, at $\sqrt{\varepsilon_L}\omega/\omega_0$=1.9.

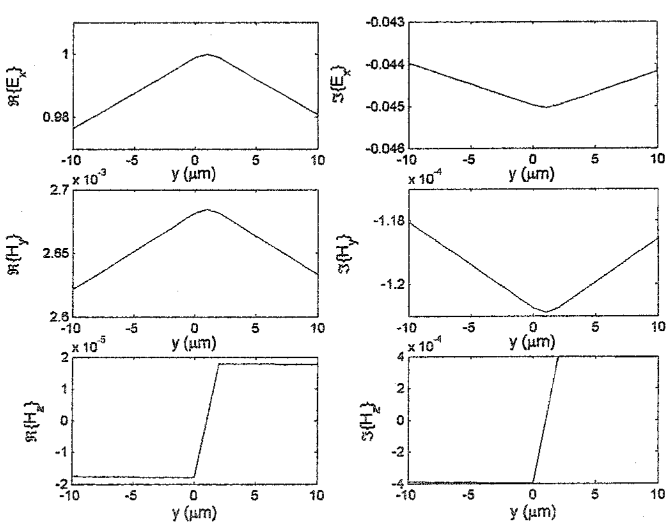

Figure 4.48 The primary field components (E_x, H_y, H_z) for branch 6 of the simulated dispersion curves for a very thin unsupported semiconducting film with an external magnetic field in the perpendicular configuration, at $\sqrt{\varepsilon_L}\omega/\omega_0$=1.9.

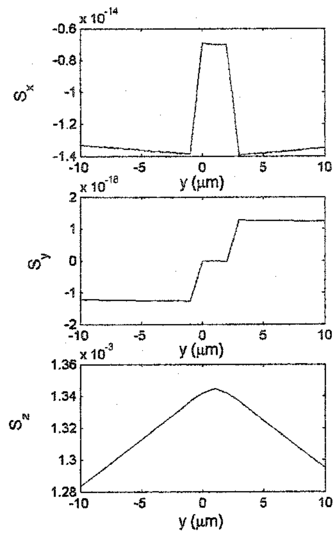

Figure 4.49 The Poynting vector components (S_x, S_y, S_z) for branch 6 of the simulated dispersion curves for a very thin unsupported semiconducting film with an external magnetic field in the perpendicular configuration, at $\sqrt{\varepsilon_L}\omega/\omega_0 = 1.9$.

There are six modes whose dispersion curves are shown in Figure 4.29 for an externally applied magnetic field in the perpendicular orientation. By examining the fields, it has been found that the modes in branches 1 and 4 are an asymmetric plasmon-polariton modes which are one mode for frequencies below $\sqrt{\varepsilon_L}\omega/\omega_0 = 1$ and become two distinct modes for frequencies above $\sqrt{\varepsilon_L}\omega/\omega_0 = 1$, which is the point at which the permittivity tensor component ε_{yy} changes sign. The mode in branch 2 is a combination of an asymmetric plasmon-polariton mode and a transverse electric total internal reflection mode. It only exists for frequencies below $\sqrt{\varepsilon_L}\omega/\omega_0 = 0.5$, above which the mode in branch 3 exists. The mode in branch 3 is similar to the mode in branch 2 but has stronger plasmon-polariton characteristics. The modes in branches 5 and 6 are both symmetric transverse electric total internal reflection modes with very similar characteristics. They exist as a single mode for frequencies above $\sqrt{\varepsilon_L}\omega/\omega_0 = 1$, which is the point at which the permittivity tensor component ε_{yy} changes sign, and become two distinct modes for frequencies above approximately $\sqrt{\varepsilon_L}\omega/\omega_0 = 1.6$.

When no external magnetic field is present, the existence of plasmon-polariton modes requires that the real parts of the diagonal components of the permittivity tensor be of opposite sign for the media that make up the interface or interfaces. In this structure this requirement means that the diagonal components of the permittivity tensor are negative since the permittivity of the surrounding medium, air, is positive. As noted previously, the diagonal components of the permittivity tensor are negative only for certain intervals. Plasmon-polariton modes would not normally exist over most of the frequencies examined. However, the presence of an externally applied magnetic field induces plasmon-polariton modes in the structure.

Typically, both an asymmetric plasmon-polariton mode and a symmetric plasmon-polariton mode exist in the same structure, and both a transverse electric total internal reflection mode and a transverse magnetic total internal reflection mode exist in the same structure. This is not the case in this structure under the influence of an externally applied magnetic field in the perpendicular orientation. The externally applied magnetic field may cause a mode to evolve into another mode or it may actually cause a mode to appear. For this reason, the modes seen here are likely not those that would be seen in the same structure with no externally applied magnetic field.

4.3.4 Conclusion

It can be seen that the dispersion curves from simulations performed with the code described at the beginning of this chapter are not all in agreement with the results presented in the literature. In the literature, Halevi and Kushwaha [27, 28 and 29] simplify their dispersion relation equations in a similar manner to that shown in the previous chapter. However, they make an error while simplifying that shows up when the x-y off-diagonal elements of the permittivity tensor are null, $\varepsilon_{xy}=\varepsilon_{yx}=0$, which is the case for the perpendicular and Voigt configurations. When this simplification error is included in the simulations performed with the code described at the beginning of the chapter, the results agree closely with those from the literature, shown as squares in Figure 4.3, Figure 4.18 and Figure 4.29. When the simplification error is removed from the simulations performed with the code described at the beginning of the chapter, the results differ significantly from those in the literature in both the perpendicular and Voigt cases. The simplification error does not affect the Faraday orientation, therefore, the results from simulations performed with the code described at the beginning of the chapter agree well with the results from the literature with the exception of an extra branch, which appears both when the error is taken into account and when it is not taken into account. It is clear that if the simulation error is taken into account, the dispersion curves from simulations performed with the code described at the beginning of this chapter are in good agreement with the results presented in the literature [27, 28 and 29]. It can, therefore, be inferred that the model presented at the beginning of this chapter is valid in the case where an external magnetic field is applied in all three orientations.

As the frequency increases, more branches appear in the dispersion curve, indicating that additional modes can be supported at higher frequencies. Every branch of the dispersion curves for the corrected dispersion equations in the Voigt and perpendicular configurations as well as the dispersion curve for the Faraday dispersion equation have been explored meticulously to the best of the numerical limitations of the modelling code. An additional branch was found in the dispersion curve for the Faraday orientation and the new corrected dispersion curve in the Voigt case comprises four branches, while the new corrected dispersion curve in the perpendicular case comprises six branches. The field components of the modes represented by these branches have also been examined.

When no external magnetic field is present, the existence of plasmon-polariton modes requires that the real parts of the diagonal components of the permittivity tensor be of opposite sign for the media that make up the interface or interfaces. In this structure this requirement means that the diagonal components of the permittivity tensor are negative since the permittivity of the surrounding medium, air, is positive. As noted previously, the diagonal components of the permittivity tensor in all three cases are negative only for certain intervals. Plasmon-polariton modes would not normally exist over most of the frequencies examined. However, the presence of an externally applied magnetic field induces plasmon-polariton modes in the structure. Future work should include the examination of the modes in this structure at fixed frequency points as the externally applied magnetic field is varied to determine exactly how the externally applied magnetic field affects the nature of the modes in the structure.

5. Simulation Results for Magneto-plasmons Supported by a Gold Film Bounded by Silicon Dioxide

It has been shown recently that a thin metal film finite in width embedded in a dielectric can form passive optical waveguides at infrared frequencies [1-5]. It is of great interest to find a way to make these waveguides active. One possible way of doing so is through the application of an external magnetic field. By simulating the propagation of plasmon-polaritons along thin metal films of infinite width bounded by dielectrics under the influence of an external magnetic field, it is possible to get an understanding of the effect of an externally applied magnetic field on thin metal films of finite width embedded in dielectrics. This is possible because the characteristics of an infinite width thin metal film are similar in many ways to the finite width thin metal film. If an externally applied magnetic field has an effect on thin films of infinite width, then it can be inferred that it will have a similar effect on thin films of finite width, and the investigation of such an effect could be initiated through more complex optical modal analysis or through experiments.

The first experimental observation of the existence of long-range plasmon-polariton waves guided by a thin metal film of finite width was done by exciting a waveguide composed of an 8 μm wide, 20nm thick gold metal film embedded in silicon dioxide [4]. Previously, it has been shown that metal film waveguides comprising noble metals such as silver, gold, aluminium and copper have low losses at optical communications wavelengths. Gold was identified as having the most promising characteristics at the near infrared communication wavelength of 1550nm [4]. For this reason, it was used in the fabrication of the first finite width thin metal film optical waveguide and will be used for the following analysis of the effect of an externally applied magnetic field.

The orientation of the thin film and the direction of wave propagation of the structure that has been analysed is shown in cartesian coordinates in Figure 5.1. Notice that the gold film is positioned between y=0 and y=d, where d is the thickness of the film. The field components and Poynting vectors in the following analysis will be plotted along the y-axis.

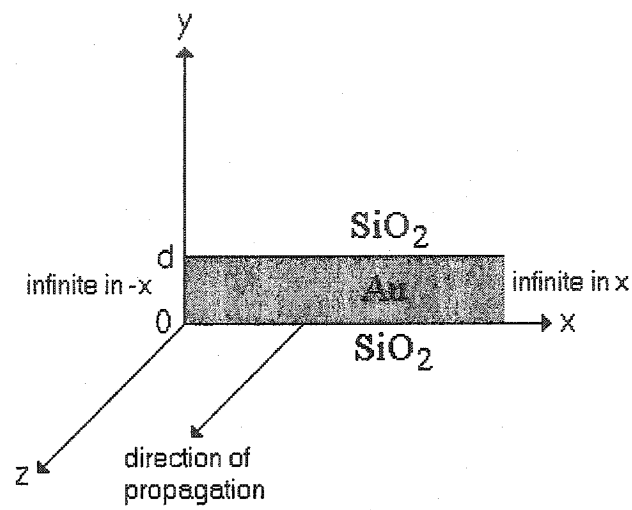

Figure 5.1 Orientation of the thin gold film bounded by silicon dioxide and the direction of wave propagation in cartesian coordinates

The analysis will be performed at a free space wavelength of 1550nm, as was done in the previous work [4]. At this wavelength, Palik [45] gives the complex refractive index of gold as N = 0.55-j11.5, from which the relative permittivity can be calculated by taking its square: ε_r = -131.9475-j12.65. The refractive index of silicon dioxide is not given by Palik for a wavelength of exactly 1550nm but can be estimated from the values that he provides for wavelengths above and below 1550nm and is found to be n = 1.444. The relative permittivity of silicon dioxide is found by taking the square of the refractive index: ε_r = 2.085136. These are the values used for the relative permittivities of gold and silicon dioxide in the following analysis, however they are slightly different from those used in reference [44] as presented in the previous chapter.

When an external magnetic field is applied to the structure, the permittivity of the gold becomes a tensor as shown in equations (2.35), (2.41) and (2.42) for a magnetic field in the Faraday, Voigt and perpendicular orientations, respectively. The nominal relative permittivity of gold is $\varepsilon_r = -131.9475\text{-}j12.65$. By using equations (2.38), (2.39) and (2.40), the plasma frequency, ω_0, and the effective electron collision frequency, ν, can be calculated from the nominal relative permittivity value. The gyro frequency is obtained by substituting the externally applied magnetic field into equation (2.19). Once the plasma frequency, the effective electron collision frequency and the gyro frequency have been calculated they are substituted into equation (2.35) to get the permittivity tensor. Once the permittivity tensor has been found it can be used in the code described in the previous chapter to determine the propagation constants at different magnetic field strengths.

5.1 No Externally Applied Magnetic Field

5.1.1 Dispersion Curves

The dispersion curves as a function of film thickness for an infinitely wide thin film of gold bounded by semi-infinite silicon dioxide using Palik's relative permittivity values are shown in Figure 5.2 and Figure 5.3.

It can be seen from Figure 5.3, that as the film thickness increases, the symmetric and asymmetric bound modes converge to the mode supported by a single metal-dielectric interface. As the film thickness decreases, the plasmon-polariton modes supported at each metal-dielectric interface become coupled by tunnelling through the metal film and the two bound modes become distinct. The effective index of refraction (β_z/β_0) of the symmetric bound mode tends towards the index of the background, 1.444, as the thickness of the film decreases. It can, therefore, be inferred that most of the power of the symmetric bound mode is in the surrounding dielectric and, thus, the value of the effective index of refraction is mainly governed by that of the supporting medium. The effective index of refraction of the asymmetric bound mode tends asymptotically towards infinity as the thickness of the film decreases, indicating that the velocity of the propagating mode decreases with thickness [44]. From this result, it can be inferred that most of the power of the asymmetric bound mode is in the metal film.

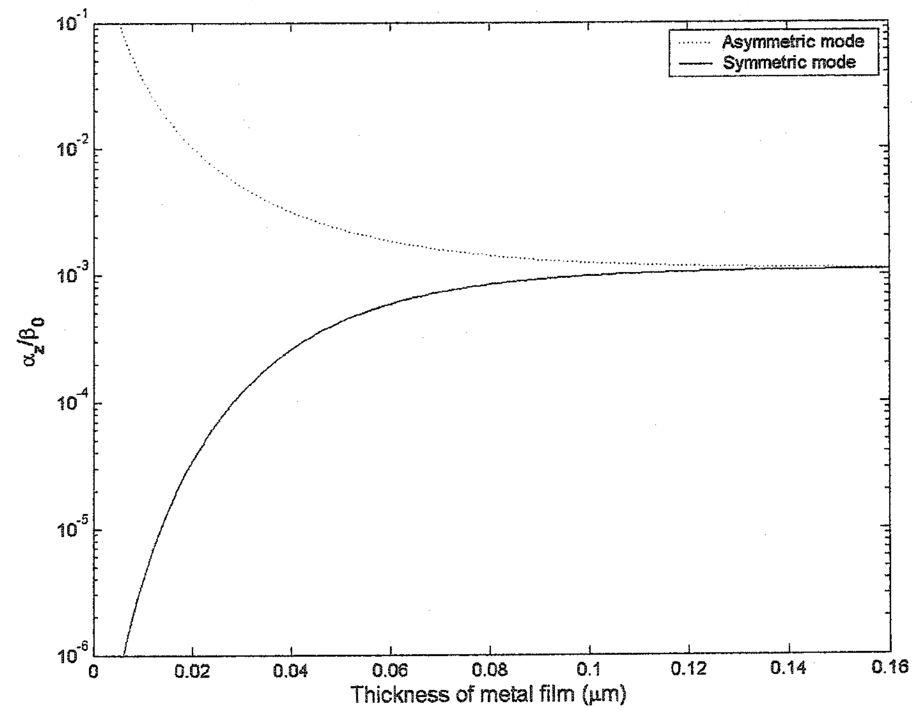

Figure 5.2 Simulated dispersion curves for the normalized attenuation constant of two bound modes supported by a thin Au film bounded by semi-infinite SiO_2, at free space wavelength of 1550nm. The relative permittivities are ε_{Au}=-131.9475-j12.65 and ε_{SiO_2}=2.085136 for gold and silicon dioxide, respectively.

Figure 5.2 presents the normalized attenuation constant for the two bound modes. It can be seen that the attenuation of the symmetric mode decreases significantly with decreasing metal thickness, whereas the attenuation of the asymmetric mode increases significantly with decreasing metal thickness. This behaviour is due to the distribution of the power of each mode: the symmetric mode has more power in the dielectric and the asymmetric mode has more power in the metal.

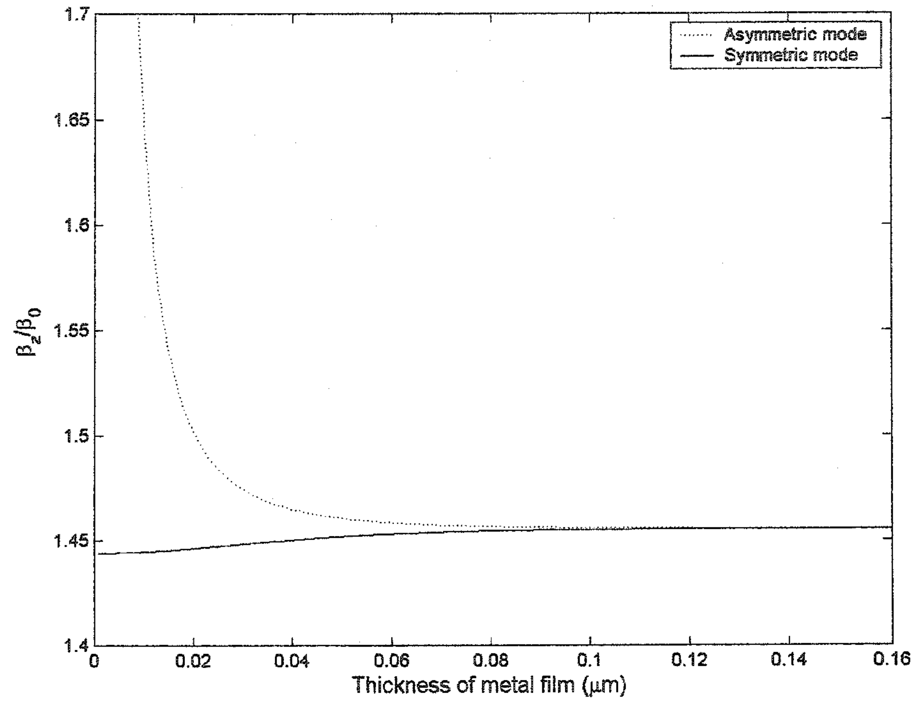

Figure 5.3 Simulated dispersion curves for the normalized phase constant of two bound modes supported by a thin Au film bounded by semi-infinite SiO_2, at free space wavelength of 1550nm. The relative permittivities are ε_{Au}=-131.9475-j12.65 and ε_{SiO_2}=2.085136 for gold and silicon dioxide, respectively.

In a real structure, there are three loss mechanisms that contribute to attenuation losses: losses in the metal, losses in the dielectric and scattering losses. In the case of silicon dioxide at this wavelength, the extinction coefficient taken from reference [45] is zero indicating that there are no losses associated with it. In addition, a perfect metal dielectric interface has been assumed in this model such that scattering losses are negligible. Therefore, the only source of loss in this structure is the absorption in the metal.

From Figure 5.2 and Figure 5.3, excitation of the symmetric bound mode in a film with the smallest possible thickness will provide the lowest loss plasmon-polariton propagation. In previous work, a thickness of 20nm was chosen [4]. This thickness may have been chosen because, at this thickness, gold can be deposited in a relatively uniform film when compared with thinner gold films. Due to its low attenuation level and its use in previous work, a thickness of 20nm will be used as the gold film thickness in this analysis.

5.1.2 Field Components

When no magnetic field is applied, the dielectric constant is not a tensor and, therefore, the modes are purely transverse magnetic in nature. That is, they only have three field components: E_y, E_z and H_x. These three field components, along with the Poynting vector of the asymmetric bound mode of a 20nm thick gold film bounded by silicon dioxide at the wavelength of 1550nm, with no external magnetic field, are shown in Figure 5.4 and Figure 5.5, respectively. The three main transverse magnetic field components and the Poynting vector of the symmetric bound mode are shown in Figure 5.6 and Figure 5.7, respectively.

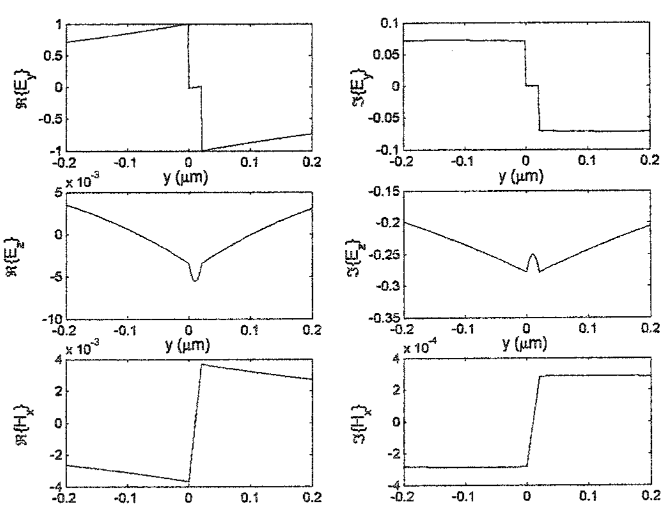

Figure 5.4 Simulated electric (E_y, E_z) and magnetic (H_x) fields of the asymmetric bound mode supported by a 20nm Au film bounded by semi-infinite SiO_2, with no external magnetic field, at free space wavelength of 1550nm. The propagation constant is 41534.60773993610 + j6088192.914047782.

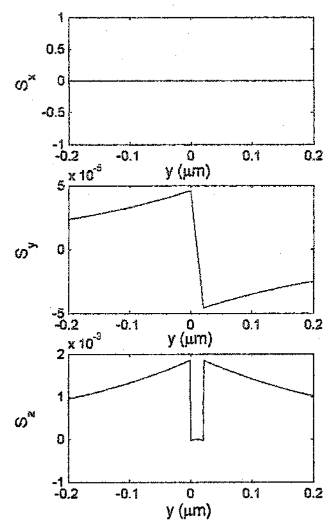

Figure 5.5 Poynting vector of the asymmetric bound mode supported by a 20nm Au film bounded by semi-infinite SiO_2, with no external magnetic field, at free space wavelength of 1550nm. The propagation constant is 41534.60773993610 + j6088192.914047782.

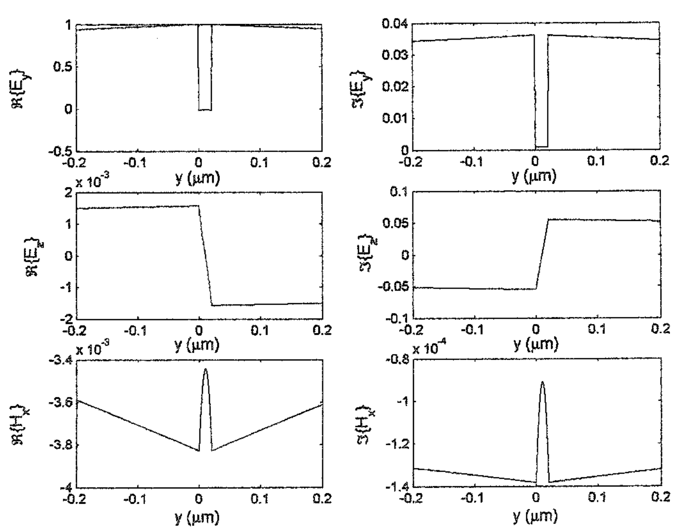

Figure 5.6 Simulated electric (E_y, E_z) and magnetic (H_x) fields of the symmetric bound mode supported by a 20nm Au film bounded by semi-infinite SiO_2, with no external magnetic field, at free space wavelength of 1550nm. The propagation constant is 139.4062040426159 + j5862484.452181567.

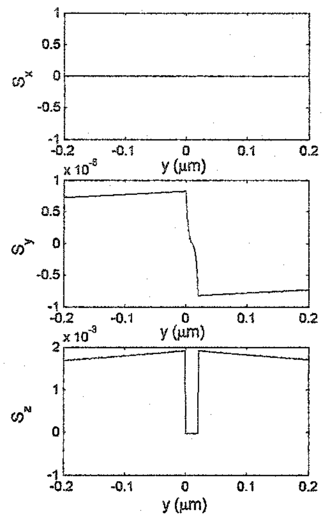

Figure 5.7 Poynting vector of the symmetric bound mode supported by a 20nm Au film bounded by semi-infinite SiO_2, with no external magnetic field, at free space wavelength of 1550nm. The propagation constant is 139.4062040426159 + j5862484.452181567.

The mode is defined as asymmetric when its E_y and H_x field components are asymmetric about the metal slab, as can been seen in Figure 5.4. Likewise, the mode is defined as symmetric when its E_y and H_x field components are symmetric about the metal slab, as can been seen in Figure 5.6. Both the asymmetric and symmetric modes have only the three field components that make them purely transverse magnetic in nature.

From Figure 5.5 and Figure 5.7, it can be seen that there is more of the energy of the symmetric mode in the surrounding dielectric when compared to the asymmetric mode. This can seen from the sloping lines in the Poynting vector as it approaches the film at y=0 and y=20nm in the asymmetric case as compared to the straighter lines in the symmetric case. The more energy there is in the dielectric, the less there is in the metal, which is lossy, making the overall mode less lossy. From the Poynting vector it can be seen that the symmetric mode is less lossy than the asymmetric mode for a 20nm gold film.

In Figure 5.2 and Figure 5.3, it can be seen that the propagation constants of the symmetric and asymmetric modes are much more similar when the film is 100nm thick than when it is 20nm. By looking at the field components and especially the Poynting vectors, it is possible to see the similarities in the asymmetric and symmetric modes at a film thickness of 100nm. The field components and Poynting vectors along the y-axis are shown in Figure 5.8 and Figure 5.9, respectively, for the asymmetric mode, and in Figure 5.10 and Figure 5.11, respectively, for the symmetric mode.

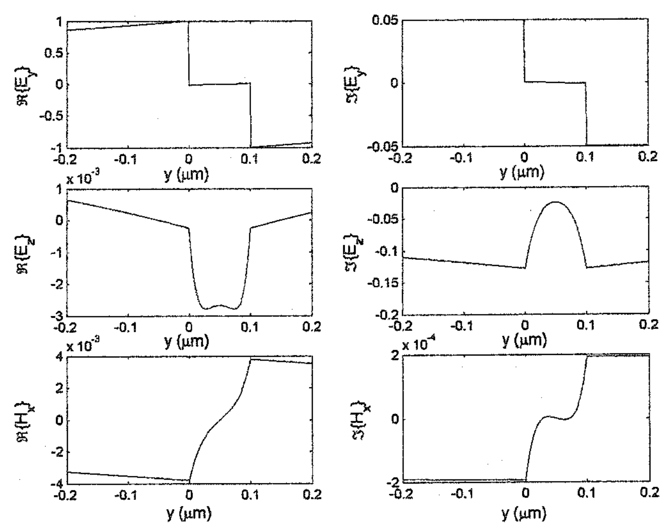

Figure 5.8 Simulated electric (E_y, E_z) and magnetic (H_x) fields of the asymmetric bound mode supported by a 100nm Au film bounded by semi-infinite SiO_2, with no external magnetic field, at free space wavelength of 1550nm. The propagation constant is 5042.763503612161 + j5901498.858084749.

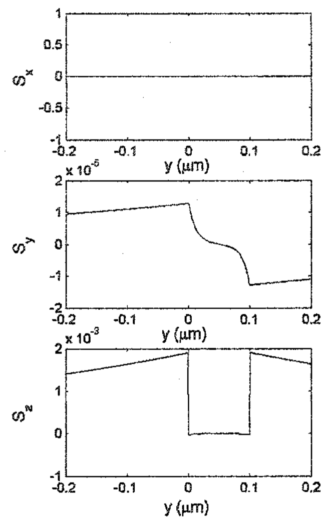

Figure 5.9 Poynting vector of the asymmetric bound mode supported by a 100nm Au film bounded by semi-infinite SiO_2, with no external magnetic field, at free space wavelength of 1550nm. The propagation constant is 5042.763503612161 + j5901498.858084749.

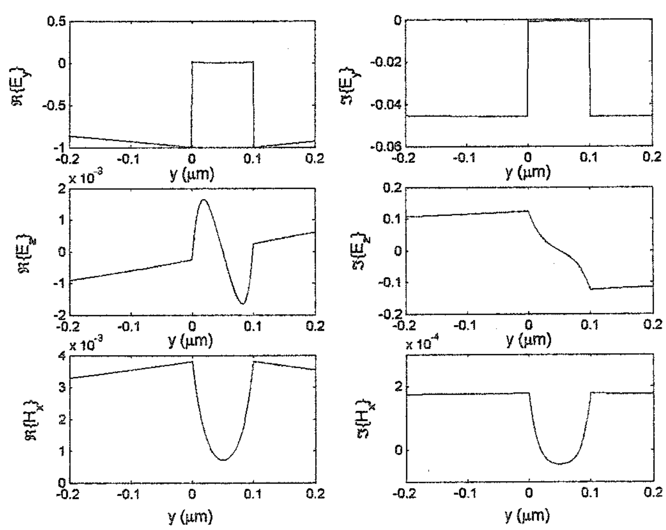

Figure 5.10 Simulated electric (E_y, E_z) and magnetic (H_x) fields of the symmetric bound mode supported by a 100nm Au film bounded by semi-infinite SiO_2, with no external magnetic field, at free space wavelength of 1550nm. The propagation constant is 3986.507952717954 + j5898285.990536048.

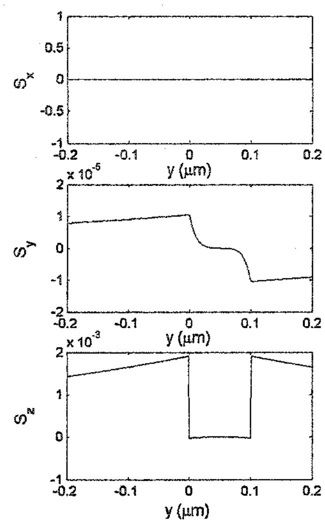

Figure 5.11 Poynting vector of the symmetric bound mode supported by a 100nm Au film bounded by semi-infinite SiO_2, with no external magnetic field, at free space wavelength of 1550nm. The propagation constant is 3986.507952717954 + j5898285.990536048.

By comparing the Poynting vectors for the asymmetric and symmetric modes, in Figure 5.9 and Figure 5.11, it can be seen that they are almost identical. This means that the asymmetric and symmetric modes have very similar characteristics, as expected because of the similarity of the propagation constants. At a film thickness of 100nm there is no real advantage of exciting the symmetric mode over exciting the asymmetric mode since they are so similar and have similar losses.

5.2 External Magnetic Field Applied in the Faraday Orientation

When an external magnetic field is applied in the Faraday orientation it is in the same direction as the wave propagation. This is in the z-direction with respect to Figure 5.1. For this reason, it induces off-diagonal field components in the permittivity tensor in all but the z positions, as shown in equation (5.1). This induces the three other field components (E_x, H_y and H_z) in addition to the transverse magnetic components (E_y, E_z and H_x). Notice that the diagonal tensor element in the z position remains constant as the external magnetic field changes since the gyro frequency is not present in this element.

$$\tilde{\varepsilon} = \varepsilon_0 \begin{bmatrix} 1+\dfrac{\omega_0^2(\omega-j\nu)}{\omega(\omega_g^2-(\omega-j\nu)^2)} & \dfrac{-j\omega_0^2\omega_g}{\omega(\omega_g^2-(\omega-j\nu)^2)} & 0 \\ \dfrac{j\omega_0^2\omega_g}{\omega(\omega_g^2-(\omega-j\nu)^2)} & 1+\dfrac{\omega_0^2(\omega-j\nu)}{\omega(\omega_g^2-(\omega-j\nu)^2)} & 0 \\ 0 & 0 & 1-\dfrac{\omega_0^2}{\omega(\omega-j\nu)} \end{bmatrix} \tag{5.1}$$

5.2.1 Dispersion Curves for the Asymmetric Mode

In this case, the dispersion curves are shown for a second thickness of 40nm, as well as at 20nm, to examine the dependence on thickness. At a thickness of 40nm, the modes are still distinct, as can be seen in Figure 5.2 and Figure 5.3, although there is more metal that will be affected by the externally applied magnetic field. The dispersion curves of the propagation constant of a 20nm thick gold film and a 40nm thick gold film bounded by semi-infinite silicon dioxide under the influence of an externally applied magnetic field in the Faraday (z) orientation have been simulated for magnetic fields ranging from 1 μ Tesla to 1 kTesla. The Earth's magnetic field is about 50μ T. A refrigerator magnet can produce a magnetic field of about 0.02T and a superconducting magnet can produce a magnetic field of about 20T. Although a pulse magnet can produce a magnetic pulse of more than 1kT it can only do so for a few millionths of a second. The range chosen for the magnetic field simulations covers the range over which magnetic fields can be produced in practice. The dispersion curves of the asymmetric bound mode for the normalized attenuation constants and normalized phase constants, at the free space wavelength of 1550nm are shown in Figure 5.12 and Figure 5.13, respectively.

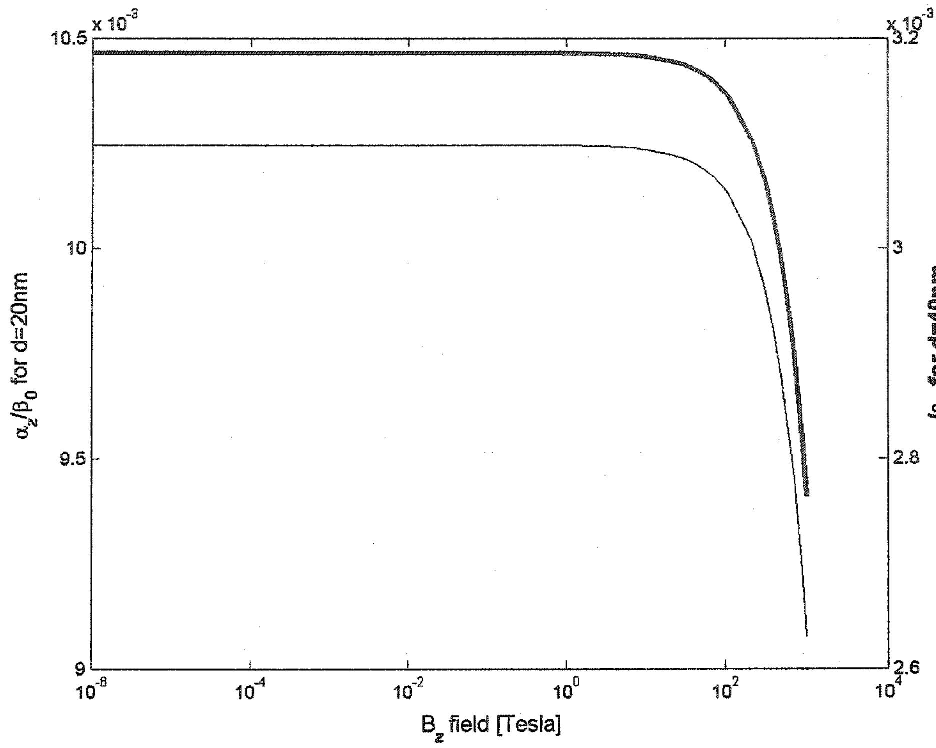

Figure 5.12 Simulated dispersion curve for the normalized attenuation constant of the asymmetric bound mode supported by a thin Au film bounded by semi-infinite SiO_2, with an external magnetic field applied in the z direction (Faraday), at free space wavelength of 1550nm. Refer to the right-hand axis for the bold curve and the left-hand axis for the regular curve.

The attenuation constant of the asymmetric bound mode supported by a thin gold film bounded by semi-infinite silicon dioxide, with an external magnetic field applied in the z direction (Faraday) decreases as the magnetic field increases. The attenuation constant decreases because the fields are less confined to the metal and therefore less energy is being lost through attenuation in the metal. When a magnetic field of 1000 Tesla is applied to the 20nm thick film, the attenuation constant decreases by 13% of its value when close to no magnetic field, 1 μ T, is applied: from 41535 to 36794. This is a change in attenuation per length of the slab of about 0.05dB/cm. The attenuation constant is thickness dependent; it has a lower initial value and does not change as rapidly for the thicker film

(40nm). However, the attenuation constants for both thicknesses follow the same decreasing trend as the externally applied magnetic field increases.

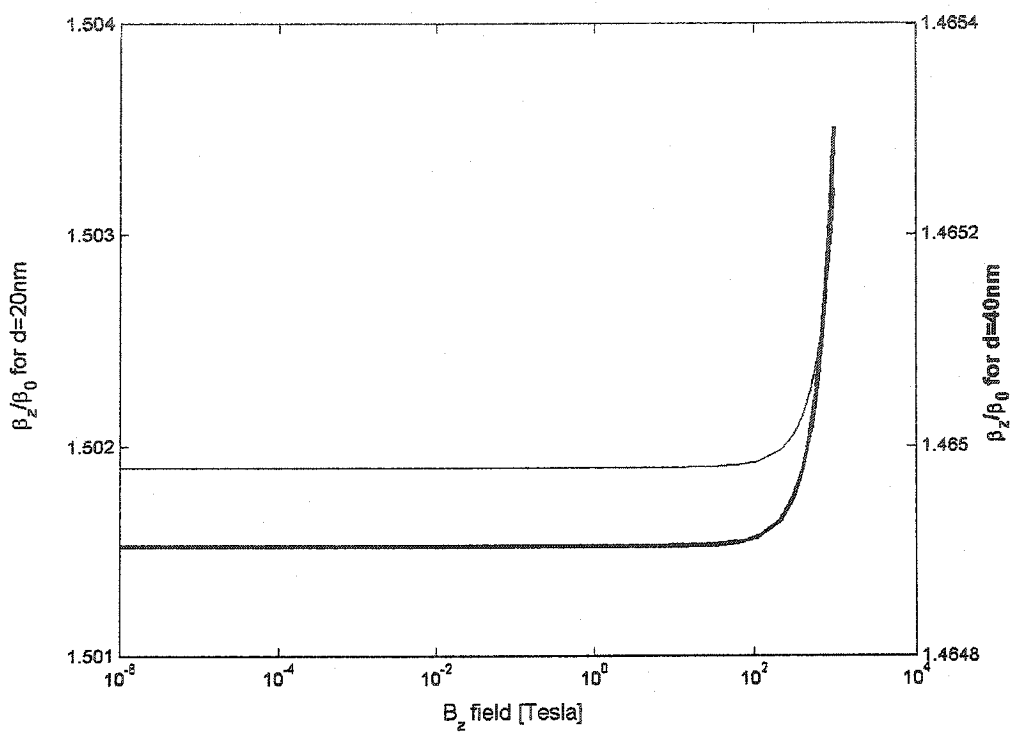

Figure 5.13 Simulated dispersion curve for the normalized phase constant of the asymmetric bound mode supported by a thin Au film bounded by semi-infinite SiO_2, with an external magnetic field applied in the z direction (Faraday), at free space wavelength of 1550nm. Refer to the right-hand axis for the bold curve and the left-hand axis for the regular curve.

The phase constant of the asymmetric bound mode supported by a thin gold film bounded by semi-infinite silicon dioxide, with an external magnetic field applied in the z direction (Faraday) increases as the magnetic field increases. When the magnetic field varies from $1\mu T$ to 1kT in the 20nm thick film case, the phase constant increases by 0.09%; it is $6.0882x10^6$ at $1\mu T$ and it is $6.0935x10^6$ at 1kT. For the 40nm thick film, the phase constant increases in the same manner as for the 20nm thick film but not as rapidly.

5.2.2 Field Components for the Asymmetric Mode

When a magnetic field is applied in the Faraday or z direction it is parallel with the direction of propagation. Therefore, it does not affect the asymmetric or symmetric nature of the modes but only stimulates additional field components. All six electric and magnetic field components of the asymmetric bound mode of a 20nm thick gold film bounded by semi-infinite-silicon dioxide at the wavelength of 1550nm, with a magnetic field of 1T applied in the Faraday direction (z), are shown in Figure 5.14 and Figure 5.15, and the Poynting vector is shown in Figure 5.16. The three main transverse magnetic field components are shown in Figure 5.14, and the other three field components are shown in Figure 5.15.

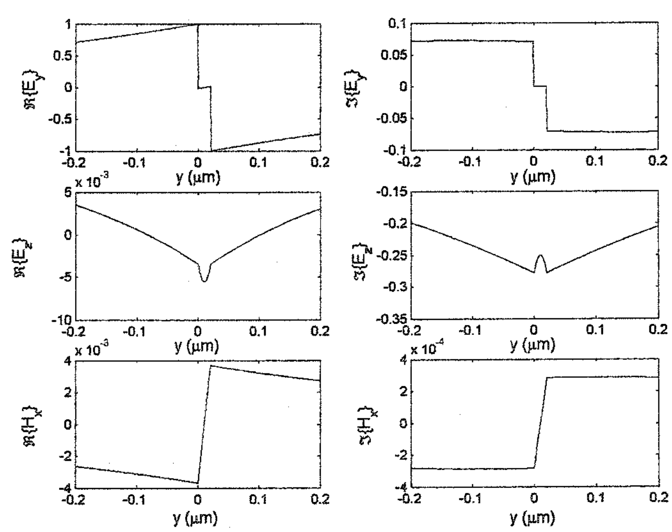

Figure 5.14 Simulated electric (E_y, E_z) and magnetic (H_x) fields of the asymmetric bound mode supported by a thin Au film bounded by semi-infinite SiO_2, with an external magnetic field of 1 T applied in the z direction (Faraday), at free space wavelength of 1550nm. The propagation constant is 41530.22007494762 + j6088193.502466070.

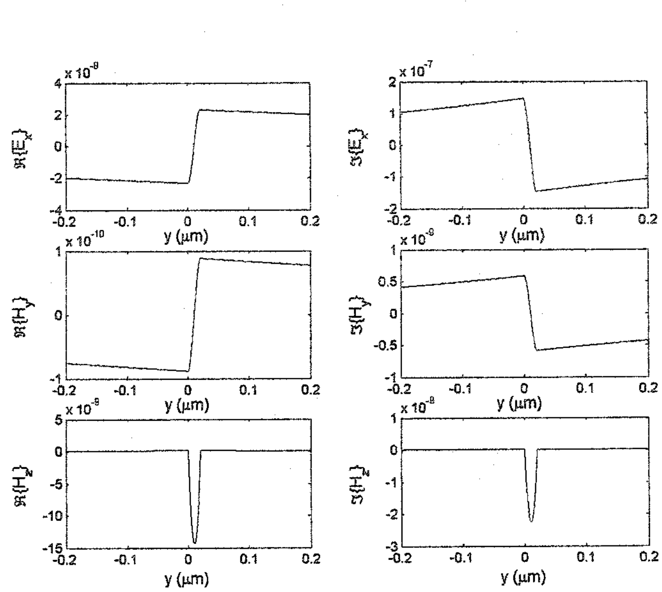

Figure 5.15 Simulated electric (E_x) and magnetic (H_y, H_z) fields of the asymmetric bound mode supported by a thin Au film bounded by semi-infinite SiO_2, with an external magnetic field of 1 T applied in the z direction (Faraday), at free space wavelength of 1550nm. The propagation constant is 41530.22007494762 + j6088193.502466070.

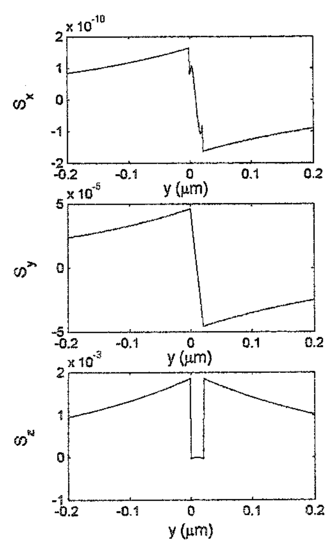

Figure 5.16 Poynting vector of the asymmetric bound mode supported by a thin Au film bounded by semi-infinite SiO_2, with an external magnetic field of 1 T applied in the z direction (Faraday), at free space wavelength of 1550nm. The propagation constant is 41530.22007494762 + j6088193.502466070.

Notice that all of the x and y field components, E_x, E_y, H_x and H_y, of the asymmetric bound mode are asymmetric about the metal slab, while both of the z field components, E_z and H_z, are symmetric about the metal slab, as seen in Figure 5.14 and Figure 5.15. The additional field components, E_x, H_y and H_z, are significantly smaller than the main transverse magnetic field components, E_y, E_z, and H_x. This indicates that the mode is still mainly transverse magnetic in nature when an external magnetic field of 1T is applied.

The real part of the Poynting vector represents power flow while the imaginary part represents stored energy. Therefore, by examining the real part of all three components of the Poynting vector it is possible to see the direction of power flow in the waveguide. The direction of power flow in the asymmetric bound mode supported by a thin Au film bounded by semi-infinite SiO_2, with an external magnetic field of 1 T applied in the z direction (Faraday) is shown in Figure 5.17.

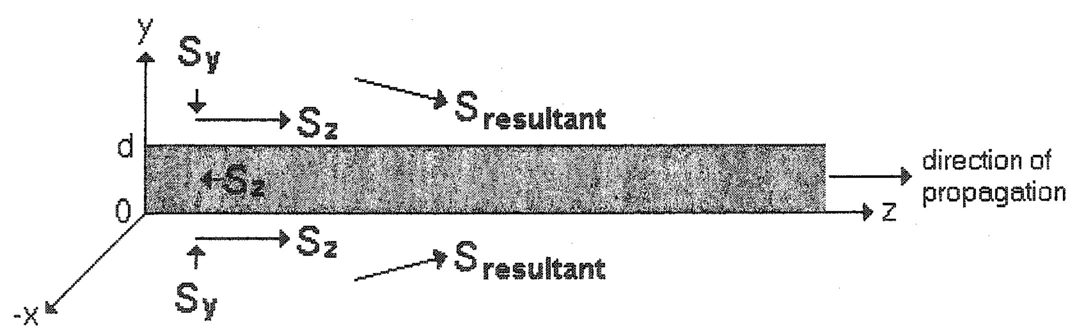

Figure 5.17 Direction of power flow in the asymmetric bound mode supported by a thin Au film bounded by semi-infinite SiO_2, with an external magnetic field of 1 T applied in the z direction (Faraday)

The Poynting vector of the asymmetric bound mode has its major component in the z-direction, which is the direction of wave propagation. Both above and below the metal slab, the power is mainly directed in the positive z-direction. However, in the metal slab the power is directed in the negative z-direction. This power is input power that was input at an earlier time and therefore appears to be flowing against the direction of propagation.

The secondary component of the Poynting vector is the y-directed component. Power flows into the metal slab from the top and the bottom. This is due to the fact that the metal is lossy and absorbs power. To maintain the steady state mode, power must flow into the metal. The greater the loss in the metal the greater the y-directed Poynting vector component. If there is no loss in the metal, the y-directed Poynting vector component would be zero. The x-directed Poynting vector component is seven and four orders of magnitude below the z-directed component and the y-directed component, respectively, therefore it is has a negligible effect on the resultant Poynting vector. The Poynting vector of the asymmetric bound mode is very similar to the unperturbed, zero externally applied magnetic field case shown in Figure 5.9. Therefore an externally applied magnetic field of 1T has very little effect on the asymmetric bound mode when applied in the Faraday orientation.

To get some insight into the effect of stronger magnetic fields on the asymmetric mode, the Poynting vector has been plotted in Figure 5.18 for an externally applied magnetic field of 1000T. By examining the real part of all three components of the Poynting vector it is possible to see the direction of power flow in the waveguide. The direction of power flow in the asymmetric bound mode supported by a thin Au film bounded by semi-infinite SiO_2, with an externally applied magnetic field of 1000 T applied in the z direction (Faraday) is shown in Figure 5.19. At an externally applied magnetic field of 1000T, the power flow is still mainly in the z-direction but the x-component of the Poynting vector is more significant when a larger magnetic field is applied. This is due to the fact that the secondary field components, due to the off-diagonal tensor elements, are becoming more significant. The x-component of the Poynting vector is positive below the film and negative above the film, indicating that the power flows in opposite directions above and below the film. A slight asymmetry is also introduced in the y-direction inside the metal. There is more y-directed power inside the metal at the upper interface than at the lower interface. Because this additional power is greater than the y-directed power in the dielectric above the metal, there is a small spike in the y-component of the Poynting vector.

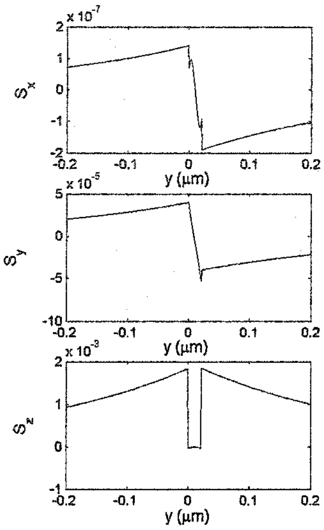

Figure 5.18 The Poynting vector of the asymmetric bound mode supported by a thin Au film bounded by semi-infinite SiO_2, with an external magnetic field of 1000 T applied in the z direction (Faraday), at free space wavelength of 1550nm.

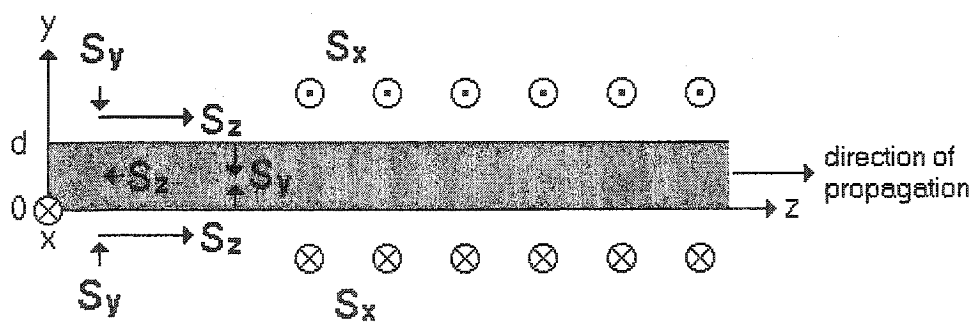

Figure 5.19 Direction of power flow in the asymmetric bound mode supported by a thin Au film bounded by semi-infinite SiO_2, with an external magnetic field of 1000 T applied in the z direction (Faraday)

The relative permittivity tensor components as a function of magnetic field are shown in Figure 5.20. As the magnetic field increases, the real and imaginary parts of the diagonal components of the permittivity tensor remain constant (ε_{zz}) or increase in magnitude (ε_{xx}, ε_{yy}). The magnitudes of the real and imaginary parts of the off-diagonal components of the permittivity tensor increase linearly with magnetic field. The real part of the permittivity tensor primarily affects the phase constant. As the real part of the diagonal components of the permittivity tensor increases in magnitude, the phase constant will also tend to increase, if this is the primary influence on the phase constant, which it is for the asymmetric mode. The imaginary part of the diagonal components of the permittivity tensor affects primarily the attenuation constant. As the externally applied magnetic field increases, the imaginary part of the diagonal components of the permittivity tensor increase, indicating that the losses in the metal are increasing. Normally this phenomenon would cause the attenuation constant to increase, however it is decreasing. This indicates that the fields are being pushed out of the metal film and are, therefore, less attenuated by its losses.

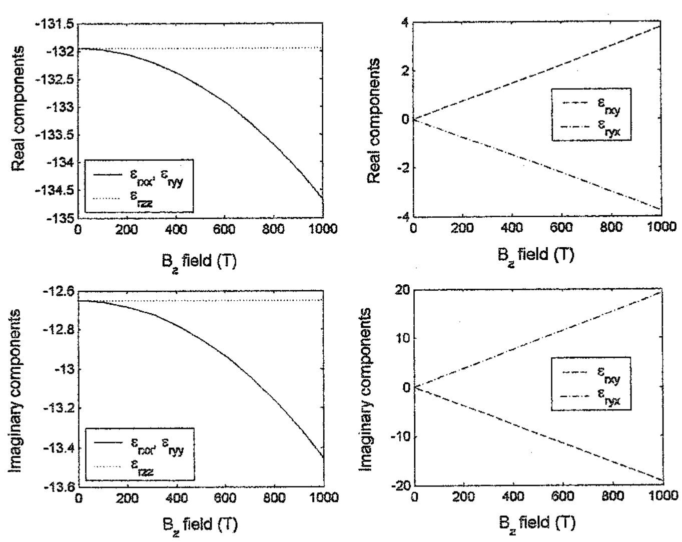

Figure 5.20 Components of the relative permittivity tensor as a function of an externally applied magnetic field in the Faraday (z) direction

5.2.3 Dispersion Curves for the Symmetric Mode

The dispersion curves of the propagation constant of a 20nm thick gold film and a 40nm thick gold film bounded by semi-infinite silicon dioxide under the influence of an externally applied magnetic in the Faraday (z) orientation have been simulated for the symmetric bound mode. The dispersion curves of the symmetric bound mode for the normalized attenuation constants and normalized phase constants, at the free space wavelength of 1550nm are shown in Figure 5.22 and Figure 5.21, respectively.

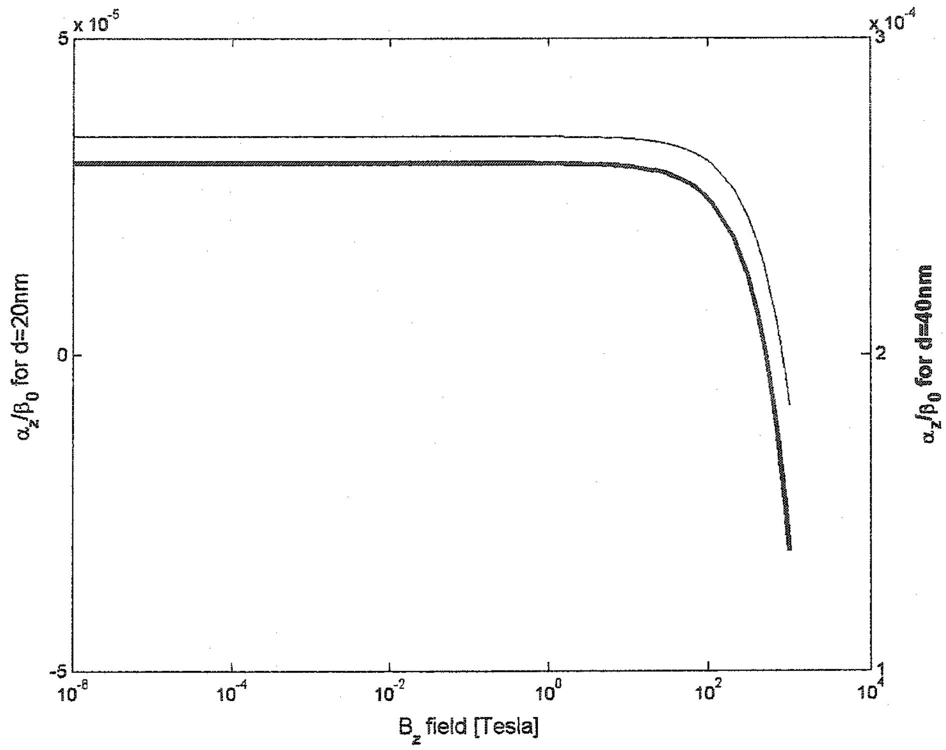

Figure 5.21 Simulated dispersion curve for the normalized attenuation constant of the symmetric bound mode supported by a thin Au film bounded by semi-infinite SiO_2, with an external magnetic field applied in the z direction (Faraday), at free space wavelength of 1550nm. Refer to the right-hand axis for the bold curve and the left-hand axis for the regular curve.

The attenuation constant of the symmetric bound mode supported by a thin gold film bounded by semi-infinite silicon dioxide, with an external magnetic field applied in the z direction (Faraday) decreases as the magnetic field increases. In the case of the 20nm thick film, the attenuation constant reaches zero and begins to go negative when the magnetic field is approximately 800 Tesla. A change of sign in the attenuation constant indicates that the mode is no longer losing energy as it propagates but gaining energy. The mode represented here is physically realizable if energy is fed into the structure from the top or bottom at a slight angle. This energy will begin to compensate for the losses in the metal and may actually exceed the losses in the metal as the tilt angle increases [46]. This will be demonstrated below by inspecting the fields.

In the case of the 40nm thick film, the mode is more tightly bound to the metal, therefore the attenuation constant is higher than in the case of the 20nm thick film and does not cross zero for any externally applied magnetic fields up to 1000 Tesla. However, the attenuation constant does follow the same trend for both thicknesses, therefore it will cross zero at a higher externally applied magnetic field in the case of the 40nm thick film.

The phase constant of the symmetric bound mode supported by a thin gold film bounded by semi-infinite silicon dioxide, with an external magnetic field applied in the z direction (Faraday) tends towards the phase constant of the background as the magnetic field increases, then it increases as the magnetic field increases. In the case of the 20nm thick film, the minimum is at about 210T. If the dispersion curve for the 40nm thick film is examined closely, it can be seen that it follows the same trend as the curve for the 20nm thick film but has its minimum around 10T. This trend indicates that the mode is evolving into another mode. When the behaviour of the attenuation constant is compared with the behaviour of the phase constant, it can be seen that as the externally applied magnetic field increases, the mode is cutting off, and more and more of the mode power is outside of the metal, therefore the attenuation constant decreases. As the original mode is replaced by the top and bottom fed mode discussed above, the phase constant begins to increase and the attenuation constant continues to decrease as the mode is fed additional energy. Once the additional energy overcomes the losses in the metal, the attenuation constant crosses zero.

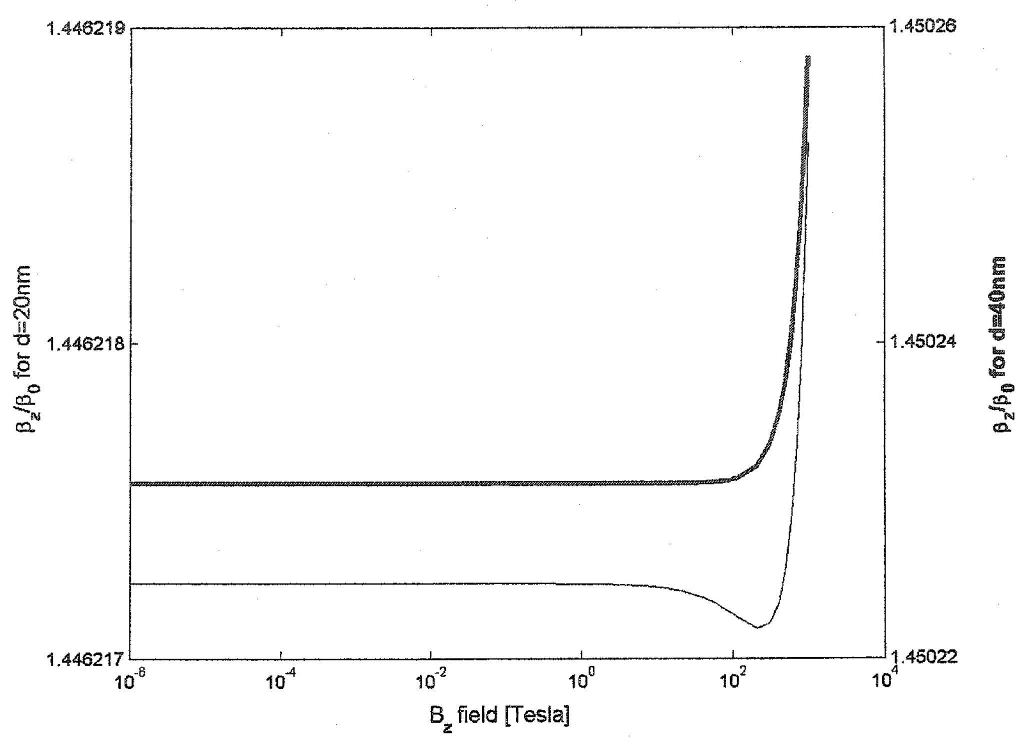

Figure 5.22 Simulated dispersion curve for the normalized phase constant of the symmetric bound mode supported by a thin Au film bounded by semi-infinite SiO_2, with an external magnetic field applied in the z direction (Faraday), at free space wavelength of 1550nm. Refer to the right-hand axis for the bold curve and the left-hand axis for the regular curve.

5.2.4 Field Components for the Symmetric Mode

The three main transverse magnetic field components, the other three field components and the Poynting vector of the symmetric bound mode with an external magnetic field of 1 T applied in the z-direction are shown in Figure 5.23, Figure 5.24 and Figure 5.25, respectively.

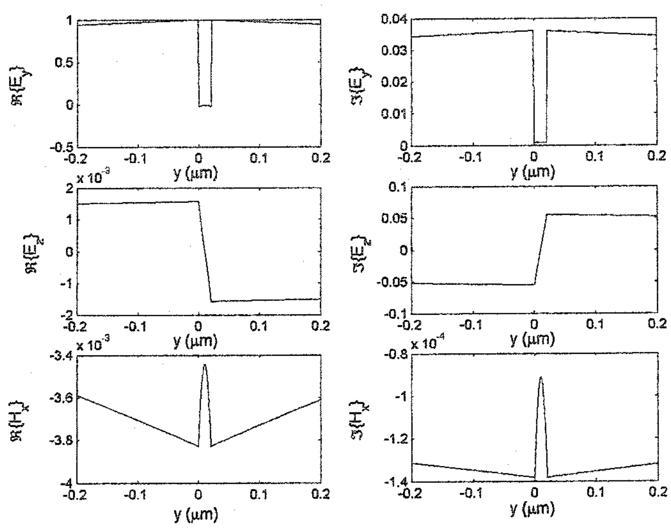

Figure 5.23 Simulated electric (E_y, E_z) and magnetic (H_x) fields of the symmetric bound mode supported by a thin Au film bounded by semi-infinite SiO_2, with an external magnetic field of 1 T applied in the z direction (Faraday), at free space wavelength of 1550nm. The propagation constant is 139.2425472023547 + j5862484.447251684.

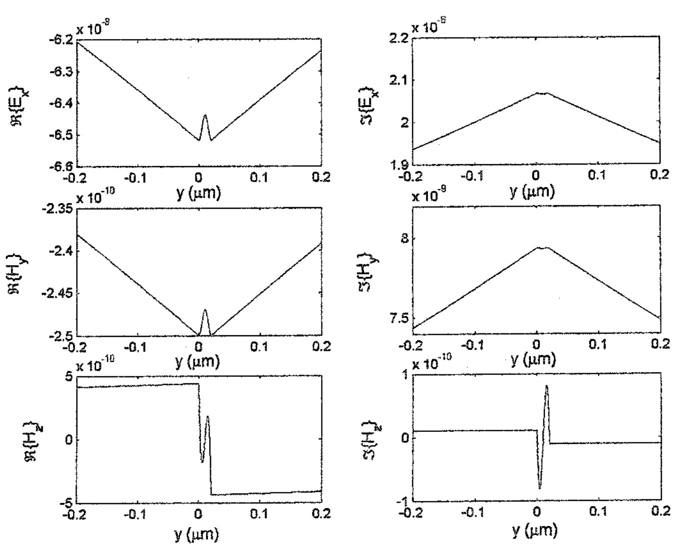

Figure 5.24 Simulated electric (E_x) and magnetic (H_y, H_z) fields of the symmetric bound mode supported by a thin Au film bounded by semi-infinite SiO_2, with an external magnetic field of 1 T applied in the z direction (Faraday), at free space wavelength of 1550nm. The propagation constant is 139.2425472023547 + j5862484.447251684.

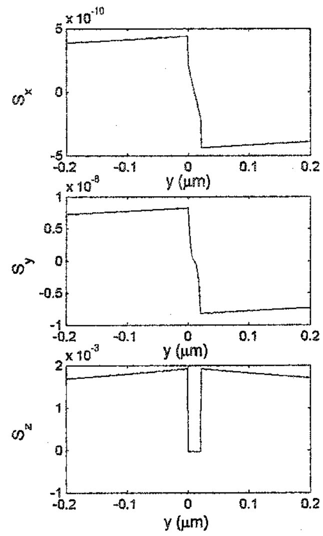

Figure 5.25 Poynting vector of the symmetric bound mode supported by a thin Au film bounded by semi-infinite SiO_2, with an external magnetic field of 1 T applied in the z direction (Faraday), at free space wavelength of 1550nm. The propagation constant is 139.2425472023547 + j5862484.447251684.

The symmetric bound mode is similar to the asymmetric bound mode in that all of its x and y field components, E_x, E_y, H_x and H_y, are symmetric about the metal slab, while both of its z field components, E_z and H_z, are asymmetric about the metal slab, as seen in Figure 5.23 and Figure 5.24. The additional field components, E_x, H_y and H_z, are also significantly smaller than the main transverse magnetic field components, E_y, E_z, and H_x, indicating that the mode is still mainly transverse magnetic in nature.

It can also be noted that the Poynting vector of the symmetric mode, in Figure 5.25, has a shape similar to the Poynting vector of the asymmetric mode in Figure 5.16. The power flow in the symmetric mode is similar to that of the asymmetric mode shown in Figure 5.17. However, there is more of the energy of the symmetric mode in the surrounding dielectric when compared to the asymmetric mode. This can seen from the sloping lines in the Poynting vector as it approaches the film at y=0 and y=20nm in the asymmetric case as compared to the straighter lines in the symmetric case. The more energy there is in the dielectric, the less there is in the metal, which is lossy, making the overall mode less lossy. From the Poynting vector it can be seen that the symmetric mode is less lossy than the asymmetric mode.

To see the effect of larger externally applied magnetic fields, the real part of the x-component of the Poynting vector and the y-component of the Poynting vector are plotted in Figure 5.26 and Figure 5.27, respectively, for various magnetic field levels: 10T, 100T, 500T, 800T, 900T and 1000T. The z-component of the Poynting vector is not plotted since it remains relatively unchanged from its value for an externally applied magnetic field of 1T over this range of externally applied magnetic field values.

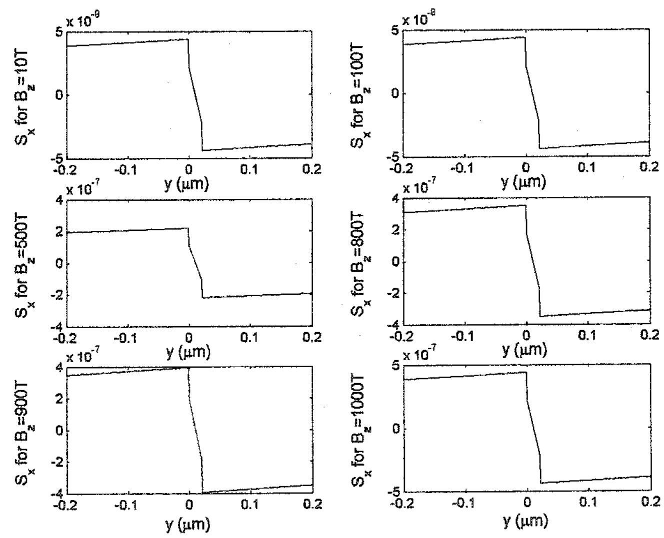

Figure 5.26 Poynting vector of the symmetric bound mode supported by a thin Au film bounded by semi-infinite SiO_2, with various external magnetic field levels applied in the z direction (Faraday), at free space wavelength of 1550nm.

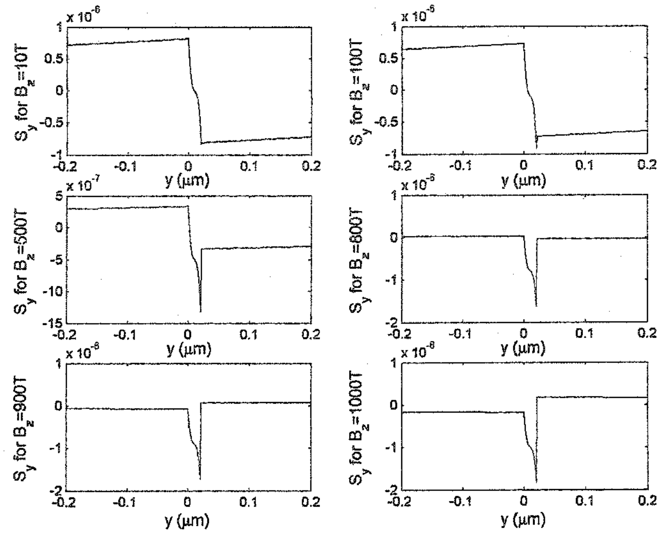

Figure 5.27 Poynting vector of the symmetric bound mode supported by a thin Au film bounded by semi-infinite SiO_2, with various external magnetic field levels applied in the z direction (Faraday), at free space wavelength of 1550nm.

It can be seen from Figure 5.26 that as the externally applied magnetic field increases, more and more power flows in the x and -x directions. When the externally applied magnetic field is 1000T, x-component of the Poynting vector is in the same range as the y-component. More interestingly, it can be seen from Figure 5.27, that as the externally applied magnetic field increases, the y-component of the Poynting vector is affected significantly. The power flowing into the waveguide from the bottom and the top decreases in magnitude and actually start flowing out of the waveguide instead of into it. This change occurs when the phase constant crosses zero just above 800T and the energy that is fed into the top and bottom fed mode overcomes the losses in the metal film. Some of the energy that is being fed into the top and bottom is absorbed by the metal and some is reflected by the metal. The reflected energy combines with previously reflected energy and radiation loss from the mode in the metal to form an increasing field above and below the metal film.

5.3 External Magnetic Field Applied in the Voigt Orientation

When a magnetic field is applied in the Voigt orientation it is parallel with the interface but perpendicular to the direction of propagation. This is in the x-direction with respect to Figure 5.1. For this reason, it induces off-diagonal field components in the permittivity tensor in all but the x positions, as shown in equation (5.2), and does not induce additional field components. Although an external magnetic field is applied, the wave remains purely transverse magnetic and only the three main field components (E_x, H_y and H_z) are present, if it is applied in the Voigt orientation. Notice that the diagonal tensor element in the x position remains constant as the external magnetic field changes since the gyro frequency is not present in this element.

$$\tilde{\varepsilon} = \varepsilon_0 \begin{bmatrix} 1 - \dfrac{\omega_0^2}{\omega(\omega - j\nu)} & 0 & 0 \\ 0 & 1 + \dfrac{\omega_0^2(\omega - j\nu)}{\omega(\omega_g^2 - (\omega - j\nu)^2)} & \dfrac{-j\omega_0^2\omega_g}{\omega(\omega_g^2 - (\omega - j\nu)^2)} \\ 0 & \dfrac{j\omega_0^2\omega_g}{\omega(\omega_g^2 - (\omega - j\nu)^2)} & 1 + \dfrac{\omega_0^2(\omega - j\nu)}{\omega(\omega_g^2 - (\omega - j\nu)^2)} \end{bmatrix} \qquad (5.2)$$

5.3.1 Dispersion Curves for the Asymmetric Mode

The dispersion curve of the propagation constant of a 20nm thick gold film and a 40nm thick gold film bounded by semi-infinite silicon dioxide under the influence of an externally applied magnetic field in the Voigt (x) orientation have been simulated for magnetic fields ranging from 1 μ Tesla to 1 kTesla. The dispersion curves of the asymmetric bound mode for the normalized attenuation constants and normalized phase constants, at the free space wavelength of 1550nm are shown in Figure 5.28 and Figure 5.29, respectively.

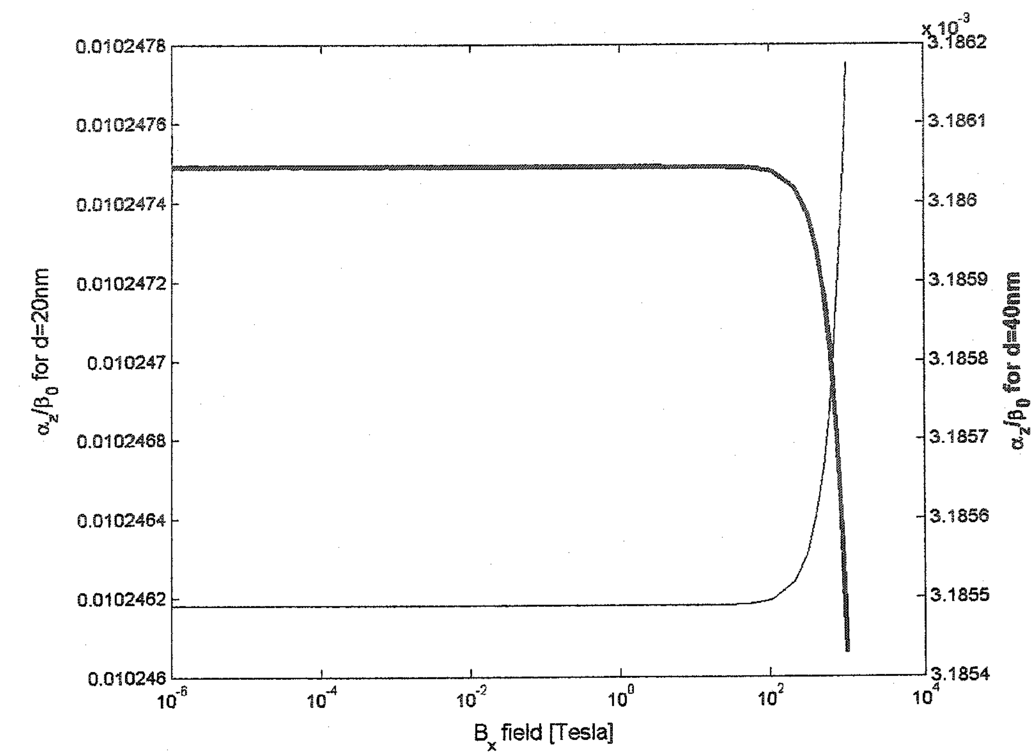

Figure 5.28 Simulated dispersion curve for the normalized attenuation constant of the asymmetric bound mode supported by a thin Au film bounded by semi-infinite SiO_2, with an external magnetic field applied in the x direction (Voigt), at free space wavelength of 1550nm. Refer to the right-hand axis for the bold curve and the left-hand axis for the regular curve.

It can been seen in Figure 5.28 that the response of the attenuation constant of the asymmetric bound mode to an external magnetic field applied in the Voigt direction is thickness dependent. In the case where the film is 20nm thick, the attenuation constant increases with increasing magnetic field, whereas, in the case where the film is 40nm thick, the attenuation constant decreases with increasing magnetic field. In both cases the changes in attenuation constant are very small. The increase in the magnitude of the imaginary part of the diagonal elements of the relative permittivity of the metal due to the application of the external magnetic field, as shown in Figure 5.20, increases the losses in the metal. As the losses in the metal go up it is expected that the attenuation constant will increase. This is the case when the metal is 20nm thick. However, the increase in magnitude of the real part of diagonal elements of the relative permittivity of the metal due to the application of the external magnetic field, as shown in Figure 5.20, causes the modes to be pushed out of the metal film. As the externally applied magnetic field increases in the case where the metal is 40nm thick, the real part of the diagonal elements of the relative permittivity cause the fields to be pushed out of the metal at a greater rate than the losses in the metal are increasing due to the imaginary part of the diagonal elements of the relative permittivity.

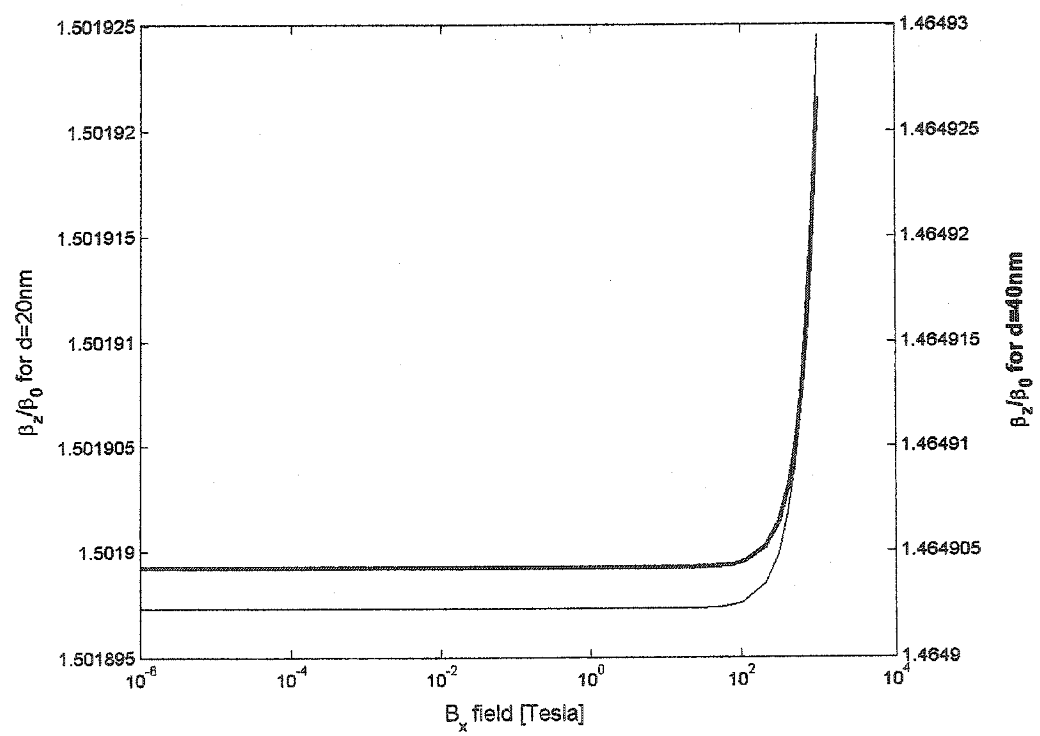

Figure 5.29 Simulated dispersion curve for the normalized phase constant of the asymmetric bound mode supported by a thin Au film bounded by semi-infinite SiO_2, with an external magnetic field applied in the x direction (Voigt), at free space wavelength of 1550nm. Refer to the right-hand axis for the bold curve and the left-hand axis for the regular curve.

It can be seen from Figure 5.29, that the phase constant of the asymmetric bound mode increases as the external magnetic field increases. The magnitude of the real part of the diagonal elements of the relative permittivity increases as the external magnetic field increases, as shown in Figure 5.20, allowing less of the mode to penetrate into the metal.

When the mode is pushed out of the metal the phase constant generally tends towards the phase constant of the background. However, when the mode is being pushed out of the metal because the magnitude of the real parts of the diagonal components of the permittivity tensor are increasing, a competing effect is present: the phase constant can increase. In this case, the latter effect overpowers the former effect and the phase constant increases as the magnetic field increases.

5.3.2 Field Components for the Asymmetric Mode

When a magnetic field is applied in the Voigt or x direction it is parallel with the interface but perpendicular to the direction of propagation. A magnetic field in the Voigt direction induces yz and zy off-diagonal components in the permittivity tensor. Since the other off-diagonal components are null, there is no x-directed electric field component. The y and z directed magnetic field components are dependent upon the x-direction field component, therefore, they are also null. This can be confirmed by examining the equations leading up to and including the dispersion relation.

The field components and the Poynting vector of the asymmetric bound mode of a 20nm thick gold film bounded by silicon dioxide at the wavelength of 1550nm, with a magnetic field of 1T applied in the Voigt direction (x), are shown in Figure 5.30 and Figure 5.31, respectively.

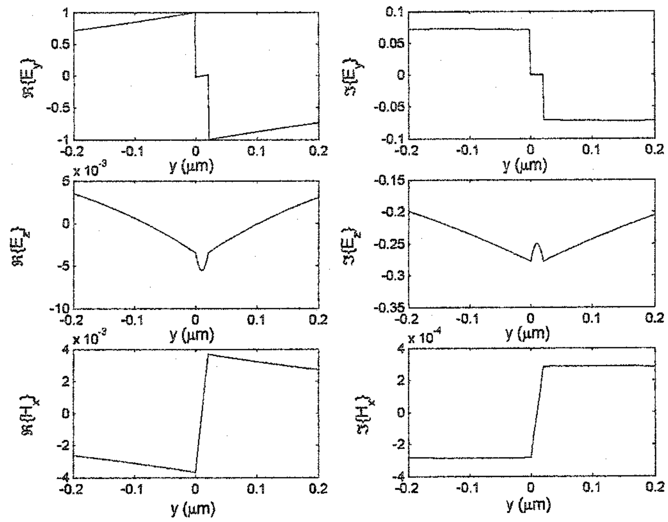

Figure 5.30 Simulated electric (E_y, E_z) and magnetic (H_x) fields of the asymmetric bound mode supported by a thin Au film bounded by semi-infinite SiO_2, with an external magnetic field of 1 T applied in the x direction (Voigt), at free space wavelength of 1550nm. The propagation constant is 41534.60774519816 + j6088192.914155815.

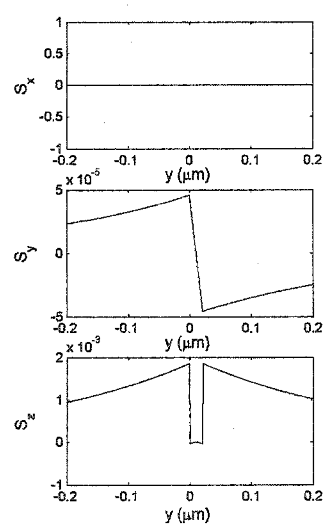

Figure 5.31 Poynting vector of the asymmetric bound mode supported by a thin Au film bounded by semi-infinite SiO_2, with an external magnetic field of 1 T applied in the x direction (Voigt), at free space wavelength of 1550nm. The propagation constant is 41534.60774519816 + j6088192.914155815.

The field components and the Poynting vector of the asymmetric bound mode of a 20nm thick gold film bounded by silicon dioxide at the wavelength of 1550nm, with a magnetic field of 1000T applied in the Voigt direction (x), are shown in Figure 5.32 and Figure 5.33, respectively.

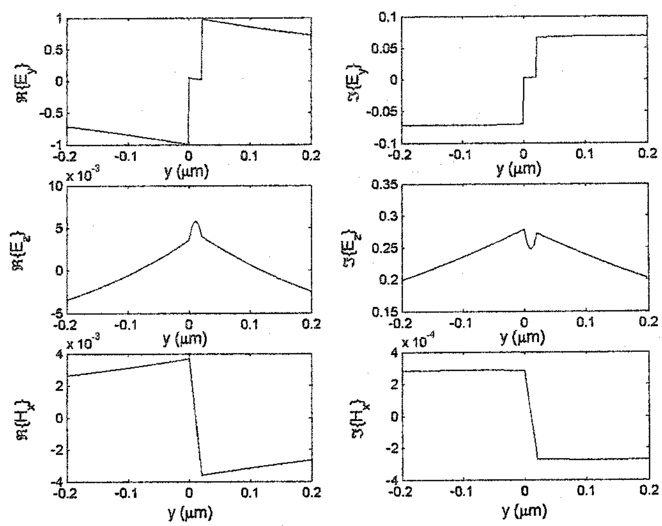

Figure 5.32 Simulated electric (E_y, E_z) and magnetic (H_x) fields of the asymmetric bound mode supported by a thin Au film bounded by semi-infinite SiO_2, with an external magnetic field of 1000 T applied in the x direction (Voigt), at free space wavelength of 1550nm.

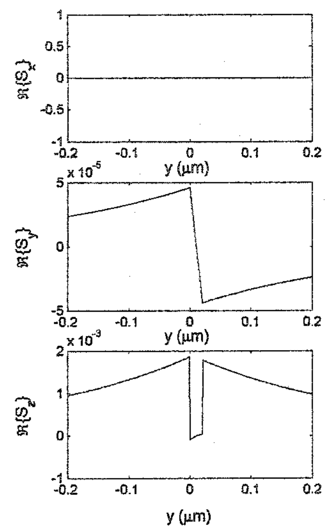

Figure 5.33 Poynting vector of the asymmetric bound mode supported by a thin Au film bounded by semi-infinite SiO_2, with an external magnetic field of 1000 T applied in the x direction (Voigt), at free space wavelength of 1550nm.

The propagation constant of the asymmetric bound mode under the influence of an external magnetic field of up to 1000T applied in the Voigt direction is slightly different from the propagation constant of the asymmetric bound mode for the nominal (no external magnetic field) case, but the fields and Poynting vector are not noticeably affected, as can be seen by comparing Figure 5.30 and Figure 5.32 with Figure 5.4, and Figure 5.31 and Figure 5.33 with Figure 5.5.

5.3.3 Dispersion Curves for the Symmetric Mode

The dispersion curves of the symmetric bound mode for the normalized attenuation constant and the normalized phase constant, at the free space wavelength of 1550nm are shown in Figure 5.34 and Figure 5.35, respectively.

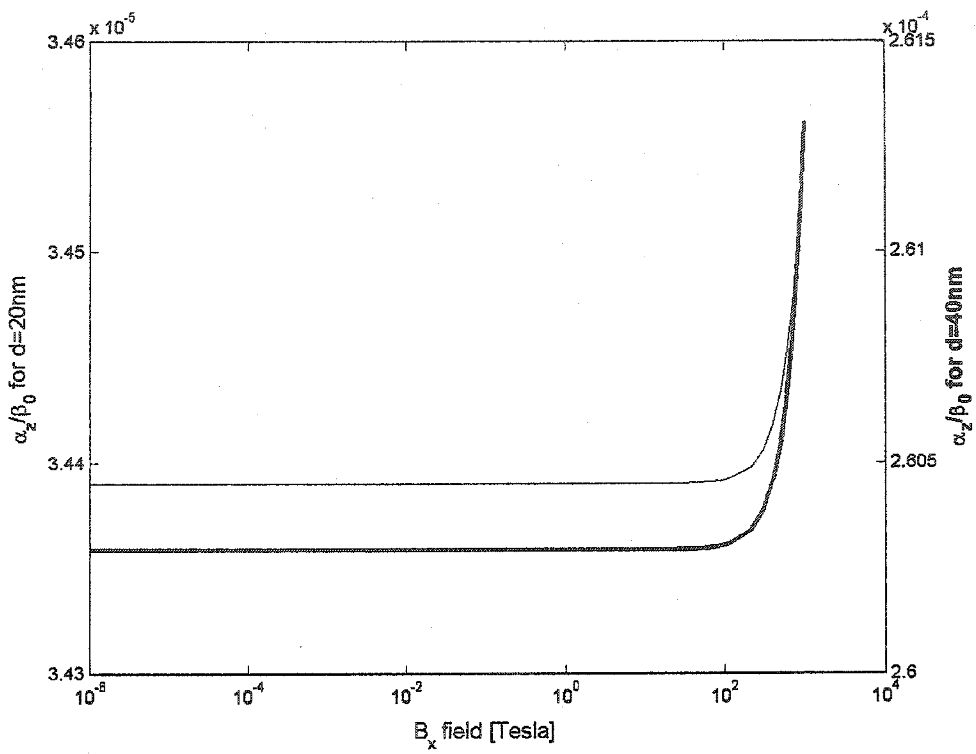

Figure 5.34 Simulated dispersion curve for the normalized attenuation constant of the symmetric bound mode supported by a thin Au film bounded by semi-infinite SiO_2, with an external magnetic field applied in the x direction (Voigt), at free space wavelength of 1550nm. Refer to the right-hand axis for the bold curve and the left-hand axis for the regular curve.

It can been seen in Figure 5.34 that the attenuation constant of the symmetric bound mode increases as the magnetic field increases. Both the 20nm thick case and the 40nm thick case increase in the same manner, but the 40nm thick case increases more rapidly. The increase in the magnitude of the imaginary part of the diagonal elements of the relative permittivity of the metal due to the application of the external magnetic field, as shown in Figure 5.20, increases the losses in the metal. As the losses in the metal increase, the attenuation constant is expected to increase if the mode is not being pushed out of the metal very rapidly. This is the case for both thicknesses.

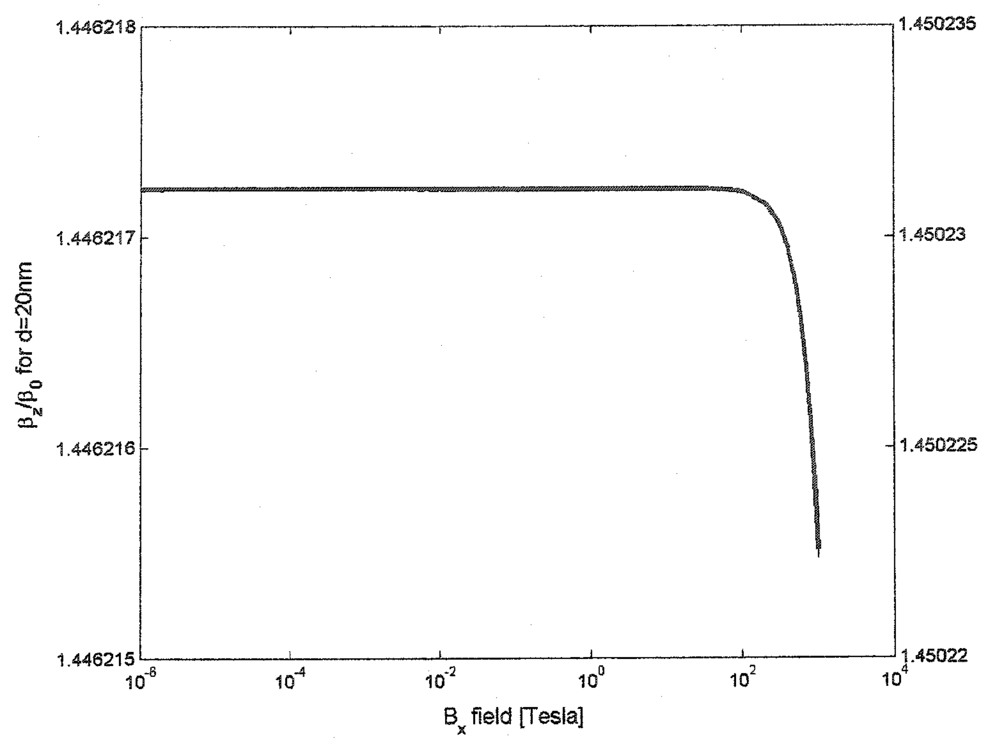

Figure 5.35 Simulated dispersion curve for the normalized phase constant of the symmetric bound mode supported by a thin Au film bounded by semi-infinite SiO_2, with an external magnetic field applied in the x direction (Voigt), at free space wavelength of 1550nm. Refer to the right-hand axis for the bold curve and the left-hand axis for the regular curve.

The phase constant of the symmetric bound mode decreases towards the value of the background dielectric as the magnetic field increases, as shown in Figure 5.35. Both the 20nm thick case and the 40nm thick case decrease in the same manner, but the 40nm thick case decreases more rapidly. The magnitude of the real part of the diagonal elements of the relative permittivity increases as the external magnetic field increases, as shown in Figure 5.20, allowing less of the mode to penetrate into the metal. Therefore, more of the mode is in the dielectric. Because this mode is a symmetric mode, the main field component, E_z, does not have a zero crossing in the metal, and it can, therefore, be easily pushed out of the metal and cut off. Since the mode is being cut off the phase constant is tending towards the value of the background dielectric, 1.444. Although the mode is being pushed out of the metal, the attenuation constant is increasing because there is still enough of the mode in the metal to be affected by the increase in the imaginary parts of elements of the relative permittivity tensor.

5.3.4 Field Components for the Symmetric Mode

The field components and the Poynting vector of the symmetric bound mode for a 20nm thick gold film bounded by silicon dioxide at the wavelength of 1550nm, with a magnetic field of 1T applied in the Voigt direction (x), are shown in Figure 5.36 and Figure 5.37, respectively.

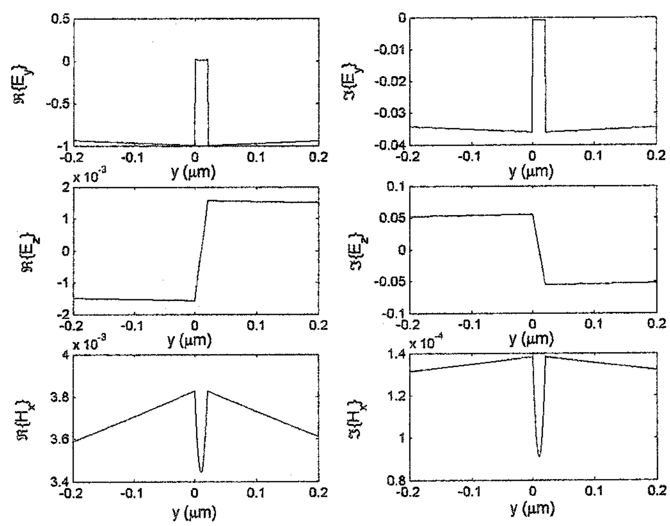

Figure 5.36 Simulated electric (E_y, E_z) and magnetic (H_x) fields of the symmetric bound mode supported by a thin Au film bounded by semi-infinite SiO_2, with an external magnetic field of 1 T applied in the x direction (Voigt), at free space wavelength of 1550nm. The propagation constant is 139.4062047238759 + j5862484.452174554.

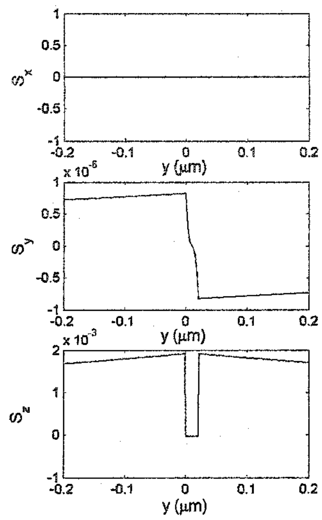

Figure 5.37 Poynting vector of the symmetric bound mode supported by a thin Au film bounded by semi-infinite SiO_2, with an external magnetic field of 1 T applied in the x direction (Voigt), at free space wavelength of 1550nm. The propagation constant is 139.4062047238759 + j5862484.452174554.

The field components and the Poynting vector of the symmetric bound mode for the same structure, with a magnetic field of 1000T applied in the Voigt direction (x), are shown in Figure 5.38 and Figure 5.39, respectively.

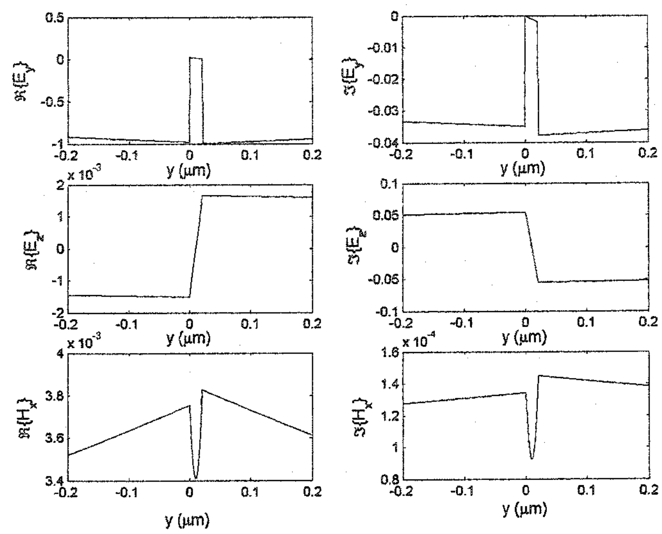

Figure 5.38 Simulated electric (E_y, E_z) and magnetic (H_x) fields of the symmetric bound mode supported by a thin Au film bounded by semi-infinite SiO_2, with an external magnetic field of 1000 T applied in the x direction (Voigt), at free space wavelength of 1550nm.

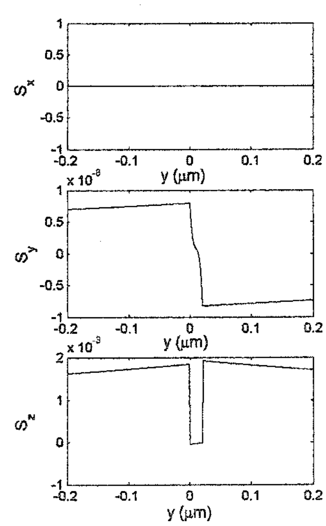

Figure 5.39 Poynting vector of the symmetric bound mode supported by a thin Au film bounded by semi-infinite SiO_2, with an external magnetic field of 1000 T applied in the x direction (Voigt), at free space wavelength of 1550nm.

As in the asymmetric case, the propagation constant of the symmetric bound mode under the influence of an external magnetic field of up to 1000T applied in the Voigt direction is slightly different from the propagation constant of the symmetric bound mode for the nominal (no external magnetic field) case, but the fields and Poynting vector are not noticeably affected, as can be seen in by comparing Figure 5.36 and Figure 5.38 with Figure 5.6, and Figure 5.37 and Figure 5.39 with Figure 5.7.

5.4 External Magnetic Field Applied in the Perpendicular Orientation

When an external magnetic field is applied in the perpendicular orientation it is perpendicular to both the direction of wave propagation and the interface. This is in the y-direction with respect to Figure 5.1. For this reason, it induces off-diagonal field components in the permittivity tensor in all but the y positions, as shown in equation (5.3). This induces the three other field components (E_x, H_y and H_z) in addition to the transverse magnetic components (E_y, E_z and H_x). Notice that the diagonal tensor element in the y position remains constant as the external magnetic field changes since the gyro frequency is not present in this element.

$$\tilde{\varepsilon} = \varepsilon_0 \begin{bmatrix} 1 + \dfrac{\omega_0^2(\omega - j\nu)}{\omega(\omega_g^2 - (\omega - j\nu)^2)} & 0 & \dfrac{j\omega_0^2\omega_g}{\omega(\omega_g^2 - (\omega - j\nu)^2)} \\ 0 & 1 - \dfrac{\omega_0^2}{\omega(\omega - j\nu)} & 0 \\ \dfrac{-j\omega_0^2\omega_g}{\omega(\omega_g^2 - (\omega - j\nu)^2)} & 0 & 1 + \dfrac{\omega_0^2(\omega - j\nu)}{\omega(\omega_g^2 - (\omega - j\nu)^2)} \end{bmatrix} \tag{5.3}$$

5.4.1 Dispersion Curves for the Asymmetric Mode

The dispersion curve of the propagation constant of a 20nm thick gold film and a 40nm thick gold film bounded by semi-infinite silicon dioxide under the influence of an externally applied magnetic field in the perpendicular (y) orientation have been simulated for magnetic fields ranging from 1 μTesla to 1 kTesla. The dispersion curves of the asymmetric bound mode for the normalized attenuation constants and normalized phase constants, at the free space wavelength of 1550nm are shown in Figure 5.40 and Figure 5.41, respectively.

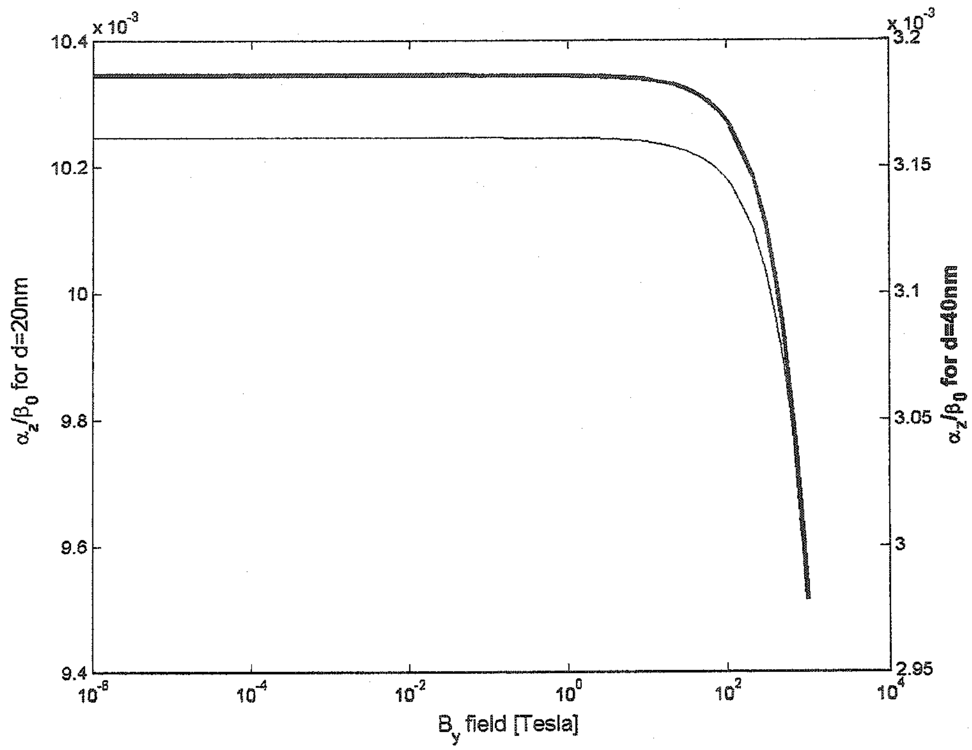

Figure 5.40 Simulated dispersion curve for the normalized attenuation constant of the asymmetric bound mode supported by a thin Au film bounded by semi-infinite SiO_2, with an external magnetic field applied in the y direction (perpendicular), at free space wavelength of 1550nm. Refer to the right-hand axis for the bold curve and the left-hand axis for the regular curve.

It can been seen in Figure 5.40 that the attenuation constant of the asymmetric bound mode supported by a thin gold film bounded by semi-infinite silicon dioxide, with an external magnetic field applied in the y direction (perpendicular), decreases as the magnetic field increases. This occurs because the mode is being pushed out of the metal and less of the mode power is being attenuated by the losses in the metal. Both the 20nm thick case and the 40nm thick case decrease in the same manner, but the 20nm thick case decreases more rapidly.

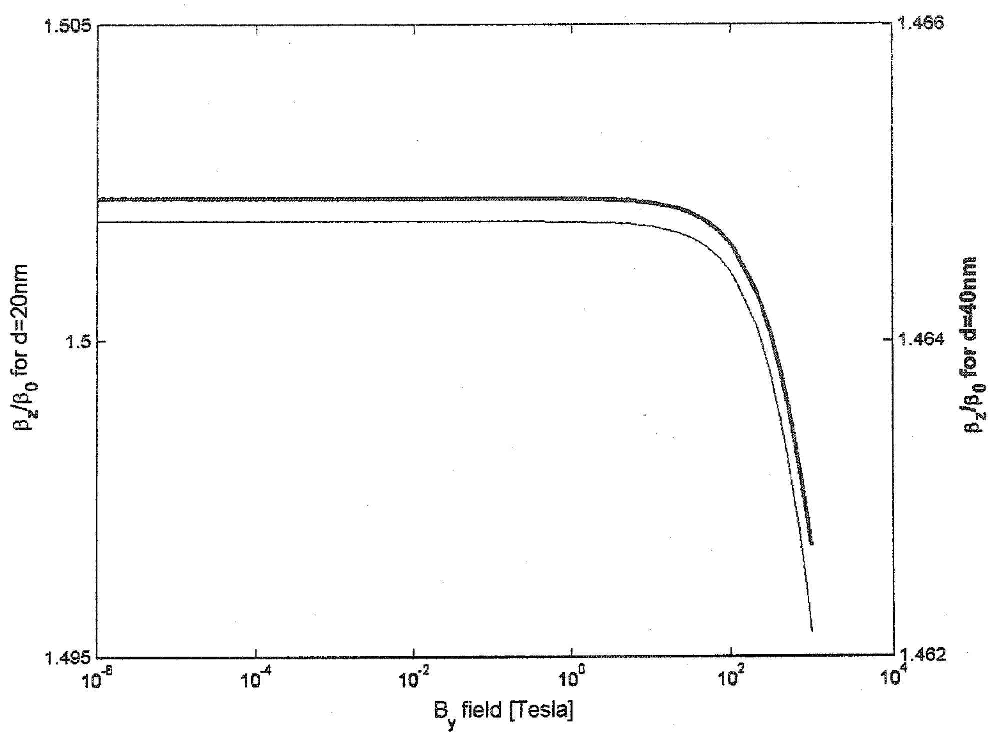

Figure 5.41 Simulated dispersion curve for the normalized phase constant of the asymmetric bound mode supported by a thin Au film bounded by semi-infinite SiO_2, with an external magnetic field applied in the y direction (perpendicular), at free space wavelength of 1550nm. Refer to the right-hand axis for the bold curve and the left-hand axis for the regular curve.

It can be seen from Figure 5.41 that the phase constant of the asymmetric bound mode supported by a thin gold film bounded by semi-infinite silicon dioxide, with an external magnetic field applied in the y direction (perpendicular), decreases towards the value of the background dielectric, 1.444, as the magnetic field increases for metal films of both 20nm and 40nm in thickness. Both the 20nm thick case and the 40nm thick case decrease in the same manner, but the 20nm thick case decreases more rapidly. This indicates that the mode is being pushed out of the metal into the dielectric and is being cut off. This cut-off is also supported by the mode fields shown in Figure 5.42. They become severely distorted when an external magnetic field is applied because the mode is being cut off.

5.4.2 Field Components for the Asymmetric Mode

When a magnetic field is applied in the perpendicular or y direction it is perpendicular to both the interface and the direction of propagation. It stimulates additional field components. All six electric and magnetic field components of the asymmetric bound mode of a 20nm thick gold film embedded in silicon dioxide at the wavelength of 1550nm, with a magnetic field of 1T applied in the perpendicular direction (y), are shown in Figure 5.42 and Figure 5.43. The three main transverse magnetic field components are shown in Figure 5.42, and the other three field components are shown in Figure 5.43. The Poynting vector is shown in Figure 5.44.

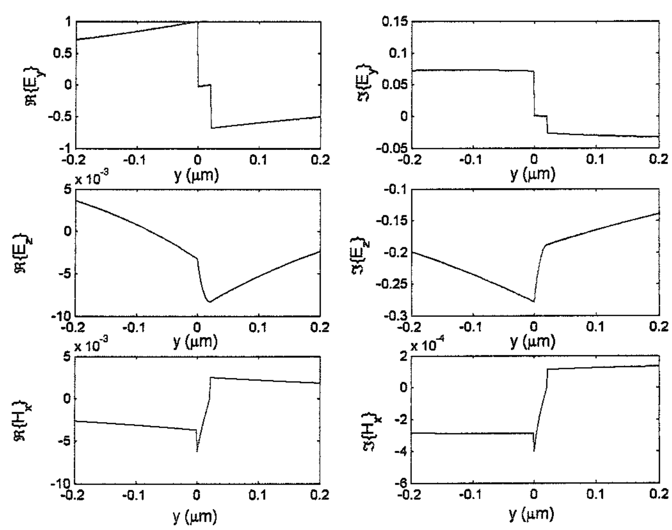

Figure 5.42 Simulated electric (E_y, E_z) and magnetic (H_x) fields of the asymmetric bound mode supported by a thin Au film bounded by semi-infinite SiO_2, with an external magnetic field of 1 T applied in the y direction (perpendicular), at free space wavelength of 1550nm. The propagation constant is 41531.92044917875 + j6088158.814474985.

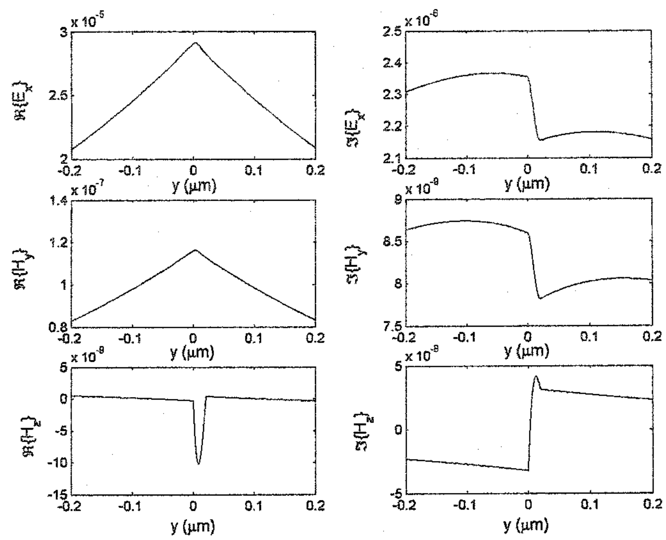

Figure 5.43 Simulated electric (E_x) and magnetic (H_y, H_z) fields of the asymmetric bound mode supported by a thin Au film bounded by semi-infinite SiO_2, with an external magnetic field of 1 T applied in the y direction (perpendicular), at free space wavelength of 1550nm. The propagation constant is 41531.92044917875 + j6088158.814474985.

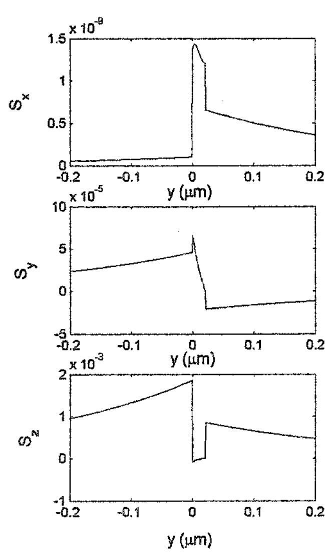

Figure 5.44 Poynting vector of the asymmetric bound mode supported by a thin Au film bounded by semi-infinite SiO_2, with an external magnetic field of 1 T applied in the y direction (perpendicular), at free space wavelength of 1550nm. The propagation constant is 41531.92044917875 + j6088158.814474985.

By comparing Figure 5.4 and Figure 5.42, it can be seen that the main three field components of the asymmetric mode remain relatively unchanged in the negative y half-space, that is to say, below the waveguide, when a magnetic field of 1T is applied in the perpendicular direction. However, the amplitude of the field decreases above the metal slab when the magnetic field is applied. The additional field components, E_x, H_y and H_z, are significantly smaller than the main transverse magnetic field components, E_y, E_z, and H_x, indicating that the mode is still mainly transverse magnetic in nature. The z-component of the Poynting vector is reduced above the waveguide, and the y-component of the Poynting vector experiences a sharp increase at the lower metal-semiconductor interface. The x component of the Poynting vector is 6 and 4 orders of magnitude smaller than the z component and the y component, respectively, therefore it does not have a great influence on the direction of power flow. The power flow is shown schematically in Figure 5.45.

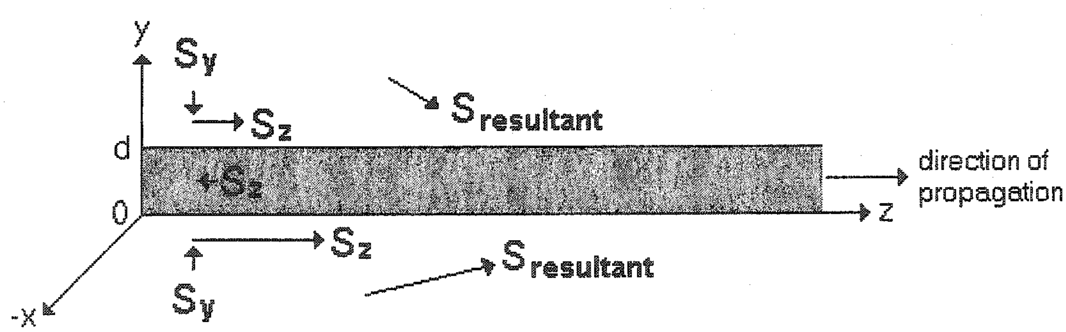

Figure 5.45 Direction of power flow in the asymmetric bound mode supported by a thin Au film bounded by semi-infinite SiO_2, with an external magnetic field of 1 T applied in the y direction (perpendicular)

To get a better understanding of the effect of a perpendicularly oriented externally applied magnetic field, the Poynting vector for the asymmetric bound mode with an external magnetic field of 1000T applied in the perpendicular direction is plotted in Figure 5.46.

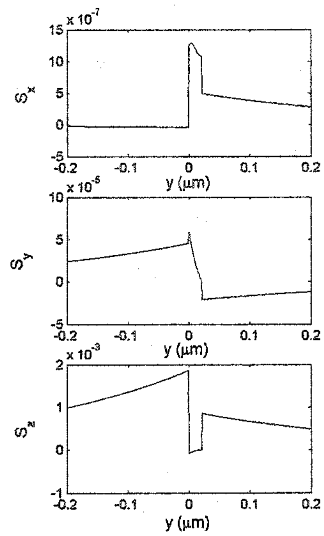

Figure 5.46 The Poynting vector of the asymmetric bound mode supported by a thin Au film bounded by semi-infinite SiO_2, with an external magnetic field of 1000 T applied in the y direction (perpendicular), at free space wavelength of 1550nm.

When the externally applied magnetic field is increased to 1000T, the x component of the Poynting vector becomes more important relative to the other components. Power flows above the metal film in the positive x-direction and more power flows in the metal film in the positive x-direction but very little power flows in the x-direction below the metal film. The direction of power flow is shown schematically in Figure 5.47.

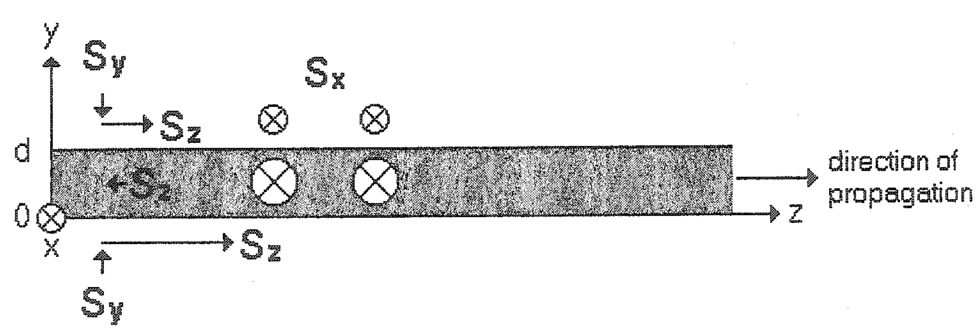

Figure 5.47 Direction of power flow in the asymmetric bound mode supported by a thin Au film bounded by semi-infinite SiO_2, with an external magnetic field of 1000 T applied in the y direction (perpendicular)

5.4.3 Dispersion Curves for the Symmetric Mode

The dispersion curves of the symmetric bound mode for the normalized attenuation constants and normalized phase constants, at the free space wavelength of 1550nm are shown in Figure 5.48 and Figure 5.49, respectively.

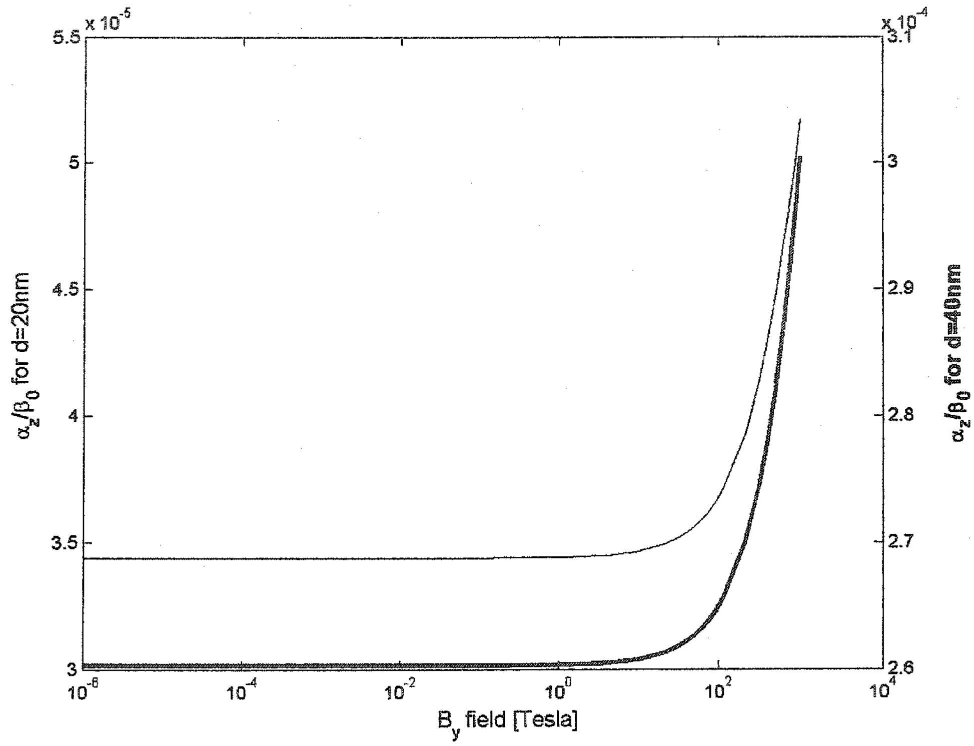

Figure 5.48 Simulated dispersion curve for the normalized attenuation constant of the symmetric bound mode supported by a thin Au film bounded by semi-infinite SiO_2, with an external magnetic field applied in the y direction (perpendicular), at free space wavelength of 1550nm. Refer to the right-hand axis for the bold curve and the left-hand axis for the regular curve.

It can been seen in Figure 5.48, that the attenuation constant of the symmetric bound mode supported by a thin gold film bounded by semi-infinite silicon dioxide, with an external magnetic field applied in the y direction (perpendicular), increases as the magnetic field increases for both film thickness values shown. Both the 20nm thick case and the 40nm thick case increase in the same manner, but the 40nm thick case increases more rapidly. The increase in the magnitude of the imaginary part of the diagonal elements of the relative permittivity of the metal due to the application of the external magnetic field, as shown in Figure 5.20, increases the losses in the metal. As the losses in the metal increase, the attenuation constant is expected to increase if the mode is not being pushed out of the metal very rapidly. This is what is seen in this case. However, in the asymmetric case, the mode is pushed out of the metal more rapidly than the losses in the metal are increasing, therefore the attenuation constant behaves in the opposite manner.

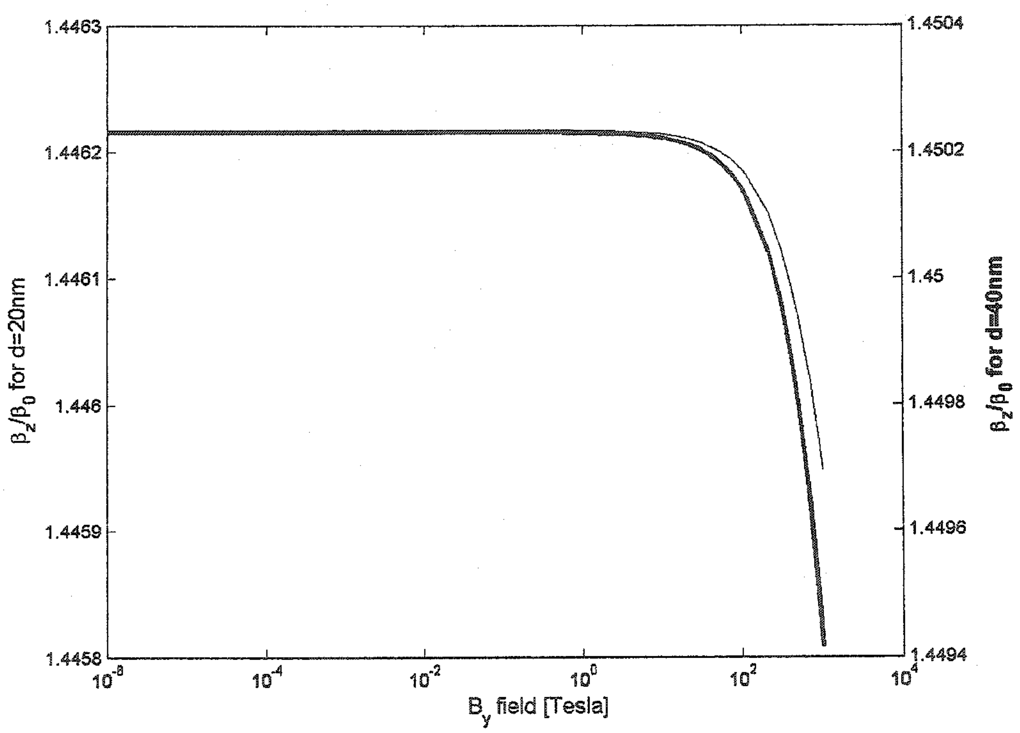

Figure 5.49 Simulated dispersion curve for the normalized phase constant of the symmetric bound mode supported by a thin Au film bounded by semi-infinite SiO_2, with an external magnetic field applied in the y direction (erpendicular), at free space wavelength of 1550nm. Refer to the right-hand axis for the bold curve and the left-hand axis for the regular curve.

It can be seen from Figure 5.49 that the phase constant of the symmetric bound mode, with an external magnetic field applied in the y direction (perpendicular), decreases towards the value of the background dielectric, 1.444, as the magnetic field increases for metal films of both 20nm and 40nm in thickness. Both the 20nm thick case and the 40nm thick case decrease in the same manner, but the 40nm thick case decreases more rapidly.

As is the case for the asymmetric bound mode, this indicates that the mode is being pushed out of the metal into the dielectric and is being cut off. This cut-off is also supported by the mode fields shown in Figure 5.50. They become distorted when an external magnetic field is applied because the mode is being cut off.

5.4.4 Field Components for the Symmetric Mode

The three primary transverse magnetic field components, the three secondary field components and the Poynting vector of the symmetric bound mode of a 20nm thick gold film embedded in silicon dioxide at the wavelength of 1550nm, with a magnetic field of 1T applied in the perpendicular direction (y), are shown in Figure 5.50, Figure 5.51 and Figure 5.52, respectively.

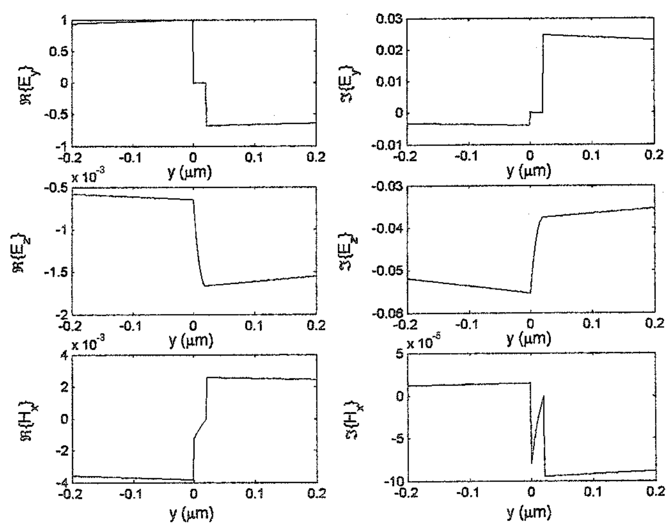

Figure 5.50 Simulated electric (E_y, E_z) and magnetic (H_x) fields of the symmetric bound mode supported by a thin Au film bounded by semi-infinite SiO_2, with an external magnetic field of 1 T applied in the y direction (perpendicular), at free space wavelength of 1550nm. The propagation constant is 139.5084114223609 + j5862483.142525522.

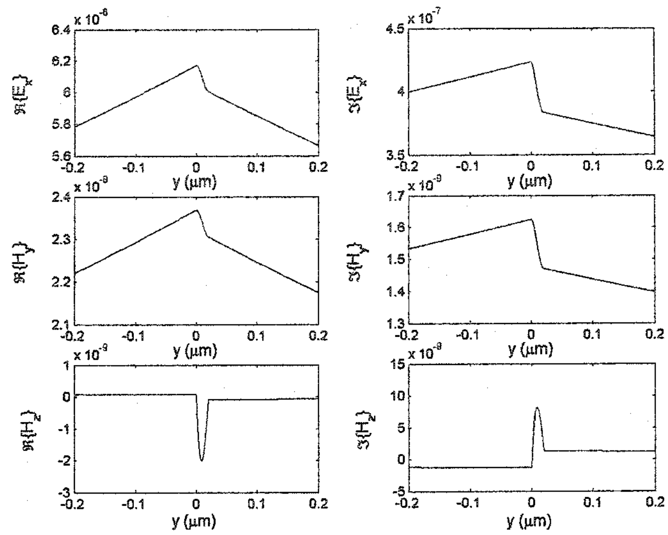

Figure 5.51 Simulated electric (E_x) and magnetic (H_y, H_z) fields of the symmetric bound mode supported by a thin Au film bounded by semi-infinite SiO_2, with an external magnetic field of 1 T applied in the y direction (perpendicular), at free space wavelength of 1550nm. The propagation constant is 139.5084114223609 + j5862483.142525522.

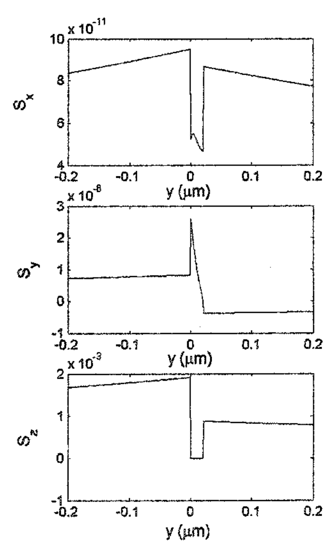

Figure 5.52 Poynting vector of the symmetric bound mode supported by a thin Au film bounded by semi-infinite SiO_2, with an external magnetic field of 1 T applied in the y direction (perpendicular), at free space wavelength of 1550nm. The propagation constant is 139.5084114223609 + j5862483.142525522.

By comparing Figure 5.6 and Figure 5.50, it can be seen that the field components of the symmetric bound mode change quite a bit when a magnetic field of 1T is applied in the perpendicular direction. The real part of the y-directed electric field component, E_y, reverses sign and experiences a significant reduction in amplitude below the metal film, but only experiences a small reduction in amplitude above the metal film. The opposite is true for the imaginary part of the y-directed electric field component, E_y. The real part of the z-directed electric field component, E_z, remains relatively unchanged below the metal film, but above the metal film it is no longer of equal but opposite amplitude but reverses sign and approaches the amplitude of the part below the waveguide. Once again the exact opposite is true for the imaginary part: the part above the waveguide remains relatively unchanged while the part below the waveguide reverses sign and approaches the amplitude of the part above the waveguide. The x-directed magnetic field component, H_x, behaves in the same manner as the y-directed electric field component, E_y. The additional field components, E_x, H_y and H_z, are significantly smaller than the main transverse magnetic field components, E_y, E_z, and H_x, indicating that the mode is still mainly transverse magnetic in nature. However, due to the sign reversal of the y-directed electric field component and the x-directed magnetic field component above the waveguide, the mode has become asymmetric. The Poynting vector, in Figure 5.52, seems to indicate that there is more energy at the bottom metal-semiconductor interface since there is a sharp increase in energy at the interface for the y-component of the Poynting vector.

In order to see how the mode evolves as the magnetic field increases, the x-component, y-component and z-component of the Poynting vector are plotted in Figure 5.53, Figure 5.54 and Figure 5.55, respectively, for several external magnetic field levels: 1μT, 10μT, 1mT, 1mT, 1T, 10T, 1000T.

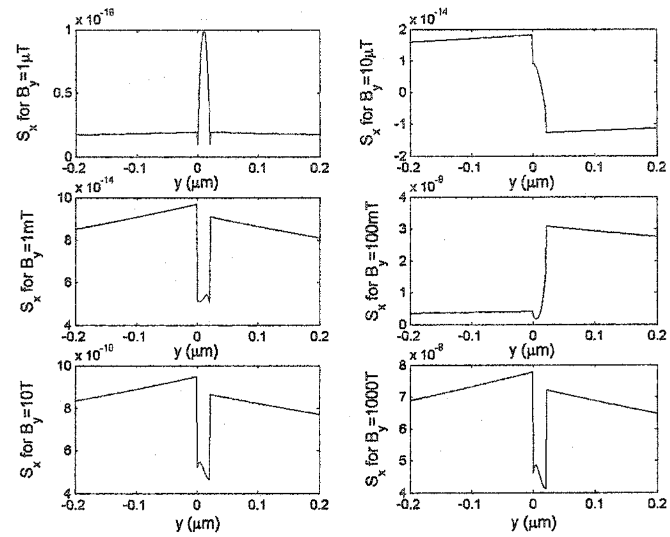

Figure 5.53 Poynting vector of the symmetric bound mode supported by a thin Au film bounded by semi-infinite SiO_2, with various external magnetic field levels applied in the y direction (perpendicular), at free space wavelength of 1550nm.

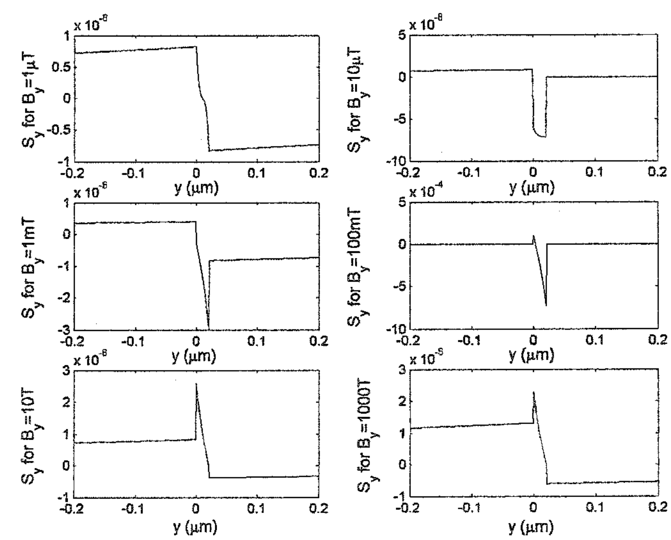

Figure 5.54 Poynting vector of the symmetric bound mode supported by a thin Au film bounded by semi-infinite SiO_2, with various external magnetic field levels applied in the y direction (perpendicular), at free space wavelength of 1550nm.

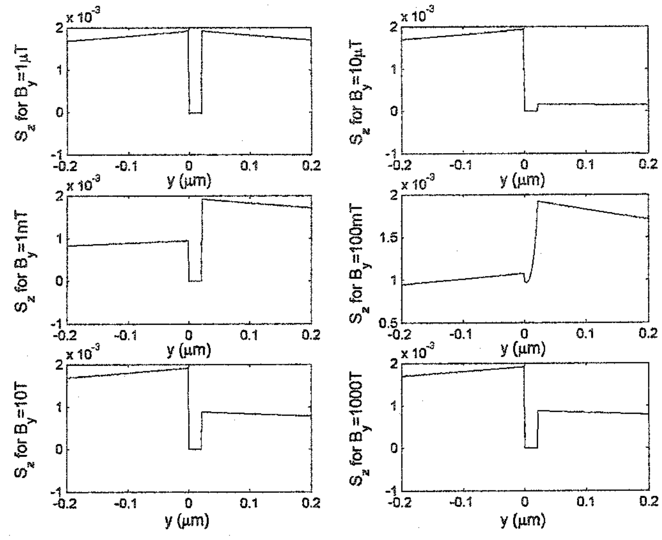

Figure 5.55 Poynting vector of the symmetric bound mode supported by a thin Au film bounded by semi-infinite SiO_2, with various external magnetic field levels applied in the y direction (perpendicular), at free space wavelength of 1550nm.

From Figure 5.53, Figure 5.54 and Figure 5.55, it can be seen that the Poynting vector of the symmetric mode is greatly affected by an external magnetic field applied in the perpendicular direction. The z-component of the Poynting vector always points in the direction of propagation above and below the metal film, although it varies in amplitude as the externally applied magnetic field changes. In the metal film the z-component does not change very much except at around 100mT, where it increases in amplitude and changes direction. At 100mT, the other two Poynting vector components also exhibit interesting behavior. The x-component is much larger above the metal film than below it. The y-component has the majority of its power in the metal film with very little above and below the waveguide. The symmetric mode evolves into an asymmetric mode around 1mT. This can be noted by the changes in the Poynting vector in all three dimensions. After this point, more and more of the mode power is drawn into the metal film as the mode continues to evolve as an asymmetric mode. When the externally applied magnetic field reaches 1000T the Poynting vector is starting to resemble the Poynting vector of a mode unaffected by an external magnetic field, with the noted exception that the x-component is present and becoming more important. This is due to the secondary field components that grow in magnitude as the externally applied magnetic field increases.

5.5 Conclusion

The application of an external magnetic field will perturb a plasmon polariton mode in a finite width gold film bounded by semi-infinite silicon dioxide. The way and extent to which this externally applied magnetic field influences the mode depends on its orientation with respect to the gold film, the direction of propagation and the film thickness. The externally applied magnetic field has the least influence on the asymmetric and symmetric plasmon polariton modes when it is applied in the Voigt direction because additional field components are not introduced. The externally applied magnetic field has a greater influence on the plasmon polariton modes when it is applied in either the Faraday or perpendicular directions. The effect on the symmetric mode in both cases is quite interesting. When an external magnetic field is applied in the Faraday orientation, the symmetric bound mode will cut off and evolve into another mode that is being fed energy from the top and bottom of the metal film at a slight angle. This energy begins to compensate for the losses in the metal and may actually exceed the losses in the metal as the tilt angle increases [46]. When an external magnetic field is applied in the perpendicular orientation, both the symmetric and asymmetric modes cut off and the phase constant tends towards the phase constant of the background dielectric.

The effect of an externally applied magnetic field on the symmetric bound mode is of more interest than its effect on the asymmetric bound mode because the symmetric bound mode has a diminishing attenuation constant for decreasing thickness, and is therefore, practical for optical devices. When the external magnetic field is applied in both the Faraday and perpendicular orientations, the attenuation constants increase and the phase constants decrease as the magnetic field increases. Both changes are much stronger when the external magnetic field is applied in the perpendicular orientation.

The change in the attenuation constant due to the application of an external magnetic field can be exploited in variable optical attenuator. A variable optical attenuaor could also be designed based on the change in phase constant due to the application of an external magnetic field. The change in phase constant could also be used to design a Mach Zehnder modulator. Although the magnetic field levels used in this study are quite large and impractical, the trends seen in this material system may be transferable to another material system in which the magnetic field levels required to see an effect are more practical. From the relative permittivity tensor, in equations (5.1), (5.2) and (5.3), it can be seen that the off-diagonal tensor elements of a material with a smaller effective electron mass will be more sensitive to the application of an external magnetic field. Therefore, a material with a smaller effective electron mass would be affected mre by an externally applied magnetic field.

6. Conclusions and Future Work

6.1 Conclusions

In this thesis, magneto-plasmons have been investigated theoretically. The broader field of plasmon polaritons has been reviewed and a literary review of the previous work conducted in this area has been presented. The dielectric permittivity tensor in the presence of a magnetic field has been derived from Drude theory. Based on Maxwell's equations a general dispersion relation, including losses, for magneto-plasmons in an infinitely wide thin film metal waveguide has been developed for what is believed to be the first time.

6.1.1 Model Validation with Corrected and Interpreted Results

The dispersion relation is used as the basis of a software model of magneto-plasmons in thin metal films. This model is validated against specific cases in the literature with and without an externally applied magnetic field. During the validation process, an error was discovered in the literature. The previous work has been corrected and the results have been interpreted.

An indium tin slab in air with an externally applied magnetic field in three orthogonal cartesian orientations was modelled. It was found that as the frequency increases, more branches appear in the dispersion characteristic, indicating that additional modes can be supported at higher frequencies. Every branch of the dispersion curves for the corrected dispersion equations in the Voigt and perpendicular configurations as well as the dispersion curve for the Faraday dispersion equation have been explored meticulously to the best of the numerical limitations of the modelling code. Numerous branches are found in each orientation. The field components of the modes represented by these branches have also been examined. The modes in these branches exhibit complex behaviour; both plasmon-polariton modes and total internal reflection modes are present.

When no external magnetic field is present, the existence of plasmon-polariton modes requires that the real parts of the diagonal components of the permittivity tensor be of opposite sign for the media that make up the interface or interfaces. In this structure this requirement means that the diagonal components of the permittivity tensor are negative since the permittivity of the surrounding medium, air, is positive. In this structure, the diagonal components of the permittivity tensor in all three cases are negative only for certain intervals. Plasmon-polariton modes would not normally exist over most of the frequencies examined. However, it is believed that the presence of an externally applied magnetic field induces plasmon-polariton modes in the structure primarily via the appearance of off-diagonal elements in the permittivity tensor.

6.1.2 Simulation Results for Thin Gold Films in Silicon Dioxide

Once the software model was validated it was used to model thin gold films bounded by semi-infinite silicon dioxide at a free space wavelength of 1550nm for what is believed to be the first time. The modelling results include the effect of the externally applied magnetic field on the propagation constant and the corresponding field components for all three cartesian orientations of externally applied magnetic field.

Through the simulations, it was discovered that an externally applied magnetic field has an effect on a thin gold film bounded by semi-infinite silicon dioxide. The way and extent to which this externally applied magnetic field influences the mode depends on its orientation with respect to the gold film, the direction of propagation and the film thickness. The externally applied magnetic field has the least influence on the asymmetric and symmetric plasmon-polariton modes when it is applied in the Voigt direction because additional field components are not introduced. The externally applied magnetic field has a greater influence on the plasmon-polariton modes when it is applied in either the Faraday or perpendicular directions. The effect on the symmetric mode in both cases is quite interesting. When an external magnetic field is applied in the Faraday orientation, the symmetric bound mode will cut off and evolve into another mode that is being fed energy from the top and bottom of the metal film at a slight angle. This energy begins to compensate for the losses in the metal and may actually exceed the losses in the metal as the tilt angle increases [46]. When an external magnetic field is applied in the perpendicular orientation, both the symmetric and asymmetric modes cut off and the phase constant tends towards the phase constant of the background dielectric.

The effect of an externally applied magnetic field on the symmetric bound mode is of more interest than its effect on the asymmetric bound mode because the symmetric bound mode has a diminishing attenuation constant for decreasing thickness, and is, therefore, practical for optical devices. When the external magnetic field is applied in either the Faraday or perpendicular orientation, the attenuation constants increase and the phase constants decrease as the magnetic field increases. Both changes are much stronger when the external magnetic field is applied in the perpendicular orientation.

The effect of an externally applied magnetic field on a finite width gold film will be similar to the effect on a slab. Limiting the width of the slab will not change the basic trends of the effect. In a finite width metal optical waveguide, the symmetric mode is of most interest. It is highly probable that the effect of an externally applied magnetic field will be strongest when it is applied in the perpendicular orientation.

The change in the attenuation constant due to the application of an external magnetic field can be exploited in a variable optical attenuator. A variable optical attenuator could also be designed based on the change in phase constant due to the application of an external magnetic field. The change in phase constant could be used to design a Mach Zehnder modulator.

6.2 Thesis Contributions

Surface magneto-plasmons have been investigated theoretically in several studies. However, most of the literature on the subject is not geared towards optical communications. In this thesis, an effort has been made to analyse the magneto-plasmons in structures that are practical at communications wavelengths. Three main thesis contributions are of interest:

- The general dispersion relation for a structure with a permittivity tensor including losses, which may be induced by an externally applied magnetic field, has been formulated for what is believed to be the first time.
- This dispersion relation is used as the basis for a model which is used to reproduce simulations of a semiconductor slab under the influence of an externally applied magnetic field for comparison with the literature. An error was discovered in the formulation in the literature, and the specific formulations in the literature have been corrected and the simulation results have been interpreted. It is believed that this constitutes the most comprehensive study on magneto-plasmons in a semiconductor film to date.
- Finally, this model is used to simulate magneto-plasmons in a thin gold film bounded by semi-infinite silicon dioxide at a free space wavelength of 1550nm for what is believed to be the first time. The behaviour of the magneto-plasmon modes in this structure have been studied and interpreted for the first time.

6.3 Future Work

The simulation work on indium tin slab in the literature and in this thesis was only done for a single value of externally applied magnetic field over a range of frequencies. Investigating this structure over a range of magnetic field levels would add to this work and aid in the interpretation of the modes. The thickness of the slab could also be varied to see how the effect of an externally applied magnetic field changes as the thickness of the slab changes.

The thickness of the thin gold films bounded by semi-infinite silicon dioxide could also be varied, as could the wavelength of the incident light. The almost free-electron gas model used in the derivation of the permittivity model does not include scattering losses at the interfaces. Their inclusion would improve the theory. Thin film resistivity models could be used as a starting point.

Finite width metallic optical waveguides are of greater interest than infinitely wide optical slab waveguides because the symmetric bound mode can be excited by end-fire excitation. Although the results from this work on slab waveguides can be extended to the expected trends in finite width optical waveguides, it would be of great interest to theoretically study the effect of an externally applied magnetic field on finite width optical waveguides. This cannot be done analytically; a numerical technique is required. The method of lines, the finite element method or the finite difference method may prove to be suitable for this task.

Although the magnetic field levels used in this study of a gold slab bounded by silicon dioxide are quite large and impractical, the trends seen in this material system may be transferable to another material system in which the magnetic field levels required to see an effect are more practical. A material with a lower effective electron mass would be affected more by an externally applied magnetic field. The model could be extended to include the permeability tensor so that the effect of an externally applied magnetic field on a magnetic material could be investigated.

It would be of great interest to experimentally investigate the effect of an externally applied magnetic field on thin gold films bounded by silicon dioxide. As mentioned previously, the magnetic fields required for this experiment are quite large in some cases so it may be necessary to use specialized equipment.

Metal optical waveguide technology is of great interest to the optical communications industry because the waveguides can be printed in the same manner as the electronic integrated circuits. For this reason, the investigation of magneto-plasmons as a method of producing active metal optical waveguide devices is of great interest.

Glossary of Symbols

Symbol	Definition	Units
$\vec{a}$	acceleration	m/s^2
α_i	attenuation constant in the *i* direction	Np/m
β_i	phase constant in the *i* direction	rad/m
β_0	free space wave constant	
$\vec{B}$	magnetic flux density	T
$\vec{B}_{DC}$	externally applied magnetic flux density	T
B_{DCz}	externally applied magnetic flux density in the z-direction	T
c	speed of light in a vacuum	m/s
d	thickness of the film	m
$\vec{D}$	electric flux density	C/m^2
$\tilde{\varepsilon}$	permittivity tensor	F/m
ε_0	permittivity of free space	F/m
ε_r	relative permittivity	
ε_r'	real part of the relative permittivity	
ε_r''	imaginary part of the relative permittivity	
ε_L	background dielectric constant	
$\vec{E}$	electric field intensity	V/m
$\vec{F}_e$	electric force	N
$\vec{F}_m$	magnetic force	N

Symbol	Definition	Units
$\vec{F}_d$	damping force	N
$\vec{F}$	total force	N
γ	propagation vector (or wave vector), $\gamma = (\gamma_x, \gamma_y, \gamma_z)$	m^{-1}
γ_x	complex directional propagation constants in x	m^{-1}
γ_y	complex directional propagation constants in y	m^{-1}
γ_z	complex directional propagation constants in z	m^{-1}
$\vec{H}$	magnetic field	A/m
i	direction of propagation constant (x, y or z)	
$\vec{J}$	current density	A/m^2
λ_0	free space wavelength	m
m	effective optical mass of the electron	kg
μ	permeability	H/m
N	density of conduction electrons	m^{-3}
N_{Au}	refractive index of gold	
N_{SiO_2}	refractive index of silicon dioxide	
q	electronic charge	C
r	position vector, $r = (x, y, z)$	
$\vec{S}$	Poynting vector	W/m^2
t	time	s
ϕ	angle of wave propagation with respect to the z axis	
$\vec{v}$	velocity of the electron due to the wave	m/s
ν	effective electron collision frequency	rad/s

Symbol	Definition	Units
ω	angular frequency of radiation	rad/s
ω_0	plasma (or critical) frequency	rad/s
ω_g	gyro (or cyclotron) frequency	rad/s

Bibliography

1 BERINI, P., “Plasmon-polariton modes guided by a metal film of finite width,” Optics Letters, Vol. 24 (15), pp. 1011-1013, (August 1999).

2 BERINI, P., “Plasmon-polariton waves guided by thin lossy metal films of finite width: bound modes of symmetric structures,” Physical Review B, Vol. 61 No. 15, pp. 10484-10503, 15 April 2000.

3 BERINI, P., “Plasmon-polariton modes guided by a metal film of finite width bounded by different dielectrics,” Optics Express, Vol. 7 (10), pp. 329-335, (November 2000).

4 CHARBONNEAU, R., BERINI, P., BEROLO, E., LISICKA-SHRZEK, E., “Experimental observation of plasmon-polariton waves supported by a thin metal film of finite width,: Optics Letters, Vol. 25 (11), pp. 844-846, (June 1, 2000).

5 CHARBONNEAU, R., BERINI, P., BEROLO, E., LISICKA-SHRZEK, E., “Long-Range Plasmon-Polariton Wave Propagation in Thin Metal Films of Finite-Width Excited Using an End-Fire Technique,” International Conference on the Application of Photonic Technology, ICAPT’2000, Proc. SPIE, Vol. 4087, pp. 534-540, (June 2000).

6 OTTO, A., “Excitation of nonradiative surface plasma waves in silver by the method of frustrated total reflection,” Z. Phys., Vol. 216, pp. 328, (1968).

7 KRETSCHMANN, E., RAETHER, H., “Radiative Decay of Non Radiative Surface Plasmons Excited by Light,” Zeitschrift fur Naturforschung Part A, Vol. 23A (12), pp. 2135, (1968).

8 KRETSCHMANN, E., "Scattering of Light at Rough Surfaces Due to Excitation of Surface Plasmons," Zeitschrift fur Physik, Vol. 227 (5), pp. 412, (1969).

9 CHIU, K. W., QUINN, J. J., "Magnetoplasma Surface Waves in Metals," Phys. Rev. B, Vol. 5 (12), pp. 4707-4709, (15 June 1972).

10 CHIU, K. W., QUINN, J. J., "Magneto-Plasma Surface Waves in Solids," Il Nuovo Cimento, Vol 10B, (1), (11 Luglio 1972).

11 BRION, J. J., WALLIS, R. F., HARTSTEIN, A., BURSTEIN, E., Phys. Rev. Letters, 28, 1455 (1972).

12 QUINN, J. J., CHIU, K. W., in: Polaritons (E. Burstein and R. de Martini, eds.) (Pergamon, New York, 1974) p. 259.

13 DeWAMES, R. E., HALL, W. F., "Magnetic Field Effect on Plasma-Wave Dispersion in a Dielectric Layer," Phys. Rev. Letteres, Vol. 29 (3) , pp. 172-175 (17 July 1972)

14 WALLIS, R. F., BRION, J. J., BURSTEIN, E., HARTSTEIN, A., "Theory of surface polaritons in anisotropic dielectric media with application to surface magnetoplasmons in semiconductors," Phys. Rev. B, Vol. 9 (8), pp. 3424-3437 (15 April 1974).

15 BOARDMAN, A. D., and ISSAC, E. D., Solid State Commun., 18, 97 (1976).

16 AERS, G. C., and BOARDMAN, A. D., J. Phys., C11, 945 (1978).

17 CHIU, K. W., and QUINN, J. J., in: Proceedings of the Eleventh International Conference on the Physics of Semiconductors (PWN-Polish Scientific Publishers, Warsaw, 1972) p. 1455

18 CHIU, K. W., and QUINN, J. J., Phys. Rev. Letters, 29, 600 (1972).

19 BRION, J. J., WALLIS, R. F., HARTSTEIN, A., BURSTEIN, E., Surface Science, 34, 73 (1973).

20 MARTIN, B. G, MARADUDIN, A. A., and WALLIS, R. F., "Theory of damped surface magnetoplasmons in n-type InSb," Surface Science 77 (1978) pp. 416-426.

21 HARTSTEIN, A., BURSTEIN, E., Solid State Commun., 14, 1223 (1974).

22 HARTSTEIN, A., BURSTEIN, E., PALIK, E. D., GAMMON, R. W., AND HENVIS, B. W., Phys. Rev., B12, 3186 (1975)

23 KAPLAN, H., PALIK, E. D., KAPLAN, R., AND GAMMON, R. W., "Calculation of attenuated-total-reflaction spectra of surface magnetoplasmons on semiconductors," Journal of the Optical Society of America, Vol. 64 (11), pp. 1551-1562, November 1974.

24 PALIK, E. D., KAPLAN, R., GAMMON, R. W., KAPLAN, H., QUINN, J. J., and WALLIS, R. F., "Surface Magnetoplasmon-Optic Phonon Modes in InSb," Phys, Letters, A45, 143 (1973).

25 SARID, D., "Enhanced surface-magnetoplasma interactions in a semiconductor," Phys. Rev. B, Vol. 29 (4), (15 February 1984) pp. 3422-2346.

26 SARID, D., "Enhanced Magnetic Interaction of Surface-Magnetoplasmon Polaritons," IEEE Journal of Quantum Electronics, Vol. QE-20 (8), (August 1984), pp. 943-948.

27 KUSHWAHA, M. S., and HALEVI, P., "Magnetoplasma modes in thin films in the Faraday configuration," Phys. Rev. B, Vol. 35 (8), 15 March 1987, pp. 3879-3889.

28 KUSHWAHA, M. S., and HALEVI, P., "Magnetoplasmons in thin films in the Voigt configuration," Phys. Rev. B, Vol. 36 (11), 15 October 1987, pp. 5960-5967.

29 KUSHWAHA, M. S., and HALEVI, P., "Magnetoplasmons in thin films in the perpendicular configuration," Phys. Rev. B, Vol. 38 (17), 15 December 1988, pp. 12428-12435.

30 YARIV, A. and YEH, P., Optical Waves in Crystals, Propagation and Control of Laser Radiation, John Wiley & Sons, New York, 1984.

31 BOARDMAN, A. D., Electromagnetic Surface Modes, John Wiley & Sons, Chester, 1982.

32 KRAUS, Electromagnetics, 2nd Ed., Chapter 15.

33 JOHNSON, P. B. and CHRISTY, R. W., "Optical Constants of Noble Metals," Physical Review B, Vol. 6, No. 12, 15 December 1972.

34 YANG, F., SAMBLES, J. R., BRADBERRY, G. W., "Long-range surface modes supported by thin tilms," Physical Review B, pp. 5855-5872, Vol. 44, No. 11, 15 September 1991.

35 KUSHWAHA, M. S., "Effect of an applied magnetic field on interface excitations in finite layered structures," Physical Review B, Vol. 35, No. 8, 15 March 1987-I.

36 KUSHWAHA, M. S., "Effect of an applied magnetic field on interface excitations in finite layered structures. II," Physical Review B, Vol. 36, No. 9, 15 September 1987-II.

37 KUSHWAHA, M. S., "Effect of an applied magnetic field on interface excitations in finite layered structures. III," Physical Review B, Vol. 40, No. 3, 15 July 1989-II.

38 IVANOV, S. T. and NIKOLAEV, N. I., "Singular waves along the boundary of gyrotropic plasma," J. Phys. D: Appl. Phys. 29 (1996) 1107-1110.

39 IVANOV, S. T., NIKOLAEV, N. I. and THOMAE, R. W., "Magnetoplasmons along the Interface of Gyrotropic Plasma Surface - Longitudinal Propagation," Physica Scripta 57, 1997, pp. 645-651.

40 IVANOV, S. T. and NIKOLAEV, N. I., "Magnetic-field effect on wave dispersion in a free semiconductor plasma slab," J. Phys. D: Appl. Phys. 32 (1999) 430-439.

41 IVANOV, S. T., NIKOLAEV, N. I. and THOMAE, R. W., "Magnetoplasmons Along the Interface of Gyrotropic Plasma Surface - Transverse Propagation," Physica Scripta 57, 1997, pp. 637-644.

42 BERINI, P., *ELG 5379 Numerical Methods in Electromagnetic Engineering Course Notes 2000 Edition.*

43 CONTE, S. D., de BOOR, C., "Elementary numerical analysis," McGraw-Hill Book Company, 1972, pp. 74-79.

44 CHARBONNEAU, R., *Demonstration of a passive integrated optics technology based on plasmons*, Master's Thesis, July 9, 2001.

45 PALIK, E. D., Handbook of Optical Constants of Solids, Academic Press, Inc., Orlando, Florida, 1985.

46 BURKE, J. J., STEGEMAN, G. I. and TAMIR, T., "Surface-polariton-like waves guided by thin, lossy metal films," Phys. Rev. B, Vol. 33, No. 8, 15 April 1986.